A Method for Estimating the Hydraulic Roughness of Unlined Bored Tunnels

GGS Pegram • MS Pennington

Report to the Water Research Commission
by the
Department of Civil Engineering
University of Natal

WRC Report No 579/1/96

A METHOD FOR ESTIMATING THE HYDRAULIC ROUGHNESS OF UNLINED BORED TUNNELS

by

GGS Pegram

and

MS Pennington

WRC Report No: 579/1/96

ISBN No: 1 86845 219 0

REPORT DESCRIBING A RESEARCH PROJECT CARRIED OUT IN THE DEPARTMENT OF CIVIL ENGINEERING, UNIVERSITY OF NATAL, DURBAN, UNDER CONTRACT TO THE WATER RESEARCH COMMISSION

DEPARTMENT OF CIVIL ENGINEERING
UNIVERSITY OF NATAL
DURBAN

ACKNOWLEDGEMENTS

This report resulted from a research project financed by the Water Research Commission. The original proposed title of the project was "Hydraulic Roughness of Tunnels bored by Machine through Various Rock Types".

The steering committee responsible for the project consisted of the following members :

Mr DS van der Merwe	Water Research Commission
Mr HC Chapman	Water Research Commission
Dr JM Jordaan	Dept of Water Affairs and Forestry
Prof GGS Pegram	University of Natal
Dr HD Schreiner	University of Natal
Mr JR Metcalf	Keeve Steyn Inc
Prof A Rooseboom	University of Stellenbosch
Prof A van Schalkwyk	University of Pretoria

The financial support of the WRC made the entire project possible, and is acknowledged with thanks. So too, are the contributions from the steering committee members.

Thanks are also due to Keeve Steyn Inc., especially Mr JR Metcalf, who arranged access into various water tunnels and thereby made possible the tunnel roughness data collection.

After his contribution to its development, Mr J Hamar, senior technician of the Department of Civil Engineering, University of Natal, serviced and modified the roughness data collection apparatus as was required by the researchers, who are grateful for this service.

EXECUTIVE SUMMARY

THE PROBLEM

The hydraulic engineer who is presented with the problem of designing a tunnel to be excavated by tunnel boring machine (TBM) has (among others) the following question to answer:

- given the route or alignment of the tunnel and the quantity of water it is to transport
- given a geological prediction of the rock-types likely to be encountered in the tunnel,
- **what is the hydraulic resistance of the tunnel walls likely to be in situations where head loss is important?**

To answer this question, the answer to a new question must be found:

- **how rough is the surface inside the tunnel likely to be, and how is this physical roughness related to hydraulic resistance?**

Hard rock is no longer beyond the capacity of the TBM. However, at the outset of this study, there were relatively few kilometres of tunnel excavated by TBM (when compared to the more traditional method of drill-and-blast) on which to base an answer to this question. There are nowadays a number of hard rock TBM excavated tunnels. There nevertheless continues to be a paucity of information on the resistance coefficients to be used for unlined bored tunnels. The information that is available has been almost exclusively derived from hydraulic tests.

THE PURPOSE OF THIS REPORT

The purpose of this report is to form the link between measurements of physical roughness obtained from bored tunnels on the one hand with hydraulic resistance on the others. To this end, it was necessary to make a start in the systematic collection of data useful for predicting the hydraulic resistance of bored tunnels. The following actions were taken and are reported on here:

- an extensive literature search was undertaken to find out what had already been done in directly relating physical roughness to hydraulic resistance

- a methodology using a laser scanner was developed to collect accurate roughness data at 0,5mm (scanning) intervals over a 1m base length and store them directly in a file in a notebook computer while in a tunnel

- such roughness samples and accompanying photographs were collected at 100m (spacing/sampling) intervals in 15,1 kilometres of freshly bored tunnels in Lesotho and KwaZulu-Natal during 1994

- several statistical parameters for quantifying physical roughness of the tunnel wall from the measured data were defined and studied using time series analysis and spectral analysis

- theoretical fluid dynamics investigations were made into the nature of flow in large water conduits and an improved velocity distribution for turbulent flow in conduits was developed

- by comparing predictions of resistance with those obtainable in the literature, a selection was made between the various roughness statistics as to which was best for predicting hydraulic resistance

- recommended values of hydraulic resistance are offered for a range of surfaces.

The Report is divided into three main sections (beside this executive summary):

- the body containing the main points
- the appendices, containing the detailed argument, supporting the body
- the available pictorial and electronic data of the tunnels appearing in photographs and stored on diskettes at the end of the report.

THE FINDINGS

In most tunnels, the diameters and velocities are such that the flow is in the hydraulically "rough" zone. In rough flow, it cam be shown that the diameter is measured from a "boundary" which is at the median height of the surface. In addition, argument is presented to show that resistance in "rough" turbulent flow does not explicitly depend on the spacing of the roughness elements as when flow is "transitional"; it is sufficient to define the appropriate Nikuradse k value for the surface.

It turns out that a good method of estimating hydraulic resistance is to equate the equivalent Nikuradse sand grain diameter, k, to the mean range, h_λ, corresponding to the mean wavelength, λ, of the surface as defined by the sample spectrum. When estimate of k is substituted into the Colebrook-White equation for the Darcy-Weisbach friction factor, f, it gives a more robust estimate of the hydraulic resistance than does its close competitor based on the standard deviation of the surface roughness, $h_\sigma = 2{,}83\sigma$.

In tunnels excavated by TBMs through hard rock it was found, from the tunnels sampled, that the Manning's n value within the range of the reported values found in the literature. In particular, the mean n values for cast *in situ* concrete, sandstone, granite and shotcrete surfaces turn out to be :

Surface	Mean	Standard Deviation
concrete lining	n=0.0119	0.0009
sandstone	n=0.0154	0.0010
granite	n=0.0157	0.0008
shotcrete	n=0,0161	0.0011

These findings should be of interest to the community of engineers involved with the hydraulics of tunnels excavated by TBMs.

Geoffrey GS Pegram
Mark S Pennington

DURBAN 30th October 1995

LIST OF CONTENTS

APPENDICES

LIST OF TABLES

LIST OF FIGURES

LIST OF SYMBOLS

A	=	cross-sectional area
A'	=	plan area
A_p	=	projected area normal to flow
$\mathbf{B}$	=	body force vector
B_0	=	constant
C_D	=	drag coefficient
C_{xx}	=	sample spectrum
d	=	diameter
f	=	Darcy-Weisbach friction factor (as in $h_f=4flu^2/2gd$)
$\mathbf{F}_s$	=	total surface force vector
g	=	acceleration due to gravity ($=9.81 m/s^2$)
G	=	constant for boundary roughness
H_f	=	head lost due to friction
h	=	radial roughness height (crest to trough)
h_λ	=	roughness height from the mean range
h_σ	=	roughness height from variance $= 2.83\sigma$
k	=	equivalent sand grain diameter (Nikuradse)
l	=	length
l	=	mixing length (Prandtl)
m	=	hydraulic radius ($m=A/P$)
n	=	resistance coefficient "Manning's n"
p	=	pressure or power (depending on context)
P	=	wetted perimeter
Q	=	volume rate of flow
R	=	conduit radius
R_0	=	radius of eddy
Re	=	Reynolds Number
s	=	peripheral roughness spacing
S_0	=	bed slope of open channel
t	=	time

T	=	number of time points (length of series)
u	=	velocity in x-direction
$\bar{u}$	=	mean velocity
u'	=	fluctuating velocity component
u_*	=	shear velocity
v	=	velocity in y-direction
V	=	velocity vector = $u_i+v_j+w_k$
w	=	velocity in z-direction
y	=	distance from boundary
y_s	=	origin of log law for smooth boundary
y_0	=	origin of log law for rough boundary
Γ_{xx}	=	theoretical spectrum
γ	=	concentration of roughness elements
δ	=	thickness of viscous sub-layer
ϵ	=	eddy viscosity
η	=	y/R
κ	=	universal turbulence constant
λ	=	longitudinal roughness spacing or wavelength
λ_C	=	mean wavelength = $1/\phi_C$
μ	=	dynamic viscosity
ν	=	kinematic viscosity
ρ	=	density
σ	=	standard deviation
σ^2	=	variance
τ	=	shear stress
τ_0	=	shear stress at boundary
τ_s	=	viscous shear stress
τ_r	=	shear stress due to form drag of roughness elements
Φ	=	function of
ϕ	=	frequency
ϕ_C	=	centroidal frequency
χ	=	resistance coefficient (Heerman)

CHAPTER 1

INTRODUCTION

The purpose of this study was to collect physical roughness data from unlined, bored tunnels and from these estimate the expected hydraulic roughnesses of the tunnels sampled with a view to assist hydraulic engineers with good estimates of hydraulic resistance for given surface types in the design process. This involved the development of apparatus for data collection, and establishing the link between the physical roughness and hydraulic resistance of the surfaces encountered.

Tunnel excavation using Tunnel Boring Machines (TBM's), has been shown to be faster and more efficient then by traditional drill-and-blast methods. Bored tunnels have the added advantage of, in many cases, not requiring lining of any sort. Because the technology is relatively new in its application to hard rock, there are few data relating the physical roughness of the bored tunnels to their hydraulic resistance. The aim of this study was to find out what the expected roughness of bored tunnels is likely to be and also to provide a method for calculating hydraulic resistance of such surfaces by comparing them with physical roughness measurements made on other similar surfaces.

A universally accepted measure of roughness is Nikuradse's k, the dimension of equivalent sand grain diameter. It is not clear to many engineers what the relationship is between surface characteristics and k. This study attempts to provide that link.

It is also not clear how to define the diameter of a tunnel (conduit) with a rough wall. Is the measurement taken to peaks of the roughness, the troughs of the roughness, or somewhere in between? Although this is a point of academic interest, it does affect the choice of origin of the velocity distribution. It turns out that the diameter is that of a smooth cylinder of equal volume.

It is found that Nikuradse's k is equal to the mean range heights at the mean wavelength of the roughness and that the diameter should be measured from the mid range of the roughness,

which is the effective "wall" of the pipe from the point of view of the velocity distribution in rough turbulent flow.

This study was timed for a period in which there has been a large amount of tunnelling activity in Southern Africa. Because of this, many tunnels were potentially available for roughness measurement "in the dry" before commissioning. In most of these tunnels provision was made for head loss measurements to be made once the tunnels are commissioned, and from these some sort of correlation between the physical and hydraulic roughnesses was hoped to be obtained. Only one of the tunnels examined so far has been commissioned, and these data are used herein.

This report is divided into three main parts : the executive summary, the body of the report (in which the main findings appear) which comprises four short chapters, and the Appendices, where the theoretical and more detailed aspects of the study appear. There are five appendices. The two core ones are Appendix B, describing physical roughness measurement and interpretation, and Appendix C describing the hydraulic resistance of closed conduits flowing full at equilibrium and at high Reynolds numbers.

The first aspect of the study was a literature survey in which an attempt was made at locating all of the relevant information regarding head losses incurred in fluids flowing in closed conduits. The survey was focused mainly on head losses in bored tunnels and in concrete pipes.

A full description of the roughness data collection, description and analysis then follows in Chapters 2 and 3. The apparatus used for data collection is described, together with a description of its operation. Methods of analysis and physical roughness representation are then presented.

Using these methods of roughness description in conjunction with fluid dynamics theory, links between physical and hydraulic roughness are made, and are tested on physical roughness data from surfaces of known hydraulic roughness. This material appears in Chapter 4. From this a technique is developed for calculating hydraulic roughness, and this

is applied to the tunnel roughness data, for which estimates of hydraulic roughness are then made.

All of the data collected and used in this study have been made available for future research and analysis and accompany the report in the form of ASCII files on diskettes with relevant programs. The data sets are also presented photographically.

CHAPTER 2

PHYSICAL ROUGHNESS MEASUREMENT

The type of roughness under review in this study is that created by a TBM on a rock surface. TBMs produce physical roughness which is not greatly affected by rock type or machine characteristics (such as diameter).

The roughness pattern produced is comprised of features on both micro and macro scales. The most common macro features are steps due either to steering changes made during boring, or to the slight increase in diameter which occurs when worn gauge cutters are replaced. Diameter changes also occur at changes between shotcreted and non-shotcreted sections.

Aside from this, the micro roughness of bored tunnels appears visually to be unaffected by rock type. Waviness or periodicity is usually evident on TBM-bored surfaces, and the "ridges" formed, created by the rotating gauge cutters, usually have wavelengths between 5 and 50 mm and amplitudes less than 10 mm. Superimposed on this ridging is the grain roughness of the rock itself. This varies from coarse to fine, has relatively small amplitude and is essentially random.

The main objective of this study was to investigate the roughness of TBM-bored tunnel walls, and to establish corresponding hydraulic resistance. In the past a number of similar attempts have been made. A commonly used technique of collecting roughness data was by taking plaster casts of typical sections which were then further analysed in a laboratory. Burchell (1983) measured physical roughness of bored tunnels by means of a comb-like profiler which comprised movable steel pins mounted in a wooden spine, through which the pins were free to slide. When pressed firmly against a tunnel wall the pins move to assume the profile of the wall, which were then traced onto paper and later digitised.

2.1 Physical roughness data collection apparatus

In a contract between the Department of Civil Engineering, University of Natal, Durban and

the Water Research Commission (WRC), an apparatus was developed that uses a laser distance measuring device to read physical roughness, which is then converted to digital form and stored in a computer. The laser distance-measuring unit is mounted on a one metre rail inside a protective casing, and is driven along this rail by a stepper motor (taken from a printer, incidentally), controlled from a portable (lap-top) computer. In either 1/2 or 1/4 mm steps along its track, readings of distance to the tunnel wall are taken (the interval is chosen by the operator). Knowing both distance to the wall and position along the track, points may be plotted consecutively to give the profile of the tunnel wall from the information stored in a (portable) computer.

Each digitized data set taken in this way was complemented by a photograph of the wall at that particular chainage. Side lighting was used for the photography to highlight the relief of the wall.

The laser scanner, within its protective casing, was made to stand on a detachable leg and lean against the tunnel wall. It was later decided that just a single run of the scanner at each setup was not sufficient for a full three-dimensional roughness representation, and so the leg was modified to enable three parallel runs to be made, five millimetres apart, at each setup.

The apparatus is shown in Plate 1 (a). In Plate 1(b) the scanner is shown with the protective casing removed. Clearly visible are the rail, the belt to move the laser, and the laser unit itself on the right hand side. Plate 1(c) shows the one author, Pennington, operating the equipment in the Emolweni Tunnel. The photographs were taken by Pegram.

In all but one case the scanning apparatus was taken into each tunnel by rail, on a flatcar connected to a locomotive. It was initially thought that if the flatcar were towed to the upstream end of the tunnel, then the locomotive could exit the tunnel, leaving the scanner operators to push their way out. This proved to be slower and, obviously, much more tiresome than having the locomotive remain with the equipment and tow the flatcar between setups. In the one tunnel where access was by foot only, a small trolley was used to carry the batteries, while all the other equipment was carried either by hand or in backpacks.

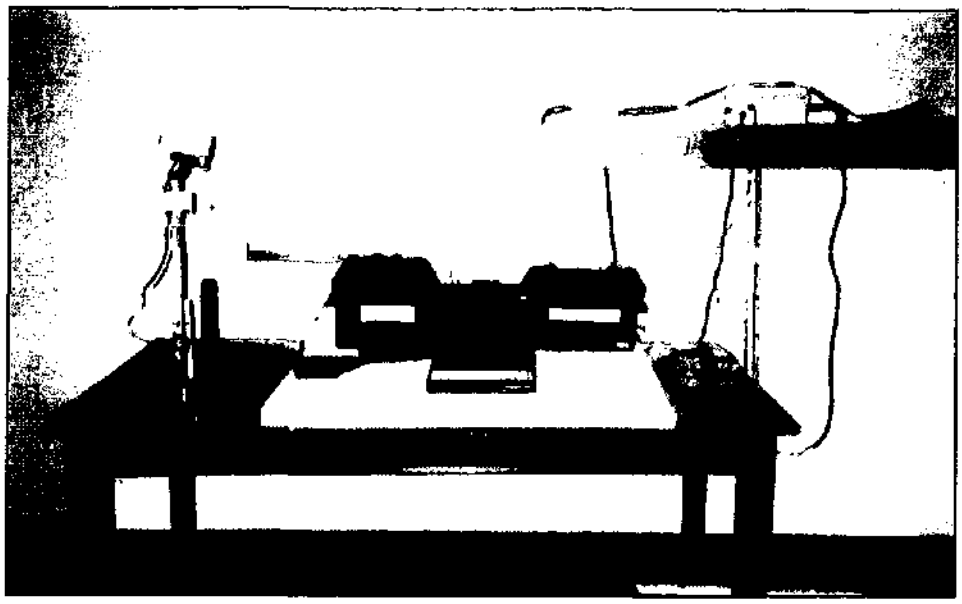

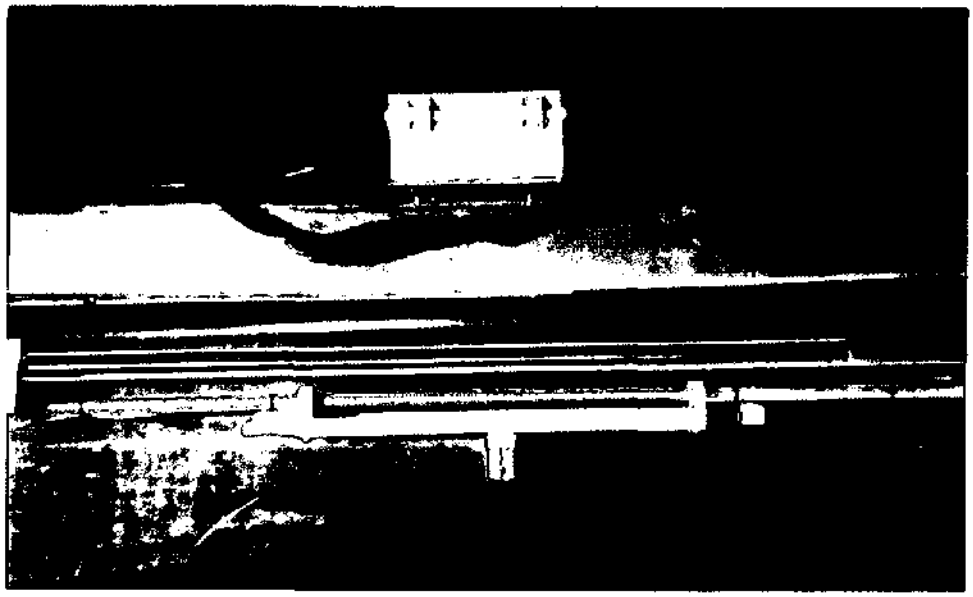

Plate 1 (a) apparatus (b) internal detail (c) operation

Actual measurement presented some difficulties which needed to be overcome by experience. Because the laser scanner depends on a reflection from the wall for its calculation of distance, any areas of dark or non-reflective rock posed a potential problem. This was countered by spraypainting these areas with matt white paint before scanning. A painting guide was specially made to ensure that the paint was applied over the correct area, which minimised wastage.

Problems were experienced when scanning very wet rock. The reflected beam would scatter somewhat off the film of moisture, causing inaccuracy in measurement. This was overcome by drying the wall with paper towel immediately before scanning.

At each setup the profile of the wall was plotted on the computer. This was done to check the data set obtained. Any dark or wet spots showed up as spikes in the plot, and the problem could be rectified before rescanning that section, to ensure that good data sets were always obtained. A feel for which rock would require painting was soon gained, and time could be saved if in these cases the rock were painted before being scanned. It was found that stippled shotcrete would almost always require painting, while granite required very little painting. Sandstone often needed to be painted, and all wet areas in all rock types needed drying.

The typical routine at each setup started with a decision of whether or not the wall needed painting or drying. The necessary surface preparation was carried out and the scanner was set up and started. Immediately after a scan was complete, the data were plotted on the computer screen to check for spikes or irregularities that did not match what was visible on the tunnel wall. If spikes were present, the problem was identified and corrected, before that section was rescanned. Once a good data set was taken the scanner was removed from the wall and the side lighting was switched on for the photograph. All the equipment was then loaded onto the flatcar and covered with plastic sheet to guard against water dripping from the tunnel crown before moving on to the next chainage point 100m away. This took typically about eight minutes when a single scan was made at each point, and when three parallel scans were made the time went up to about fifteen minutes. In this way about five kilometres could be covered in a day for single-run sampling, this distance being almost halved for triple-run sampling.

2.2 Accuracy of the apparatus

Before the apparatus was used for any data collection it was necessary to carefully test it for accuracy and to calibrate it if required. However, an opportunity to sample the Emolweni Tunnel, part of the Inanda-Wiggins Aqueduct, presented itself before this was possible and so roughness data from this tunnel were taken, trusting the accuracy of the equipment. Fortunately, the scanner when tested was found to read within the expected bounds of accuracy, and so the Emolweni Tunnel data were acceptable.

When testing the scanner, surfaces of known roughness, one smooth and the other rough were scanned. The smooth surface used was a strip of perspex, painted with a matt white paint to ensure good reflectivity. This was used to test for scatter of readings over a smooth surface. For the rough surface, a threaded bar was tested. This had a known thread height and pitch which could be compared to what the scanner read.

Scanning of both of these surfaces was carried out at varying distances between scanner and target to establish whether this affected the readings in any way.

This testing served to confirm that the scanner does, in fact, read distance to an accuracy of within the 0.1mm expected. The details of the testing, together with results, may be found in Appendix A.

2.3 Roughness Data Samples from Tunnels

In this study, physical roughness data were collected from four different bored tunnels. Two of these form part of the Lesotho Highlands Water Project, namely, the Ngoajane North and Ngoajane South Drives. The remaining two, the Emolweni and Clermont Tunnels, are part of the Inanda-Wiggins Aqueduct in Kwazulu-Natal, South Africa. Details regarding the sampling from these tunnels are summarised in Table 2.1 below. All of the data collected in this study are presented on computer diskettes which may be found in the sleeve at the back of this document. See Appendix E for details.

Table 2.1 Summary of tunnel roughness samples

Tunnel Name	Predominant Rock Type	diameter (m)	length (km)	no. of samples
Emolweni	granite	3.5	5.5	50
Clermont	sandstone	3.5	5.5	66
Ngoajane South	sandstone	5.0	5.2	37
Ngoajane North	sandstone	5.0	5.2	108

In all of the tunnels, shotcreted sections were encountered and, in addition, in the Emolweni Tunnel a short length of concrete lining was sampled. The data collected may be grouped in terms of rock or surface type, as done in Table 2.2 below.

Table 2.2 Numbers of Samples

surface type	no. samples
granite	27
sandstone	181
shotcrete	48
concrete lining	5

Within these groupings, the surfaces themselves appear to vary quite considerably. Typical plots obtained from the scanner of representative samples of these surface types are shown in figure 2.1 below.

An important characteristic of the shotcrete is that it is very seldom applied in a layer of uniform thickness. This is evident in figure 2.1. These plots have all been detrended using a linear least squares best fit line. The differences in nature of the roughnesses of the various surface types are evident here, so too are the similarities between the finishes obtained by the TBM in different rock types.

2.4 Qualitative and quantitative roughness description

Wall roughness may be described either qualitatively or quantitatively. The qualitative description is useful for communication purposes whereas quantitative description is required for analysis.

Concrete Lining - Emolweni

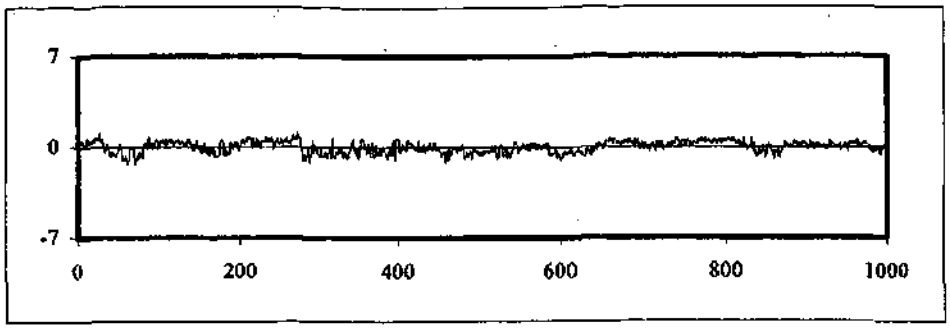

Granite - Emolweni - chainage 3200

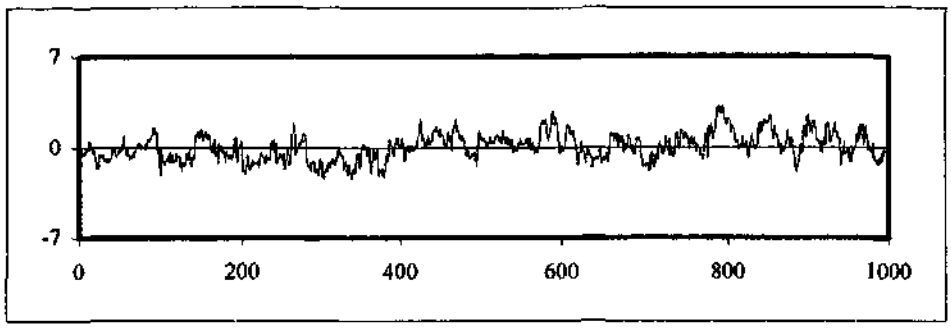

Sandstone - Ngoajane South - chainage 3500

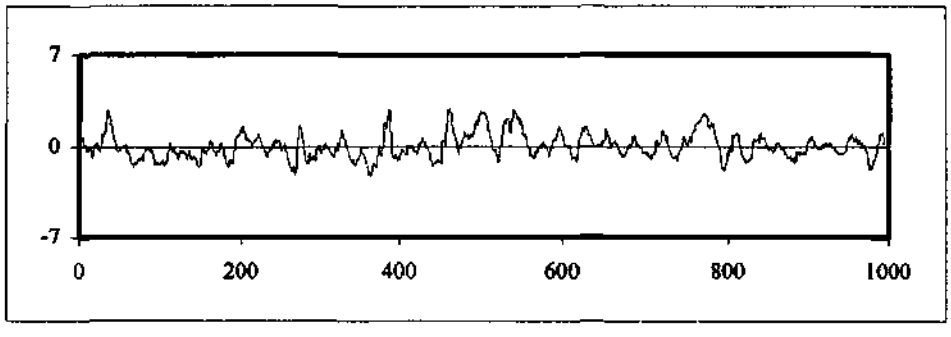

Shotcrete - Emolweni - chainage 1600

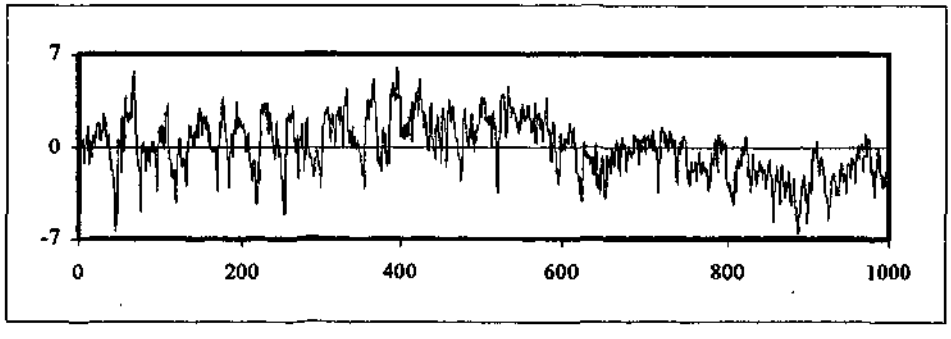

Figure 2.1
Typical wall roughness plots – all measurements in millimetres.

Qualitative Roughness Descriptors

A set of roughness descriptors has been developed in order to describe the visual appearance of various roughness patterns. These are tabulated in Table 2.3 below, and typical photographs relating to these descriptors appear in Plate 2.

Table 2.3 Roughness Descriptors

Descriptor	Definition
Wavy	Obvious repetitive grooved pattern with "wavelength" typically 5-50mm.
Stippled	Very rough surface with no directional trends in roughness character (unlike wavy).
Rutted	Ruts or grooves typically 3-10mm deep over surface in one or more directions.
Uneven	Term to describe non-uniform shotcrete layer thickness, causing slight radius changes.
Irregular	Surface has at least one outstanding feature not described by other descriptors.
Stepped	Steps in wall profile due to steering adjustments made during TBM operation.
Coarse	Surface has coarse grain texture with minimum bump dimension greater than 3mm.
Fine	Converse of coarse. Maximum bump dimension 3mm or less.
Chipped	Non-directional, angular surface without sharp crests.

These descriptors may be used alone, or in conjunction with one or more other one. For example, a surface may be described as "coarse-wavy" or "coarse-rutted-stepped".

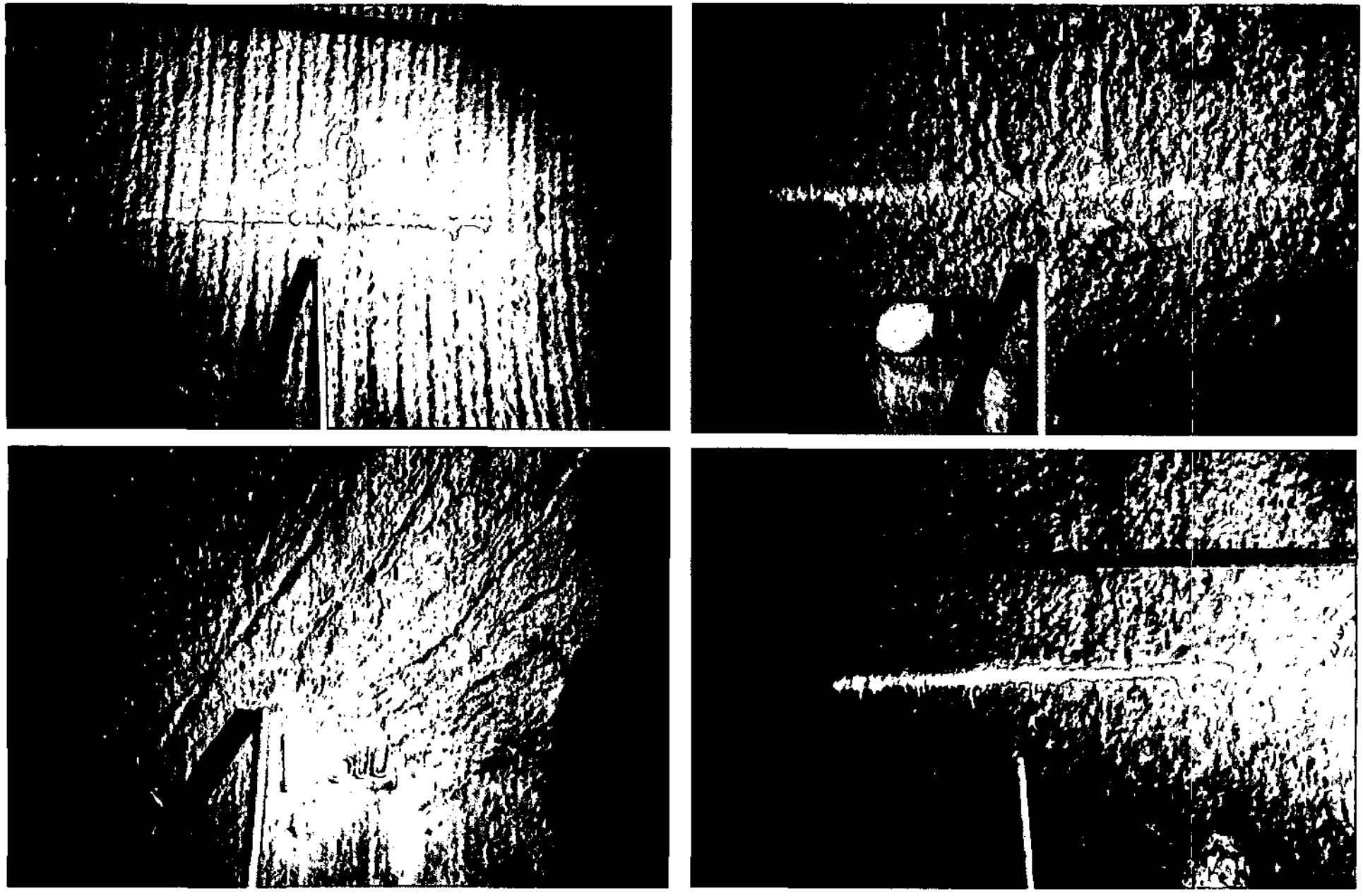

Plate 2 Roughness Types

(from top left, clockwise) wavy, stippled, chipped, rutted

Quantitative Roughness Description

Variance : The variance of a set of surface roughness data is proportional to the square of the bump heights and its square root, the standard deviation, thus gives an indication of average amplitude. In Appendix B1 details of the calculation of variance and its relation to mean roughness height are given.

Power Spectra : In the original proposal to the Water Research Commission concerning this project, Pegram (1993) suggested that the roughness data could be described using time series analysis, in particular, by means of a power spectrum. The reasoning behind this was that the shape of the roughness, ie the way in which the variance is distributed in space, was thought to affect the hydraulic resistance. The power spectrum of a set of physical roughness data shows how the variance of the data is distributed with frequency. From this, dominant frequencies (and hence wavelengths or spacings) occurring in the data may be found.

A brief overview of the time series analysis techniques used in this study is given in Appendix B2. A full treatment of this topic is given, for example, by Jenkins & Watts (1968). Schumway (1988) presented various time series analysis programs, one of which calculated power spectra of input data sets. This was modified for use in this study. A listing of one of the modified versions of the program used is given in Appendix B3.

Mean Range : The power spectrum of the roughness data does provide an effective description of the physical roughness. However, further information is required so that this description may be applied to the correlation of physical roughness and hydraulic resistance. The physical roughness needs to be described in terms of as few representative parameters as is meaningful to enable this correlation to be made.

From the spectrum the dominant frequencies of bumps making up the overall roughness may be found. The heights of the roughness elements associated with each of these frequencies needs description. These heights may successively be calculated from the actual roughness data, x(t), over intervals of length equal to λ, the wavelength corresponding to the particular frequency (ϕ) being considered (where $\lambda = 1/\phi$).

The mean range (between maximum and minimum values) within successive intervals of λ is calculated, and the mean range of the sample determined.

That is, for x(t), $0 \leq t \leq T$ (T=no. points in series)

$$\text{range } r_i \quad = \quad \max[x_i, x_{i+\lambda}] - \min[x_i, x_{i+\lambda}] \qquad \text{for } 1 \leq i \leq T-\lambda$$

Thus the mean range corresponding to frequency ϕ (or wavelength λ), h_λ, is given by

$$h_\lambda = \frac{1}{T-\lambda} \sum_{i=1}^{T-\lambda} r_i \qquad (2.1)$$

In this way the physical roughness data may be represented by a set of dominant or significant wavelengths and their associated mean ranges.

An example of the relationship between h and λ is given in figure 2.2 below.

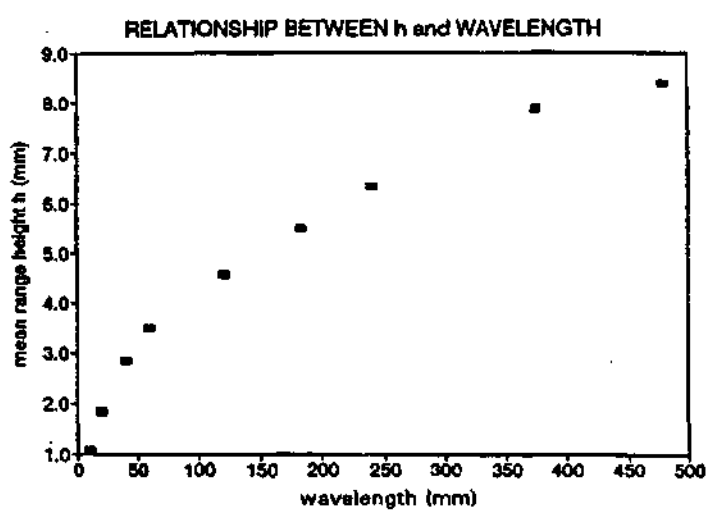

Figure 2.2 Relationship between h and λ for roughness data from chainage 4000, Ngoajane South Drive

Equivalent Sinusoid : Another way of quantitatively describing physical roughness is by finding a sinusoid of "equivalent" characteristics to those displayed by the actual data.

The total area under the spectrum is equal to the variance of the roughness data. This may

either be computed from the spectrum or directly from the data, x(t). Using this, the amplitude of a sinusoid with the same variance may be found.

$$\text{var}[a.\sin(2\pi x/\lambda)] = \sigma^2 = a^2/2$$

where a = amplitude of sinusoid

That is

$$a = \sqrt{2}\sigma \tag{2.2}$$

or

$$h_o = 2a = 2.83\sigma \tag{2.3}$$

which is independent of λ because

$$var[\ \sin(2\pi x/\lambda)\ ] = \frac{1}{\lambda}\int_0^{\lambda} \sin(2\pi x/\lambda)^2\, dx = \frac{1}{2}$$

Thus the variance is independent of the wavelength of sinusoids with the same amplitude, and this measure does not help in deriving an equivalent shape.

By analogy, the height h_o of the sinusoid as given by equation (2.3) will be used to define the effective height of a random surface with variance σ^2.

To find the wavelength of the "equivalent" sinusoid, the centroidal frequency of the power spectrum is calculated. To find this, the centroid (the horizontal co-ordinate of the centroid) is inverted to give the wavelength representative of the entire roughness pattern.

As shown in Appendix B, section B2, the centroidal frequency of the sample spectrum $C_{xx}(\phi)$ is given by

$$\phi_c = \frac{1}{\sigma^2} \sum_{i=1}^{N} \phi_i . C_{XX}(\phi_i) . \Delta\phi$$

where $\Delta\phi$ = 1/2N

This gives the centroidal frequency in cycles per point. From this the centroidal wavelength, λ_C, may be found by

$$\lambda_C = \frac{1}{\phi_C}$$

This wavelength is used to compute the effective range in equation (2.1) in the case where the range is used as a roughness measurement to be related to Nikuradse's k. In that context, the mean range will be called h_λ, dropping the subscript C, but, as is evident from figure 2.2 it is a function of λ in general.

A plot of the physical roughness data from chainage 4000 of Ngoajane South Drive, with its equivalent sinusoid superimposed, is shown in figure 2.3 below. Judged visually the equivalent sinusoid appears to be a reasonable approximation of the roughness.

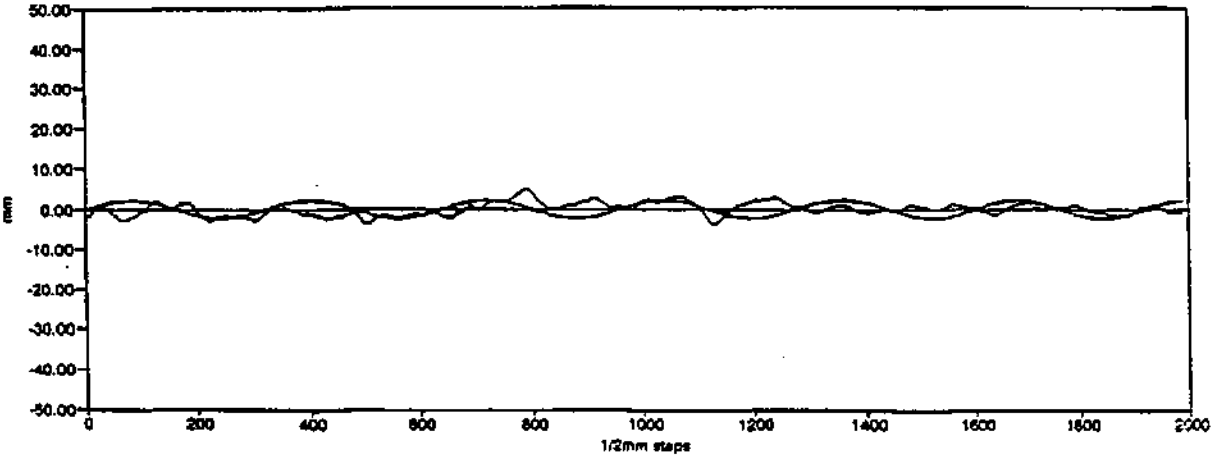

Figure 2.3 Physical roughness and equivalent sinusoid of chainage 4000, Ngoajane South Drive data

Summary : It has been shown how physical roughness data may be represented by the following :

- standard deviation
- power spectrum
- mean range
- equivalent sinusoid

The standard deviation gives a measure of the average deviation from the mean of the roughness data. This is a very broad means of quantifying the roughness as all effects are averaged over the sample. It is susceptible to outliers because it is the root mean square of the data.

The power spectrum displays how the variance is distributed with frequency. On its own, the power spectrum is not very useful for roughness description as too many parameters are required for its description. However, from the power spectrum, the dominant frequencies (those associated with the greatest variance) may be found and, using this, the average spacing (or wavelength) between roughness elements may be calculated.

The mean range technique yields the average heights of roughness elements spaced in these intervals.

The equivalent sinusoid is generated from the centroidal wavelength and a measure of roughness height obtained from the standard deviation, and thus incorporates both spacing and roughness height in the roughness description.

What remains to be done is to relate physical roughness (as outlined in this chapter) to hydraulic roughness. This is done in the following chapter.

CHAPTER 3

HYDRAULIC RESISTANCE OF UNLINED BORED TUNNELS

In terms of friction factor, f, the Colebrook-White equation (equation C3) is generally regarded as the relationship which best fits experimental data, re-stated here for convenience.

$$\frac{1}{\sqrt{f}} = -4\log_{10}\left(\frac{k}{3.71\ d} + \frac{1.26}{Re\sqrt{f}}\right) \qquad (3.1)$$

where f = Friction factor in the Darcy Weisbach equation: $H_f = 4flv^2/2gd$

k = Nikuradse's equivalent sand grain diameter

d = diameter of conduit

Re = Reynolds number = $\rho du/\mu$

For fully-developed, rough turbulent flow (ie high Re), equation (3.1) reduces to

$$\frac{1}{\sqrt{f}} = 4\log_{10}\left(\frac{3.71\ d}{k}\right) \qquad (3.2)$$

The problem regarding the use of equations (3.1) and (3.2) is in the determination of k, the equivalent sand grain diameter. It should be emphasized here that k is a linear dimension *representative* of the entire roughness, and is an hydraulic resistance parameter (as are f and n), as opposed to some physical roughness measurement which can be read directly off the conduit wall.

It is generally regarded that k is some function of the height, spacing, density and nature (shape) of the physical roughness under consideration. A number of attempts have been made to link k to one or more of these, and, in so doing, establish the required link between hydraulic resistance and physical roughness.

In section 3.1 a brief summary of some of the literature which attempts to link physical roughness descriptors (h, σ, etc) to hydraulic resistance descriptors (k, f, n), is given. A

recommendation is given as to estimating k from h.

In section 3.2 some of the estimates of roughness of bored tunnels are presented. These came to hand either from the literature reviewed or via unpublished reports.

In section 3.3 the recommendations made in 3.1 are used to estimate Manning's n values in the tunnels sampled.

3.1 Correlation of physical roughness with hydraulic resistance

3.1.1 ***Heerman (1968)*** presented a complete method for calculating friction factor, f, from the standard deviation of physical roughness data. He defined a roughness parameter χ which is related to the one-dimensional standard deviation, σ, by

$$\chi = 12.9\ \sigma^{1.66} \tag{3.3}$$

where σ = standard deviation in feet.

This roughness parameter, χ, is incorporated in an expression for the mean velocity, $\bar{u}$, derived from the universal log law for the velocity distribution in rough turbulent flow :

$$\frac{\bar{u}}{u_*} = 6.06\ \log_{10}\left(\frac{m}{\chi}\right) \tag{3.4}$$

where m = hydraulic radius in feet

u_* = shear velocity $= (\tau_0/\rho)^{1/2}$

By comparison with the universal log law, $u/u_* = (2\pi)^{1/2}\ln(y/y_0)$ (equation C10), it can be seen that χ is related to y_0, the distance from the boundary that the log law expression for this velocity distribution tends to zero.

Substitution of equations (3.3) into (3.4) for conduits flowing full yields

$$\frac{\bar{u}}{u_*} = \sqrt{\frac{2}{f}} = 6.06 \log_{10}\left(\frac{d}{51.6\sigma^{1.66}}\right)$$

where d and σ are measured in feet.

Adapting the above equation for use with metric units, and rearranging, gives

$$\frac{1}{\sqrt{f}} = 4.285 \log_{10}\left(\frac{d}{\sigma^{1.66}}\right) - 8.798 \qquad (3.5)$$

Heerman suggested that equation (3.5) may be used in estimating f directly from the standard deviation of a physical roughness data set.

In order to justify the σ-χ relationship of equation (3.1), Heerman presents the results of testing done over a number of different surfaces which were sinusoidal in section and of varying amplitude and wavelength, moulded into pipes carrying air. However, the range of Re over which these tests were performed was limited. The maximum value for Re used in any test was slightly more than $3x10^4$, which arouses the suspicion that the flow may still have been in the transition zone between laminar and fully turbulent, rough flow. Nevertheless, this data source was one of the few where hydraulic resistance was linked experimentally with wall roughness shape and was thus invaluable in selecting an appropriate k-h relation.

An important conclusion made by Heerman is that the standard deviation of a rough surface is, on its own, sufficient for complete description of the roughness of the surface and that a separate spacing parameter *need not* be included. He also concludes that the σ-χ relationship of equation (3.1) also holds for surfaces of random roughness.

For example, the data set obtained at chainage 4000 in Ngoajane South Drive is considered. The one-dimensional standard deviation was σ=1.557mm. Equation (3.5) above yields a value of the friction factor of f=0.0056 for this. This corresponds to a Manning's n value of n=0.0175 which will be shown to be too high.

3.1.2 ***Morris (1955 & 1959)*** presented a rational method of calculating friction factor, f, using physical roughness dimensions for each of the five flow types he identified.

The methods presented by Morris were found to be inapplicable to this study (see Appendix D) and therefore further detail is not gone into here. However, certain concepts suggested by Morris are worth a mention. If a surface has such variable roughness that flow of more than one type is produced, then Morris suggests that friction factors for each type may be added together to give the apparent friction factor for the surface as a whole. This only applies under certain conditions, when the wake effects of the different roughnesses do not interfere with each other. For example, this approach is suitable in calculating the effect of isolated roughness elements such as rock bolts in a bored tunnel.

3.1.3 ***LeCocq and Marin (c.1976)*** investigated the relationship between physical roughness and hydraulic resistance in the unlined Echaillon Tunnel (France). They identified the roughness height, h, and concentration, γ, as the two parameters which most affect the hydraulic resistance of tunnel walls. The concentration is defined by

$$\gamma = N\frac{A_p}{A'}$$

where N = number of roughness elements on the plan area A' of the surface

A_p = projected area of average roughness normal to the flow.

The roughness height, h, is related to equivalent sand grain diameter, k, through the concentration, γ, as shown in figure 3.1 below, whose derivation is obscure.

The analysis of 21 roughness data sets gave the value of γ to be slightly higher than $\gamma=0.05$.

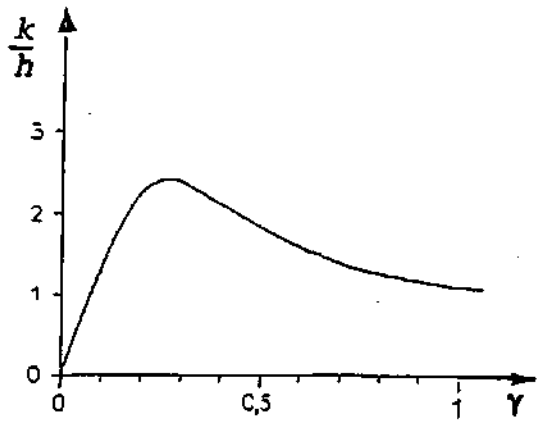

Figure 3.1 Effect of concentration (LeCocq & Marin c.1976)

From figure 3.1, this value of $\gamma=0.05$ implies that

$$\frac{k}{h} = 1$$

That is, equivalent sand grain diameter is taken to be equal to physical roughness height. It is, however, in calculating this height, h, where difficulties arise.

LeCocq and Marin estimated h from plaster casts taken from typical sections of the wall surface within the Echaillon Tunnel. It is not clear exactly how these estimates were made, but from them, estimates of Manning's n were made. These estimates varied from $n=0.0147$ to $n=0.0154$, and an average value of $n=0.0150$ was found to be representative. Further discussion of this result will be deferred until the end of section 3.3.

3.1.4 ***This study :*** In Appendix C it is shown how the universal log law is invalid near the centre of a closed conduit flowing full. There equation (C12) is derived, taking the linear variation of shear stress over a section into account, which is valid throughout the main body

of the flow. Integration of this, using the model of cylindrical eddies at the bed (as proposed by Rooseboom, personal communication, 1995[1]), in which k=2h (see Appendix C), yields an equation for friction factor for fully developed, rough turbulent flow. This equation (C30) is repeated here for ease of reference.

$$\frac{1}{\sqrt{f}} = 4.08 \log_{10}\left(\frac{d}{k}\right) + 1.82 \qquad (3.6)$$

This is of the same general form as the Colebrook-White equation (3.2), which may be rewritten as

$$\frac{1}{\sqrt{f}} = 4 \log_{10}\left(\frac{d}{k}\right) + 2.28 \qquad (3.7)$$

These two equations (3.6 and 3.7) differ only in the constant terms used. These constants may be adjusted so that the equations fit the experimental data found in the literature.

Equation (3.7) was developed to fit experimental data and therefore does so. However, equation (3.6) was derived from an analytical analysis of fully-developed turbulent pipe flow over rough boundaries. It is based on relatively few assumptions and empirical relationships and the fact that this yielded an equation of the correct form to fit experimental data is very encouraging. A shift is, however, still required to ensure that the derived equation actually fits the data. The necessity of this shift could indicate that the boundary model proposed (of cylindrical eddies formed behind roughness elements) is not entirely correct but is a reasonable approximation.

If it is accepted that equation (3.7) does accurately fit experimental data, then the question arises as to what value of k should be used to yield the correct f-value. Two suggestions have been made, (one by LeCocq and Marin (1976+) summarised in section 3.1.3 and the other in the theoretical development in Appendix C of this study) namely, k=h and k=2h; where h has yet to be properly defined.

---

[1] Professor A Rooseboom, one of the members of the steering committee, privately drew attention to Water Research Commission report WRC 236/1/93, and indicated that the nature of energy transfer at the wall of a conduit was outlined there.

By small modification of the constants in equation (3.7), using either k=h or k=2h will yield results consistent with those found by experimentation.

This then raises the question of how h should be measured. In Chapter 2 two methods of finding h for a rough surface were suggested. These were (a) from the mean range using h_λ as defined in equation (2.1) and (b) from the standard deviation using h_σ as defined in equation (2.3). As an example, both of these methods were applied to the physical roughness data set taken at chainage 4000 of Ngoajane South Drive (Lesotho) with the following results:

using mean range	h_λ = 5.53mm.
using standard deviation	h_σ = 4.40mm

To decide which value of k (Heerman's, h_λ, $2h_\lambda$, h_σ or $2h_\sigma$) should be used in equation (3.7), other experimental data must be used. Such data had to include physical roughness data and the corresponding hydraulic resistance. This was obtained from two different sources, namely, roughness data from spun concrete pipes and sinusoidal roughness artificially created and tested by Heerman. The details of these are given in Appendix D. Also in Appendix D, the method of calculation of f from σ is tested against the experimental data. Here the conclusions from that investigation are used.

In short, two basic methods for the calculation of f from physical boundary roughness measurements have been suggested. The first was that of Heerman, using the standard deviation. The second was by means of the Colebrook-White equation. Using the latter, there were four proposals as to how k and h are related. It was found that by manipulating the constant term in the Colebrook-White equation, any relationship between k and h could be supported. However, keeping equation (3.7) as is, it was found that using $k=h_\sigma$ or h_λ gives better agreement with the experimental data than $k=2h_\sigma$ or $2h_\lambda$.

As far as the value of h to be used goes, there is very little difference between h_λ calculated from the mean range and h_σ from the standard deviation. However, the mean range is preferred to the standard deviation. This is because the standard deviation is particularly

susceptible to the influence of outliers or trends in the data. The mean range estimation is a far more robust estimator in this respect.

It is important that the interval chosen (ie λ) is representative of the roughness. The suggested value to be used is that taken by finding the centroid of the sample spectrum of the roughness data. The effect of λ on the resultant mean range height, h_λ, was shown in figure 2.2 from which it is clear that h is not independent of wavelength.

Summary

The recommended procedure for the estimation of f from a set of physical roughness data is as follows :

- Calculate the sample spectrum of the roughness data set. Find the centroid of this to yield the mean wavelength λ_c representative of the roughness (use the BASIC program called SPEC.BAS on disk 1 at the back of this document).

- Calculate the mean range height h_λ by averaging the differences between maxima and minima within intervals of the representative wavelength (use a spreadsheet).

- Use the Colebrook-White equation with $k=h_\lambda$ to estimate friction factor.

As an alternative to using the mean range height in the Colebrook-White equation, the height calculated from the standard deviation may be used so $k=h=2.83\sigma$, although care should be exercised when dealing with data which have outliers or trends.

3.2 Values of Manning's n from literature and unpublished reports

Manning's n is frequently used as an hydraulic resistance parameter in tunnels because it is practically independent of diameter and effectively depends only on the surface roughness. A variety of surface finishes is obtainable for TBM-bored tunnels. In poor quality rock, tunnels are generally lined with either precast concrete segments (segmentally-lined tunnels)

or with placed in-situ concrete. In very good quality rock, lining may not be necessary at all, except for the occasional zone which may require shotcreting. All of these surface finishes have different hydraulic roughness characteristics. This study is confined entirely to unlined TBM-bored tunnels, but includes shotcreted sections.

Much of the literature pertaining to roughness of unlined rock tunnels deals with tunnels constructed using drill-and-blast methods. The roughnesses of such tunnels are very much larger than those for TBM-bored tunnels, and shall not be considered further here.

Total head loss was made up of contributions by the inlet, unlined sections, shotcreted sections, concrete-lined sections, steel linings, bends and transitions, and the estimates of n-values relating to each of these were made ensuring that the total head loss would sum to that actually measured. These estimates over the sections sampled in this study are presented in Table 3.1.

Table 3.1 Preliminary Estimates of n for Inanda-Wiggins Aqueduct (Metcalf, 1995)[2]

Surface type	Clermont	Emolweni
shotcrete (assumed)	0.016	0.016
concrete lining (assumed)	0.012	0.012
unlined (derived)	0.0141	0.0141

In a paper by Stutsman (1988) concerning the Kerckhoff 2 Hydroelectric Project in California, the estimated Manning's n value for unlined bored rock was n=0.015, equivalent to that of very rough concrete. This value was arrived at through consultation with companies and individuals who had been involved in similar tunnelling contracts. During the boring of the tunnel, Stutsman refers to three different types of TBM cutters which were used, namely button head cutters, standard "60-90" cutters and constant section cutters. Of these, the constant section and the 60-90 cutters yielded relatively smooth surfaces, while the button

[2] Metcalf (personal communication 1995) presented preliminary total head loss measurements made together with estimates of roughness coefficients over various sections in the Inanda-Wiggins aqueduct (incorporating the Clermont and Emolweni Tunnels).

head cutters created a very much rougher surface. Plaster casts of each of these two roughness types were taken. By measuring the "deviation between the highs and lows" of each surface and, knowing velocity, diameter and viscosity, estimates for Darcy-Weisbach f were made (using the Moody diagram). These values for f were then converted to Manning's n values. It is not clear from the paper how the deviations between highs and lows were measured, nor how these were converted to equivalent k values for use in the Moody diagram. It would appear that Stutsman equated the deviation with equivalent grain diameter, k.

Stutsman's estimated n-values for the two roughness types varied between n=0.0153 and n=0.0172 for the smoother and rougher surfaces respectively, an appreciable difference. Since approximately 30 per cent of the tunnel had been bored using the button head cutters, the expected value for n as reported by Stutsman was calculated by proportion to be n=0.0159 for the tunnel as a whole.

Head loss measurement equipment was installed in the tunnel and so friction factor estimates could be confirmed by measurement after commissioning. The representative Manning's n measured in this way was reported by Stutsman to be n=0.01542 for the tunnel. This compares favourably with the value predicted before commissioning.

A report by the Highlands Delivery Tunnel Consultants, HDTC (1988), included a thorough review of available literature on friction losses in tunnels. The report typically presents three values for Manning's n for each surface, n_{min}, n_{typ} and n_{max}, the subscripts of which are self-explanatory. In Table 3.2 below the values for Manning's n recommended from the findings of that report are given for both shotcreted and bored rock surfaces.

Table 3.2 Recommended n-values (HDTC, 1988)

Manning's n	Shotcrete	Bored Rock
n_{min}	0.014	0.015
n_{typ}	0.016	0.016
n_{max}	0.017	*

* Indeterminate - depends on too many ageing factors.

The report also draws attention to the effect ageing can have on hydraulic performance. Certain tunnels are prone to algae build up, while others may experience corrosion, both of which may affect hydraulic roughness.

LeCocq and Marin (c.1976) measured physical roughness of bored tunnel walls in the Echaillon Tunnel (France) by means of a mechanical instrument which plotted, on paper, the wall profile as it ran along the wall in the direction of flow. Each run was one metre in length, and the precision of the instrument was of the order of 0.1mm. A total of 21 samples were taken, approximately fifty meters apart, seventeen of which were of gneiss and the remaining four of sandstone. Three plaster casts were also taken.

This led to a value of n=0.016 for the predicted head loss coefficient. Using this, the total head loss in the Echaillon Tunnel was predicted to be 6.30 metres, but 11.94 metres was actually measured.

This would immediately suggest that the calculated value of n=0.016 is incorrect, and that the method should be reviewed. However, within the Echaillon Tunnel there were twenty changes in section between surfaced and non-surfaced zones. At each of these there is a change in diameter which contributes to the head loss. LeCocq and Marin propose that the difference between predicted and measured head loss in the tunnel is due to the extra head lost at these diameter changes, and that n=0.016 is, in fact, representative of the micro surface roughness of the tunnel wall itself.

The above findings and recommendations for the hydraulic resistance of bored rock are summarised in point form below.

Stutsman :	initial (use n for rough concrete)	n=0.0150
	estimate from roughness measurement	n=0.0159
	calculated from measured head loss	n=0.0154

HDTC : $n_{min}=0.015$

$n_{typ}=0.016$

LeCocq & Marin : estimate from roughness measurement $n=0.016$

3.3 Values of n for tunnels sampled

For every set of physical roughness data obtained from the tunnels, the values for Manning's n were calculated using each of the methods described in Appendix D. These methods are

A Heerman's method (see section 3.1.1)

B The Colebrook-White equation, using $k=h_\sigma$

C The Colebrook-White equation, using $k=2h_\sigma$

D The Colebrook-White equation, using $k=h_\lambda$

E The Colebrook-White equation, using $k=2h_\lambda$

where h_σ = standard deviation height

h_λ = mean range height

The results from this are summarised in Figure 3.2.

In this figure the maximum and minimum values for each method are shown by the ends of the lines corresponding to each method. The upper and lower tick marks on each of these represent one standard deviation either side of the mean value calculated, while the horizontal marker on each line represents the median value, which, due to skewness does not coincide with the mean.

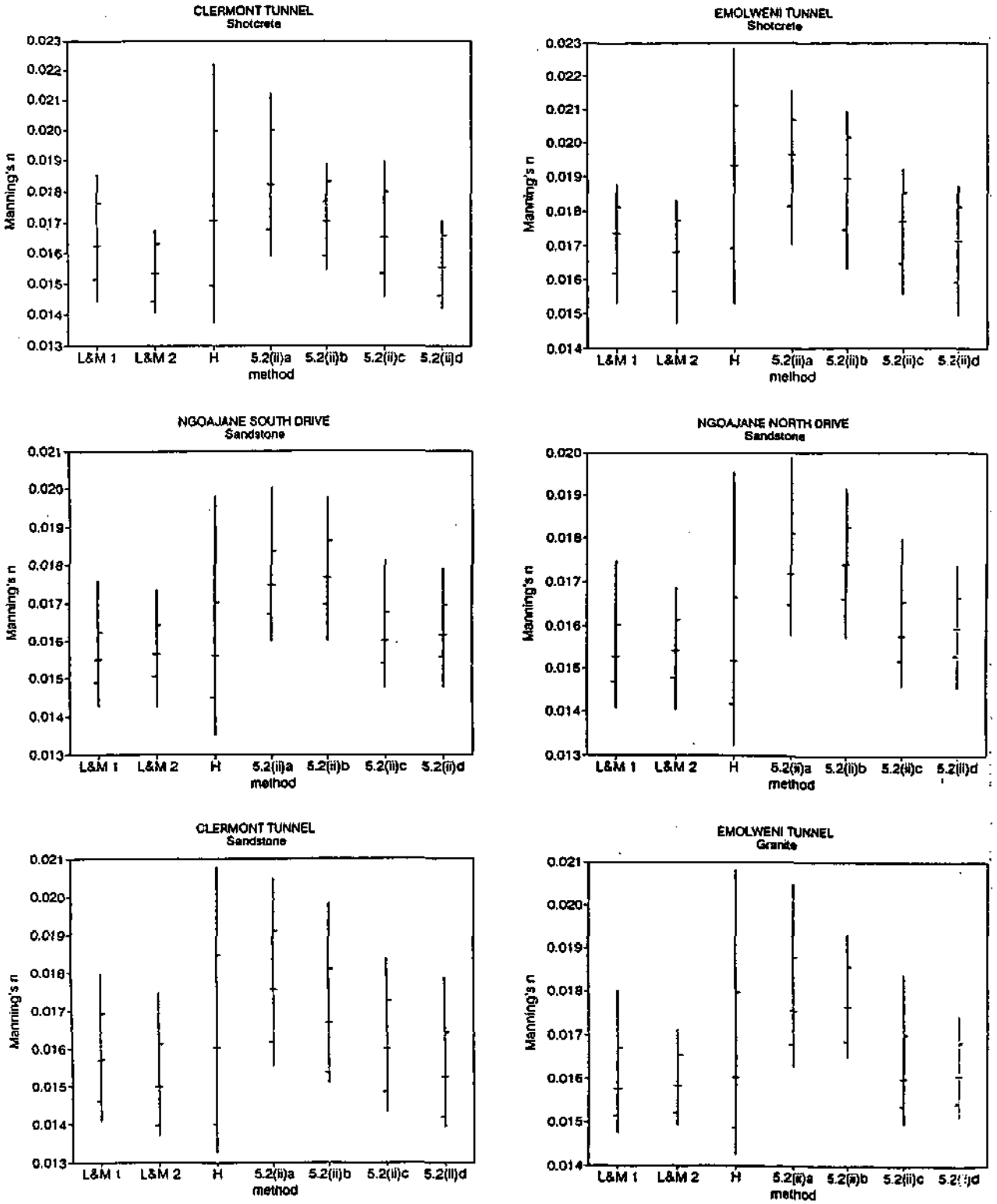

Figure 3.2 Values for *n* estimated by various methods

From this figure (figure 3.2) and from the least squares fit to Heerman's data summarised in Table D4 of Appendix D, it may be seen that methods B and D yield the best results. The following emerge as the suggested values for n for the various surfaces as estimated by methods B and D :

Table 3.3 Estimates of n-values for tunnels

method	concrete (placed)	sandstone (bored)	granite (bored)	shotcrete (placed)
B	0.0124±0.0008	0.0155±0.0010	0.0157±0.0007	0.0169±0.0012
D	0.0119±0.0009	0.0154±0.0010	0.0157±0.0008	0.0161±0.0011

Comparing these figures with those presented in section 3.2 two points are apparent.

The first point is that the estimates of the mean of the resistance of the various rock types are quite close to each other, as shown below:

this study	n = 0.0156
Stutsman	n = 0.0154
HDTC	n = 0.016
LeCocq and Marin	n = 0.016

This suggests that the method of estimating Manning's n in tunnels recommended in this study seems to accord with the wisdom of other professionals, which is comforting. The figures calculated using method D are preferred because they were nearly as good (sum of squares within 0.5%, see Table D4) as B at fitting Heerman's data and make use of the mean range, a more robust roughness height estimate than the standard deviation. This is because h_σ the standard deviation is computed as the square root of the sum of the squares of the variation of the surface around a mean line which is more sensitive to occasional outliers than the mean range h_λ.

The second point that arises from these figures is that the variation in measuring the roughness in each of figures 3.2 is smaller for method D (h_λ) than method B (h_σ).

CHAPTER 4

CONCLUSIONS AND RECOMMENDATIONS

4.1 Conclusions

There are four main conclusions that come from this study: that the method of roughness measurement in the field was successful, that the description of physical roughness is appropriate as h_λ, that a direct link has been made between h_λ and the Nikuradse k and that an improved velocity distribution has been derived.

Roughness measurement

The apparatus developed for the collection of physical roughness data in this study was shown to provide measurements of acceptable accuracy. The apparatus was also used successfully inside tunnels, provided that the correct surface preparation was carried out prior to use. This involved either drying or painting, or both, to ensure adequate reflectivity of the rock surface for the functioning of the laser unit.

Describing physical roughness

A number of different techniques for describing surface roughness were presented. These were all used in establishing links between physical and hydraulic roughness.

Contrary to the suggestion made by Morris (1955), the spacing of boundary roughness elements is not always of primary importance. In fact, at high Reynolds numbers, the resistance to flow offered by the boundary becomes completely independent of this roughness spacing.

The two statistics used in the roughness height estimation, namely the mean range and the standard deviation, yielded comparable results. It was found that for the surfaces tested, neither technique afforded any greater accuracy. However, because the variance is a quadratic function it is more susceptible to outliers in the data than the linear mean range.

For this reason, the mean range estimate of h is preferred to that of the variance, in spite of it being computationally more expensive.

Linking h and k

In Chapter 3 it was also shown that methods B ($k=h_\sigma=2.83\sigma$) and D ($k=h_\lambda$) yielded comparable results of reasonably good accuracy. However, methods C and E, using double the k-values of B and D respectively, were found to overestimate expected values by up to 28 per cent in concrete pipes, and were found to yield consistently higher values for n or f when used on the sinusoidal and bored tunnel roughness data. This would tend to indicate that the assumption that $k=2h$ is not correct, and that using $k=h_\lambda$ in the Colebrook-White equation is the best estimator for hydraulic resistance.

The results obtained using methods B and D on the tunnel roughness data of unsurfaced sections agree with those obtained by estimate from total head loss measurement in the Inanda-Wiggins Aqueduct. However, similar agreement is not obtained for the data from shotcreted sections. From the evidence presented in this document it may be concluded that shotcrete is, in fact, rougher than bored rock.

Hydraulics of conduits

It has been shown that the "universal" log law is only applicable near the boundary in turbulent pipe flow (see Appendix C). This is because it is based on the assumption that the shear stress is constant over the entire section. When the linear variation of shear stress over a pipe is taken into account, the full or true velocity distribution may be derived, yielding equation (C18) given by

$$\frac{u}{u_*} = \frac{1}{\kappa}\left[2z + \ln\left|\frac{z-1}{z+1}\right| + \ln\left(\frac{Ru_*}{\nu}\right) - 0.614\right] + 5.3 \qquad \text{(C18)}$$

where

and u=velocity, u_*=shear velocity, R=pipe radius, y=distance from pipe wall, k is the von Karman constant $\simeq 0.4$.

$$z = \sqrt{1 - \frac{y}{R}}$$

This equation was shown to accurately fit experimental data over the main body of the flow. On the other hand, the so-called "universal" log law (to which equation C18 reduces in the vicinity of the wall) fails near the centre of the pipe. For comparison, equation (C10) is repeated here:

$$u = \sqrt{2\pi}\, u_* \ln(\frac{y}{y_0}) \qquad \text{(C10)}$$

Combining the true velocity distribution with power balance relationships, the equations for flow over smooth and rough boundaries were derived. These theoretically-derived equations closely matched the phenomenologically-derived relations which have been confirmed experimentally. This indicated that the boundary geometry used in the derivation of the theoretical equations was a good model of reality.

4.2 Recommended values for Manning's n

Estimating the hydraulic roughness of bored tunnels, using method D (*substituting* $k=h_A$ *in* the Colebrook-White equation) the following values for Manning's n for the various surface types encountered are suggested :

Surface	Mean	Standard Deviation
concrete lining	n=0.0119	0.0009
sandstone	n=0.0154	0.0010
granite	n=0.0157	0.0008
shotcrete	n=0,0161	0.0011

It must be emphasized here that these values pertain specifically to the roughness of the surfaces, and do not include additional roughness affects due to steps in the wall profile, holes, bends and transitions.

4.3 Future Research

Suggestions for future research include :

- Extension of the velocity distribution to the viscous sub-layer, to give an equation applicable over the entire cross-section.
- Investigate the effect that rock characteristics such as boreability and unconfined compressive strength have on the hydraulic resistance of tunnels.
- Quantify the effects of section changes (shotcrete/unlined) on hydraulic resistance.
- Tunnel inverts - what effect is there due to the non-circular shape of the invert?
- Continuing collection of tunnel roughness and hydraulic resistance data, and refinement of the $k \sim h_\lambda$ relationship.

APPENDIX A

TESTING OF APPARATUS

Before the apparatus was first used for any data collection it was desirable to carefully test it for accuracy and calibrate it if necessary.

As mentioned in Chapter 3, testing of the scanner comprised scanning two different surface types, one smooth and the other rough.

A1 : Testing of Scanner over Smooth Surface

A strip of perspex was selected as the smooth surface for this testing. This was painted by spraycan with matt white paint to ensure good reflectivity of the laser for distance measurement. The distance between scanner and perspex was varied for various runs of the scanner. Four sets of data were taken for each new distance. The complete set of results is presented in Table A1 below. The average distance calculated for each data set is taken to be the distance, d, separating the scanner and the perspex. The variability of the surface is represented by σ, the standard deviation of each data set.

Each time the distance, d, was changed, it was possible that the section of perspex being scanned was also changed. This explains the slight variation in σ for each new position. However, for each position the values of σ are all close together, indicating that the exact same strip of perspex was scanned with little error between readings.

The mean value of σ obtained from all of the testing summarised above was σ=0.135mm. For perfectly smooth perspex and completely accurate measurement this value should be zero. Thus the value of σ=0.135mm represents the sum of the scanner error and the deviation of the painted perspex from perfectly smooth. If the physical deviation from perfectly smooth of the painted perspex is 35 microns or greater, which would appear to be reasonable, then the accuracy of the scanner may be taken to be 0.1mm over smooth surfaces.

Table A1 Perspex Test Results

d (mm)	σ (mm)
29.16	0.131
28.66	0.131
28.54	0.132
28.46	0.131
37.58	0.137
37.44	0.136
37.32	0.137
37.25	0.134
41.46	0.126
41.41	0.124
41.38	0.129
41.35	0.130
53.60	0.141
53.59	0.138
54.66	0.148
53.81	0.144
67.46	0.134
67.40	0.139
68.01	0.138
67.55	0.134

A2 : Scanner testing on threaded bar

In early test runs of the scanner it was found that irregularities occurred at abrupt changes of depth of the target. This can be attributed to diffraction of the laser beam at such discontinuities. For this reason, the threaded bar chosen to check the accuracy of the scanner had a triangular (as opposed to square) thread of height 2.60mm. This was found by averaging the heights measured by Vernier calliper along the bar. The bar had the following dimensions:

outside diameter (o.d.)	=	38.1 mm
root diameter (r.d.)	=	32.9 mm
threads per inch (tpi)	=	6

The actual thread height, h, is given by

$$h = \frac{o.d. - r.d.}{2} = 2.6mm$$

The bar and scanner were set up together on a milling machine so that the distance between the two could be adjusted by set amounts while remaining parallel. This, of course, assumes that they were parallel at the start which is unlikely to be the case, but is unimportant here since the data are detrended before being further analysed.

Two different techniques in the analysis of the data taken from the threaded bar were adopted. As a first attempt, the standard deviations of the data sets were calculated. Standard deviation is a measure of variation from the mean value and is therefore linked to the thread height. The second technique applied to the analysis of the threaded bar roughness data was one in which the mean absolute distance between maximum and minimum over an interval of physical roughness data is found. This "mean range" should correspond exactly to the thread height. Both of these estimates are discussed and presented in Chapter 3.

Matt white paint was applied to ensure adequate reflectivity of the laser beam from the bar,

thereby enabling the most accurate readings capable of the apparatus to be taken.

A total of 20 test runs of the scanner over the threaded bar were made, at distances varying from 10 to 70 mm between scanner and bar. The complete set of results obtained is given in Table A2 below. As in section A1, the d given is the mean value of all roughness measurements over the bar, and is indicative of the distance between bar and scanner.

Table A2 Threaded bar test results

Number	d (mm)	h_a (mm)	h_r (mm)
1	10.42	2.60	2.59
2	13.53	2.52	2.58
3	17.63	2.56	2.64
4	21.73	2.53	2.66
5	25.70	2.58	2.68
6	34.03	2.63	2.71
7	42.35	2.56	2.62
8	50.47	2.53	2.60
9	58.65	2.49	2.59
10	69.77	2.55	2.59
11	20.68	2.55	2.64
12	35.15	2.57	2.70
13	41.25	2.54	2.59
14	47.14	2.58	2.63
15	51.73	2.58	2.67
16	56.26	2.51	2.59
17	59.92	2.62	2.68
18	67.41	2.56	2.66
19	72.16	2.52	2.64
20	72.19	2.48	2.60

Using the variance method of finding thread height, the average value obtained was h_σ=2.55mm, which is very close to that obtained using the mean range where h_λ=2.63mm. Both of these are well within 0.1mm accuracy of the actual height of h=2.60mm. Also evident from the data sets is that the distance between scanner and bar, d, does not noticeably affect the values obtained for thread height.

To conclude, these tests performed on the threaded bar were successful in that they confirmed that the scanner does read distances accurate to, at least, 0.1mm. This complements the testing done on smooth perspex, which showed that the variation in measuring a smooth surface is of the order of 0.1mm. The scanner may now be used with confidence in measuring roughness in tunnels.

APPENDIX B

QUANTIFYING PHYSICAL ROUGHNESS

In this Appendix the methods of physical roughness description are clarified and elaborated upon. A brief overview of the time series analysis used in this study is given, together with a listing of a program to calculate the sample spectra and hence mean wavelength of input physical roughness data. This program may also be found on one of the diskettes at the back of this document.

B1 Variance

The first very basic means of quantitatively describing surface roughness is by the variance of the roughness data. The variance is proportional to the square of the bump heights and therefore its square root, the standard deviation gives an indication of average amplitude. It is important that the data be detrended before the variance is calculated, otherwise an inflated value will result. This is done linearly using least squares. An exaggerated value for the variance also occurs when the data are taken from an uneven surface.

Variance may be one or two dimensional. Heerman (1968) described roughness in terms of a two-dimensional mean and variance. Consider a cubic roughness element placed on a square surface as shown in figure B1 below. The cube has side length = e, and the square surface side length = a.

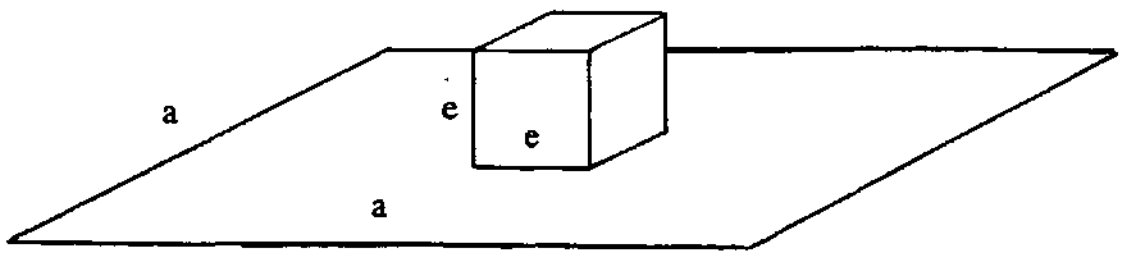

Figure B1 Cubic roughness element on square surface

The mean height of the irregularities from the surface is given by

$$\bar{z} = \frac{1}{A}\int_A z.dA = e.\frac{e^2}{a^2} = \frac{e^3}{a^2}$$

The variance of the surface is given by

$$var(z) = \sigma^2 = \frac{1}{A}\int_A (z - \bar{z})^2\, dA = \frac{1}{A}\int_A z^2\, dA - \bar{z}^2$$

which immediately gives

$$\sigma^2 = \frac{e^4}{a^2} - \frac{e^6}{a^4}$$

This method for finding the variance in two dimensions may be extended to any shape of roughness element placed on any shape of surface. If the variation of the surface is a function of one dimension as tends to be the case in a tunnel bored by a machine, then the above derivation of the variance in two dimensions naturally specializes to its more familiar one-dimensional form.

Variance may also be considered in either a local or global (total) sense. Heerman (1968) found that local variance had a higher correlation with the resistance parameter he used than the total variance. He estimated local variance by evaluating

$$\sigma_z^2 = (1-\rho^2)\sigma^2$$

where	σ_z^2	=	local variance
	σ^2	=	total variance
	ρ	=	lag 1 autocorrelation coefficient of z in the longitudinal direction (sampling at discrete intervals).

Evidently, this definition depends on the sampling interval and so is not universal.

In this document the one-dimensional variance taken from the physical roughness data is used. Because the sampling interval of the tunnel roughness is small compared to the mean wavelength of the data, the values for variance are close to the variance of the continuous surface - what Heerman would call the global variance.

B2 The Spectrum

A brief overview of the time series analysis techniques used in this study is now given. For greater detail and explanation, see, for example, Jenkins & Watts (1968).

Jenkins & Watts (1968) define a time series as a random or non-deterministic function x (ie behaviour cannot be predicted exactly) of an independent variable, t, which, in most contexts, represents time. Different sections of a time series do not necessarily resemble each other in appearance, but when their average statistical properties are compared, they are similar. Because of this it is necessary to describe time series in terms of random variables and their associated probability distributions. The behaviour of a time series may be described by a set of random variables $\{X(t)\}$ where t can have any value from $-\infty$ to $+\infty$. A *stochastic process* may be defined as the ordered set of random variables $\{X(t)\}$ and its associated probability distribution. Therefore an observed series x(t) may be regarded as doubly infinite, in that an infinite set of values is possible at each of an infinite number of time points.

There are two broad categories of time series, namely stationary and non-stationary series. Statistical properties of a stationary series are constant with time, as opposed to the changing properties of a non-stationary time series. Physical roughness data from bored tunnels constitute a non-stationary time series, with the independent variable, t, representing distance in the direction of measurement from some arbitrary datum. The non-stationarity of the physical roughness data under consideration is mainly on a macro scale, whereas on a micro scale (which is specifically being considered here) the data are usually approximately stationary.

Suppose a deterministic time series x(t) is described by the cosine function

$$x(t) = a\cos(2\pi\phi_0 t + \psi)$$

where			
	a	=	amplitude
	ϕ_0	=	frequency
	t	=	time
	ψ	=	phase shift (constant)

Then, for frequency ϕ_0, the variance is given by

$$\sigma^2 = \frac{a^2}{2}$$

In general, if x_t consists of a mixture of several cosine waves with frequencies ϕ_i and amplitudes a_i, then the variance is given by

$$\sigma^2 = \sum_i \frac{1}{2} a_i^2$$

It can be shown that if x_t is a stationary time series, the variance of the corresponding stochastic process can be decomposed into contributions at a continuous range of frequencies according to

$$\sigma^2 = \int_{-\infty}^{+\infty} \Gamma(\phi)\, d\phi$$

where			
	$\Gamma(\phi)$	=	*power spectrum*

Thus $\Gamma(\phi)\delta\phi$ is an approximate measure of average power or variance over a frequency bandwidth of $\delta\phi$.

If the probability distribution $f_X(x)$ of a series of measurements x(t) is normal, then its mean and variance are sufficient to characterise it completely. The mean, μ, and variance, σ^2, are given by

$$\mu = E[X] = \int_{-\infty}^{+\infty} x f_X(x)\, dx$$

and

$$\sigma^2 = E[(X-\mu)^2] = \int_{-\infty}^{+\infty} (x-\mu)^2 f_X(x)\, dx$$

If x(t) constitutes a time series, then neighbouring values within x(t) are only independent if the series is purely random, which is generally not the case. Therefore the mean and variance alone are usually insufficient to describe the behaviour of the series. In the case of a stationary series, specifying the autocovariance function as well as the mean and variance will be sufficient to describe the behaviour completely. Autocovariance is outlined below.

Consider a time series observed at two points in time, t and s ($t < s$). Two corresponding random variables x_t and x_s give the values of the time series at these points, as shown in figure B2 below.

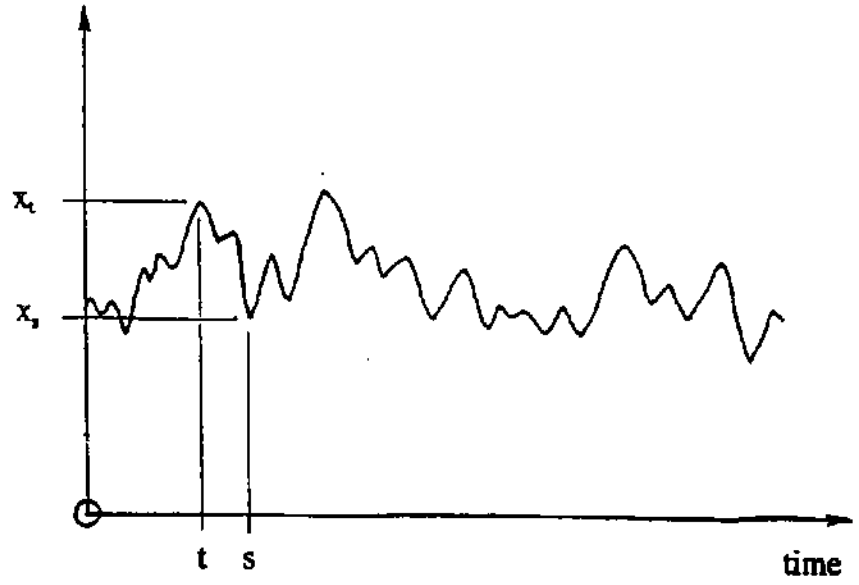

Figure B2 Time series observed at two points

The autocovariance function is defined as the second moment product

$$C(s,t) = E[(x_s-\mu_s)(x_t-\mu_t)]$$

where, because of stationarity, $\mu_s=\mu_t$.

The autocovariance measures the dependence between two points in the same series observed at different times. Very smooth series exhibit autocovariance functions that stay large even for t and s far apart, whereas "choppy" series have autocovariance functions nearly zero for $s>t$.

Note that for $s=t$

$$C(t,t) = E[(x_t-\mu)^2] = \sigma^2$$

For white noise w_t

$$C_w(s,t) = E[(w_s w_t)] = \begin{matrix} 1, s=t \\ 0, s\neq t \end{matrix}$$

That is, there is a complete lack of autocovariance in "Gaussian" white noise.

The autocovariance function $\gamma(u)$ is given by

$$\gamma(u) = E[(X(t)-\mu)(X(t+u)-\mu)]$$

This may be estimated by

$$c(u) = \frac{1}{N}\sum_{t=1}^{N-u}(x_t-\bar{x})(x_{t+u}-\bar{x})$$

If the Fourier transform of the autocovariance function of a series is taken, the power spectrum $\Gamma(\phi)$ of that series results.

Let X_m be defined as the complex amplitude at the harmonic frequency $\phi_m=m/T$. Then X_m

measures the amplitudes of the sine and cosine terms at frequency ϕ_m in x(t), and may be calculated from

$$X_m = \frac{1}{N} \int_{-\frac{T}{2}}^{+\frac{T}{2}} x(t)\ e^{-j2\pi mt/T}\ dt$$

which, for the discrete case, may be shown to be

$$X_m = \frac{1}{N} \sum_{t=-n}^{n-1} x_t e^{-j2\pi mt/N}$$

The Fourier line spectrum is obtained by plotting $|X_m|^2$ versus m.

It may be shown that, for an infinite series of length T,

$$\sigma^2 = \lim_{T\to\infty} \frac{1}{T} \int_{-\frac{T}{2}}^{\frac{T}{2}} x^2(t)\ dt$$

which may be written

$$\sigma^2 = \lim_{T\to\infty} \sum_{m=-\infty}^{\infty} (T|X_m|^2)\frac{1}{T} = \int_{-\infty}^{\infty} \Gamma(\phi)\ d\phi$$

where

$$\Gamma(\phi) = \lim_{T\to\infty} T|X_m|^2$$

The sample spectrum $C_{xx}(\phi)$ is given by

$$T|X_m|^2 = C_{xx}(\phi) = \frac{1}{T} \left| \int_{-\frac{T}{2}}^{\frac{T}{2}} x(t) e^{-j2\pi\phi t} \, dt \right|^2$$

for the continuous case, or by

$$C_{xx}(\phi) = \frac{\Delta}{N} \left| \sum_{t=-n}^{n-1} x_t e^{-j2\pi\phi t\Delta} \right|^2$$

$$(-1/2\delta \leq \phi \leq 1/2\delta)$$

for the discrete case.

The highest frequency that can be detected from data spaced δ apart, $1/2\delta$, is known as the Nyquist frequency.

To summarise, a power spectrum (or sample spectrum) of a time series gives the distribution of variance within the series with frequency, and may therefore be regarded as one way in which physical roughness can be described.

In the bored tunnels sampled, the number of data points obtained by the scanner for each run was usually close to 2000, corresponding to one distance measurement every half millimetre over a one metre length. Given this amount of data, the use of a computer in calculating the spectrum is mandatory.

Schumway (1988) presented a number of time series analysis programs, one of which was a program to calculate and plot power spectra. This program, called "SPECTRA" by Schumway, was used as a base from which to work in the development of a program suited to the specific needs of this study. A program listing of one of the modified versions is given below. This program accepts roughness data from an ASCII file, calculates the sample spectrum and outputs it back to a text file, which may be imported into a spreadsheet for manipulation and analysis. An example of a physical roughness plot (of data as supplied by the scanner) and its corresponding power spectrum is shown in figure B3 below. What is immediately obvious from the spectrum is that the variance is all concentrated near the low

frequency end of the scale, and power tapers off quickly as frequency approaches the Nyquist frequency (at ϕ=0.5 cycles per point). Note that the frequency axis in figure B3(b) has been truncated at 0.1 because the spectrum is very close to zero beyond this point. This is a characteristic common to all roughness data measured in this study and it indicates a dependent, autoregressive structure as would be expected of data of this sort.

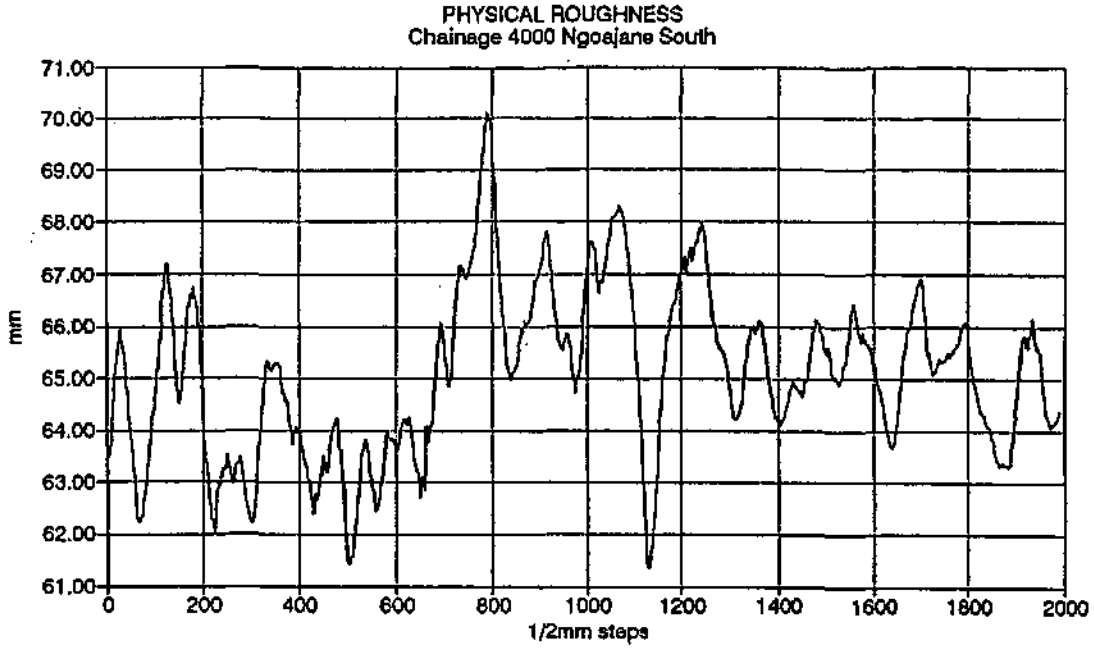

Figure B3(a) Physical roughness

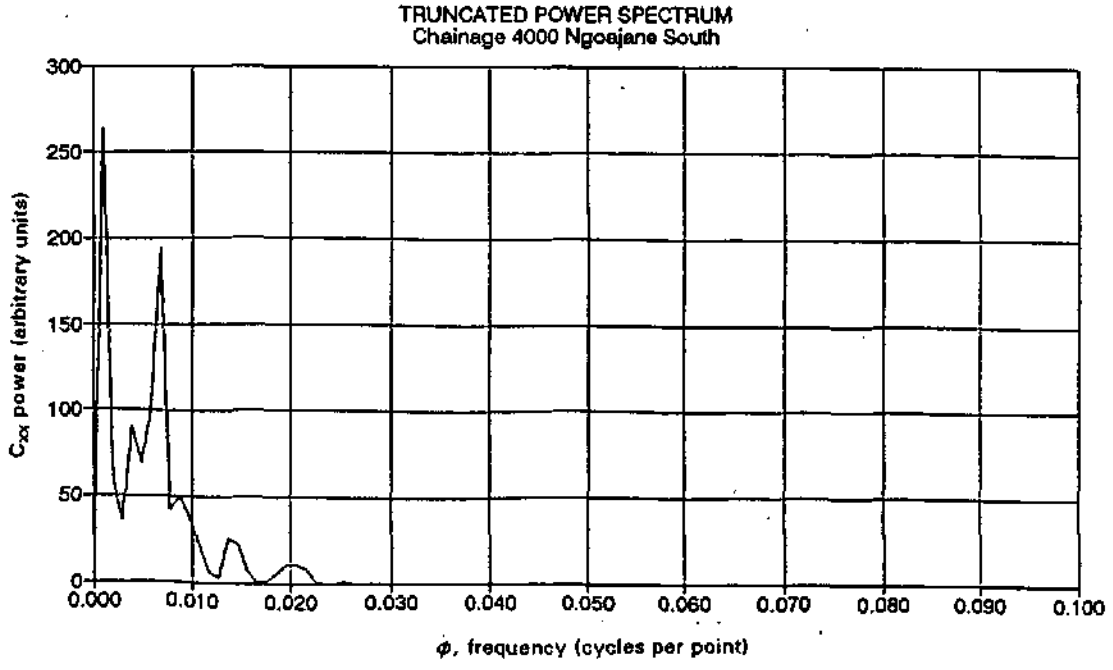

Figure B3(b) Corresponding power spectrum

No smoothing of the spectrum has been done as this was found to be unnecessary. However, because of this, very high peaks in the spectrum sometimes occur. In these cases it is often best to plot the "log spectrum", where the logarithm of the power is plotted against frequency. One big advantage of doing this is that confidence intervals remain constant on a logarithmic scale. This is explained below.

The significance of those peaks in the spectrum representing dominant frequencies needs to be investigated. On the log spectrum, the 95 per cent confidence intervals for white noise may be plotted. It is known that the theoretical spectrum for a white noise series is represented by a horizontal line of power equal to one, on a natural scale. On the log spectrum this corresponds to the zero of the vertical axis.

From Jenkins and Watts (1968)

$$\frac{2C_{xx}(\phi)}{\Gamma_{xx}(\phi)} \sim \chi^2_2$$

where $C_{xx}(\phi)$ is the sample spectrum

$\Gamma_{xx}(\phi)$ is the theoretical spectrum,

that is, twice the sample spectral estimator divided by the theoretical spectral estimator is distributed as Chi-squared with two degrees of freedom. Also

$$\frac{\nu C_{xx}(\phi)}{\Gamma_{xx}(\phi)} \sim \chi^2_\nu \qquad \text{(B1)}$$

where ν = degrees of freedom

From equation (B1)

$$P[x_\nu(\frac{\alpha}{2}) < \frac{\nu C_{xx}(\phi)}{\Gamma_{xx}(\phi)} \leq x_\nu(1-\frac{\alpha}{2})] = 1-\alpha$$

where

$$P[\chi_\nu^2 \leq x_\nu(\frac{\alpha}{2})] = \frac{\alpha}{2}$$

The interval between

$$\frac{\nu C_{xx}(\phi)}{x_\nu(1-\frac{\alpha}{2})} \quad , \quad \frac{\nu C_{xx}(\phi)}{x_\nu(\frac{\alpha}{2})}$$

is a 100(1-α) per cent confidence interval for $\Gamma_{xx}(\phi)$.

This interval may be plotted by horizontal lines on the log spectrum, and any point falling outside of this region is 95 per cent likely not white noise. Thus those peaks with power greater than the upper confidence limit may be regarded as significantly different from white noise. This is shown in figure B4 below.

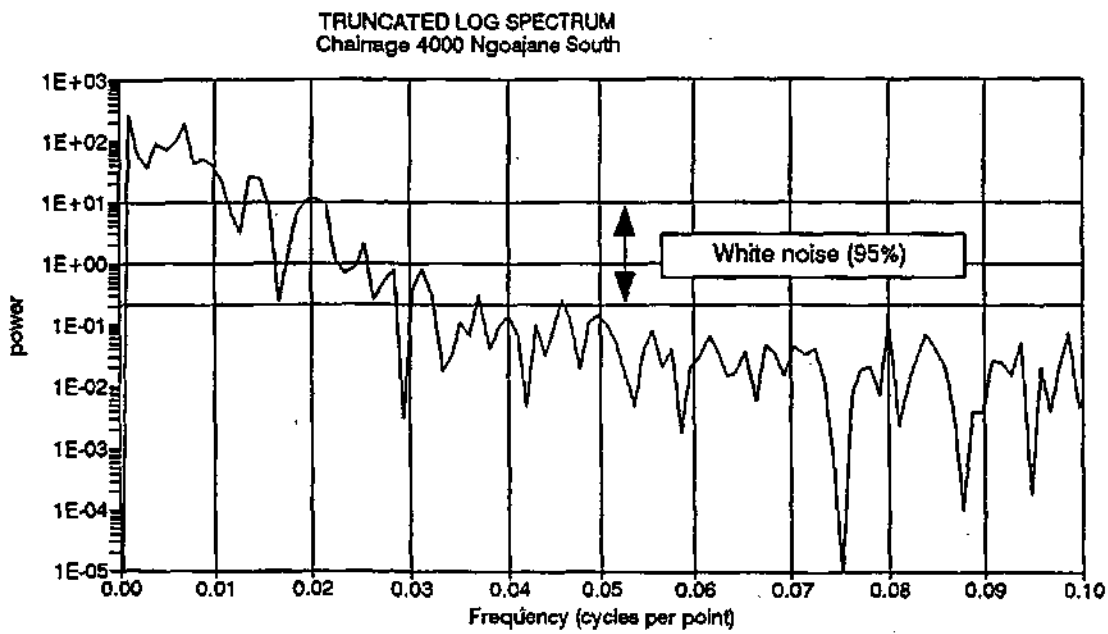

Figure B4 Log spectrum with confidence interval

In this way the dominant wavelengths of the series (highest peaks) are tested for significance.

The plots in figures B3 and B4 all relate to the same physical roughness data set. In fig B3(a) (the physical roughness plot) some periodicity of wavelength ≈ 50mm is evident. This emerges as the peak in figures B3(b) and (c), as well as in figure B4. From figure B4 it can

be seen that this wavelength is, in fact, significantly different from white noise and therefore is a definite feature of this particular roughness data set.

A test was done on the program used to calculate spectra to see whether accurate results are obtained. This was done by generating a set of second-order autoregressive (AR-2) data, and calculating the spectrum of this data set using the program. This sample spectrum is then compared to the theoretical spectrum, from which accuracy may be ascertained.

The AR-2 model used was

$$x_t = x_{t-1} - 0.89x_{t-2} + w_t$$

where w_t = Gaussian white noise

This model has a pseudo-periodicity of about 5.5 (see Box & Jenkins, 1970).

The testing showed that the program yields accurate results in that the sample and theoretical spectra matched up very well.

Thus physical roughness data from tunnel walls may be well represented by power spectra of each setup. The spread of variance (which is proportional to amplitude) with frequency is given, and the significance of dominant wavelengths may be found.

The mean wavelength is easily computed from the spectrum by numerical integration in the following way.

If the spectrum were sampled continuously, then its integral would be equal to the sample variance :

$$\hat{\sigma}^2 = \int_0^{\frac{1}{2}} C_{XX}(\phi)\, d\phi$$

where $C_{XX}(\phi)$ is the sample spectrum

The mean wavelength is then defined by $\lambda_C = 1/\phi_C$, where

$$\phi_C = \int_0^{\frac{1}{2}} \phi . C_{XX}(\phi)\, d\phi \;/\; \hat{\sigma}^2$$

is the centroidal frequency.

Using the trapezoidal rule, quadrature of this integral yields

$$\phi_C = \left[\sum_{i=1}^{N-1} \phi_i . C_{XX}(\phi_i) \Delta\phi + \frac{1}{2} C_{XX}(\phi_N) \frac{\Delta\phi}{2} \right] / \hat{\sigma}^2$$

or, with small error,

$$\phi_C = \sum_{i=1}^{N} i . C_{XX}(\phi_i) (\Delta\phi)^2 / \hat{\sigma}^2$$

where $\Delta\phi = 1/2N$

This can be conveniently computed from the spectrum using a spreadsheet.

B3 Program Listing

The program "SPECTRA" by Schumway (1988) was used as a basis for the program used in the data analysis of this study. In its original form, SPECTRA required that the data to be analysed is stored in a Random Access Memory (RAM) file, for which another program, called DATAIN, was given. Since many of the inputs which SPECTRA would normally have required were common to every data set to be analysed, the program was modified so that the user would not be prompted for these inputs for every run. SPECTRA also listed and plotted the calculated spectrum and log spectrum for each data set analysed. These subroutines consumed time and were unnecessary for the specific purposes of the analysis being performed, and were therefore removed. A further modification made was to write the power spectrum from each data set to an ASCII file, so that it could be further manipulated in a spreadsheet.

A listing of one of the many modified versions of the original program SPECTRA used in the data analysis of this study is given below. The centroidal wavelength is calculated and appears in the output by the program SPEC.BAS on disk 1 at the back of this document.

```
90 REM **PROGRAM "SPEC" TO FIND f FROM SCANNER DATA**
91 REM **PROGRAM ACCEPTS ASCII DATA, DETRENDS IT**
92 REM **FINDS VARIANCE, CALCULATES SPECTRUM**
93 REM **AND HENCE FINDS f**
94 REM ----------------------------------------
95 REM *** INPUT DATA ***
96 CLS
97 PRINT "Tunnel name ?":INPUT TNM$
98 PRINT "Tunnel diameter (metres) ?":INPUT DIA
99 DIA=1000*DIA
100 PRINT "Data file path ?":INPUT A$
101 REM PRINT "Start ?":INPUT ST:PRINT "End ?":INPUT ND
102 B1$=".PRN":EM$="PP"
103 REM FOR MSP=ST TO ND
104 PRINT "Setup number ?":INPUT C$:SF$=A$+C$+B1$
109 NR=1
110 T1=1:T2=1990:T=T2-T1+1
120 DIM X1$(NR),Y(T,NR),YY(T)
130 J=1
150 PRINT "Chainage ?":INPUT CNG$:F$=EM$+CNG$
160 OPEN SF$ FOR INPUT AS #2
170 REM ***OPEN DATA FILE***
180 OPEN "r",1,F$,4*NR
190 FIELD 1,4 AS X1$(1)
200 REM ***INPUT SERIES***
210 IF T1=1 THEN 230
220 FOR II=1 TO T1-1:INPUT #2,Z:NEXT II
230 I=0
240 FOR II=T1 TO T2:I=I+1:INPUT #2,Y(I,J):NEXT II
250 DT=1
260 FOR I=1 TO T:YY(I)=Y(I,J):NEXT I:GOSUB 500
270 FOR I=1 TO T:Y(I,J)=YY(I):NEXT I
280 REM ***WRITE DATA TO FILE***
290 FOR I=1 TO T
300 LSET X1$(J)=MKS$(Y(I,J)):PUT 1,I
310 NEXT I
320 CLOSE 2:CLOSE 1
380 REM ***MEAN AND VARIANCE***
390 K=0
400 FOR I=1 TO T:K=K+YY(I):NEXT I
410 MN=K/T:PRINT "Mean = ";MN
420 M=0
430 FOR I=1 TO T:M=M+((YY(I)-MN)^2):NEXT I
440 VAR=M/T:PRINT "Variance = ";VAR
490 ERASE X1$,Y,YY:GOTO 1001
500 REM ***DETREND***
505 REM * DETRENDED DATA STORED IN ARRAY YY *
510 K1=0:K2=0:K3=0:K4=0
520 FOR I=1 TO T:K1=K1+I:NEXT I
530 FOR I=1 TO T:K2=K2+(I*I):NEXT I
540 FOR I=1 TO T:K3=K3+YY(I):NEXT I
```

```
550 FOR I=1 TO T:K4=K4+(I*(YY(I))):NEXT I
560 A1=(K4-K1*K3/T)/(K2-K1*K1/T)
570 A0=(K4-K2*A1)/K1
580 FOR I=1 TO T
590 YY(I)=YY(I)-A0-(A1*I)
600 NEXT I
610 RETURN:END
1001 LPRINT "----------------"
1002 NR=1
1003 LPRINT TNM$:LPRINT SF$:LPRINT "Diameter = ";DIA;"mm"
1004 GOSUB 1980
1012 TP=2048
1015 DIM X(T,NR),X0$(NR),PL(TP),XX(TP),D(2*TP),B$(NR)
1016 FOR J=1 TO NR:B$(J)=F$:NEXT J
1017 PI=3.141592654#
1020 GOSUB 1960:GOSUB 1970
1029 FOR JS=1 TO NR
1030 FOR I=1 TO T:XX(I)=X(I,JS):NEXT I:DT=1
1033 NEXT JS
1048 REM *** Compute and plot spectra ***
1052 NS=512:NS=2*NS
1056 FOR JS=1 TO NR
1059 FOR I=1 TO 2*TP: D(I)=0:NEXT I
1061 FOR I=1 TO T:D(2*I-1)=X(I,JS):NEXT I
1066 REM*** Compute DFT ***
1068 SI=-1:T2=TP:GOSUB 1800
1071 REM *** Calculate periodogram ***
1072 TA$="n":SC=1
1074 FOR I=1 TO TP
1075 XC=D(2*I-1):XS=-D(2*I)
1077 PL(I-1)=(XC*XC+XS*XS)/(T*SC)
1080 NEXT I
1082 REM *** Smooth and subsample periodogram ***
1084 GOSUB 1870
1085 GOSUB 3000
1109 NEXT JS
1800 REM*** Calculate Discrete Fourier Transform ***
1802 REM*** Input Series as D(2*J-1),D(2*J),J=1,2,...,T2 ***
1804 REM*** Paired real and imaginary parts ***
1805 REM*** T2 is a power of 2 ***
1806 REM*** Output is in array  D(J) ***
1808 REM*** SI=1 for direct transform, SI=-1 for inverse transform ***
1810 REM*** Transform is not scaled by dividing out sqr(T2) ***
1812 NN=2*T2:J=1:PI=3.141592654#
1814 FOR I=1 TO NN STEP 2
1816 IF I>=J THEN GOTO 1824
1818 TR=D(J):TI=D(J+1)
1820 D(J)=D(I):D(J+1)=D(I+1)
1822 D(I)=TR:D(I+1)=TI
1824 M=NN/2
1826 IF J<=M THEN GOTO 1832
1828 J=J-M:M=M/2
1830 IF M>=M/2 THEN GOTO 1826
1832 J=J+M
1834 NEXT I
1836 MX=2
1838 IF MX>=NN THEN GOTO 1866
```

```
1840 IS=2*MX:TH=SI*2*PI/MX:SH=SIN(TH/2)
1842 VR=-2*SH*SH:VI=SIN(TH):WR=1:WI=0
1844 FOR M=1 TO MX STEP 2
1846 FOR I=M TO NN STEP IS
1848 J=I+MX
1850 TR=WR*D(J)-WI*D(J+1):TI=WR*D(J+1)+WI*D(J)
1852 D(J)=D(I)-TR:D(J+1)=D(I+1)-TI
1854 D(I)=D(I)+TR:D(I+1)=D(I+1)+TI
1856 NEXT I
1858 TR=WR
1860 WR=WR*VR-WI*VI+WR:WI=WI*VR+TR*VI+WI
1862 NEXT M
1864 MX=IS: GOTO 1838
1866 RETURN
1868 END
1870 REM *** Smooth(L point) and sample(NS values) a TP point array PL ***
1872 REM *** Returns as NS values in  XX ***
1874 JJ=0:A=TP/NS
1876 FOR K=0 TO TP/2 STEP A:SU=0
1878 FOR LL=-(L-1)/2 TO (L-1)/2
1880 LA=K+LL:IF LA<0 THEN LET LA=TP+LA
1882 SU=SU+PL(LA)
1884 NEXT LL
1886 XX(JJ+1)=SU/L
1888 JJ=JJ+1
1890 NEXT K
1900 REM *** FIND CENTROIDAL FREQUENCY ***
1905 SUM=0
1910 FOR I=1 TO 513
1912 Y=((I-1)/1024)*(XX(I))/1024
1915 SUM=SUM+Y
1920 NEXT I
1925 CRD=SUM/VAR
1930 PRINT "Centroidal frequency is ";CRD;" cycles per point"
1931 LPRINT "Centroidal frequency is ";CRD;" cycles per point"
1935 WL=1/(2*CRD)
1939 PRINT "Centroidal wavelength = ";WL;" mm"
1940 LPRINT "Centroidal wavelength = ";WL;" mm"
1941 REM *** FIND MAX POWER ***
1942 MX=0
1943 FOR I=1 TO 513
1944 IF XX(I)>MX THEN GOTO 1946
1945 GOTO 1947
1946 MX=XX(I):MF=I
1947 NEXT I
1948 PRINT "Max Power = ";MX;" corresp to wavelength = ";512/(MF-1);"mm"
1949 LPRINT "Max Power = ";MX;" corresp to wavelength = ";512/(MF-1);"mm"
1950 RETURN:END
1960 REM*** Open a data file ***
1962 OPEN "r",1,F$,4*NR
1964 FIELD 1,4 AS X0$(1)
1965 IF NR=1 THEN GOTO 1968
1966 FOR  KL=2 TO NR:FIELD 1,4*(KL-1) AS DU$,4 AS X0$(KL):NEXT KL
1968 RETURN:END
1970 REM*** Read data from a file ***
1974 I=0
1975 FOR II=T1 TO T2:GET 1,II
```

```
1976 I=I+1
1977 FOR J=1 TO NR:X(I,J)=CVS(X0$(J)):NEXT J
1978 NEXT II
1979 RETURN:END
1980 REM*** Input first point, last point and number of series ***
1982 T1=1
1983 T2=1989:T=T2-T1+1
1985 LPRINT "Chainage = ";CNG$:LPRINT DATE$:LPRINT "Start= ";T1;"End= ";T2;"Nu
er= ";T
1986 L=1:LPRINT "Smoothing const L = ";L:LPRINT "Variance = ";VAR
1987 RETURN
1988 END
3000 REM *** WRITE TO ASCII ***
3005 PN$="P.PRN"
3006 NME$=F$+PN$
3010 OPEN NME$ FOR OUTPUT AS #5
3020 FOR K=0 TO 1988:WRITE #5,XX(K+1):NEXT K
3030 CLOSE #5
3040 LPRINT "Power spectrum of ";F$;" data stored in ";NME$
4000 REM *** CALCULATE f ***
4010 KS=4*SQR(2*VAR)
4020 FI=1.7724539#*LOG(60*DIA/KS)-5.436
4025 LPRINT "Equivalent grain size Ks = ";KS;"mm"
4030 PRINT "Friction factor f = ";1/(FI*FI)
4035 LPRINT "Friction factor f = ";1/(FI*FI)
4040 PRINT:PRINT "Continue ?":INPUT QN$
4050 IF QN$="y" THEN GOTO 4060
4055 IF QN$="Y" THEN GOTO 4060
4057 END
4060 CLOSE #1:CLOSE #2
4070 ERASE X0$,X,XX,PL,D,B$:CLS:GOTO 104
```

APPENDIX C

LINKING PHYSICAL ROUGHNESS TO HYDRAULIC RESISTANCE

In C1 a brief overview of some of the fundamentals regarding flow of fluid in closed conduits and the associated friction losses is given. This is followed, in C2, by a look at the essentials of fluid dynamics. These two sections are then brought together in C3 where the particular case of turbulent flow in closed conduits is examined.

C1 Friction Losses in Closed Conduit Flow

Flow of fluid in pipes may be regarded as either laminar or turbulent. Laminar flow occurs when the paths of individual fluid particles do not cross one another and flow apparently takes place in layers or *laminae*. Viscous forces dominate over inertia forces. In turbulent flow, individual fluid particles follow random, erratic paths, with only their average velocity in the direction of flow.

The state of flow of fluid in pipes is governed by the Reynolds Number, Re, which is defined as the ratio of inertia to net viscous force in the fluid.

$$Re = \frac{\rho d\bar{u}}{\mu} = \frac{d\bar{u}}{\nu}$$

where ρ = fluid density
d = diameter of pipe
$\bar{u}$ = mean velocity
μ = dynamic viscosity
ν = kinematic viscosity

Flow is regarded as laminar for Re<2000. For Re higher than 5000 the flow is either transitional or turbulent, depending on the characteristics of the conduit.

The well-known Darcy-Weisbach[1] formula for flow in pipes, developed around the middle of the nineteenth century, relates head lost due to friction, H_f, to mean flow velocity and physical features of the pipe itself:

$$h_f = \frac{4flu^2}{2gd} \qquad \text{(C1)}$$

where f = dimensionless coefficient known as the friction factor

l = length over which H_f occurs

g = acceleration due to gravity

The assumption that f is constant, as implied by equation (C1), is only applicable to fully-developed flow.

When the flow is not fully-developed, f is variable and for laminar flow it can be shown that

$$f = \frac{16}{Re} \qquad \text{(C2)}$$

That is, friction factor f is dependent only on the Reynolds number, and is independent of the pipe roughness. Determination of f for Re > 2000 is more complicated. For sufficiently low Re, all pipes will exhibit laminar flow.

For turbulent flow of a pipe flowing full when Re > 5000, there is a zone near the wall called the viscous sub-layer. In this zone, secondary random fluctuations of velocity of fluid particles, typical of turbulent flow, die out due to their proximity to the boundary, giving rise to laminar flow. The thickness of this layer, δ, decreases with increasing Re. Flow behaviour is defined as *smooth* as long as the viscous sub-layer thickness is greater than the height of the roughness elements on the boundary. As Re increases, δ decreases and as soon as the bumps begin to protrude through the sub-layer, the flow behaviour deviates from that of

[1]According to Ven te Chow (Chow, 1959), this formula was formulated by Weisbach alone, and only because of his work on pipe flow is Darcy's name associated with it.

smooth pipes. The way in which it deviates is governed by the geometric characteristics of the conduit.

Nikuradse (1933) investigated this phenomenon in tests performed on artificially-roughened pipes. These were roughened with sand grains. Sand was sieved to obtain grains of a uniform size. Each pipe was filled with a glue which was then allowed to drain out, leaving a thin coating on the inside of the pipe. The pipe was then filled with uniformly sized sand, which was thereafter allowed to flow out, leaving those grains in contact with the glue adhered to the pipe wall.

Various pipe and grain size combinations were tested over a range of Re. These tests indicated that friction factor f was, for constant Re, governed by the ratio of sand grain size, k, to pipe diameter. This dimensionless ratio is known as the *relative roughness*.

These results are shown in figure C1.

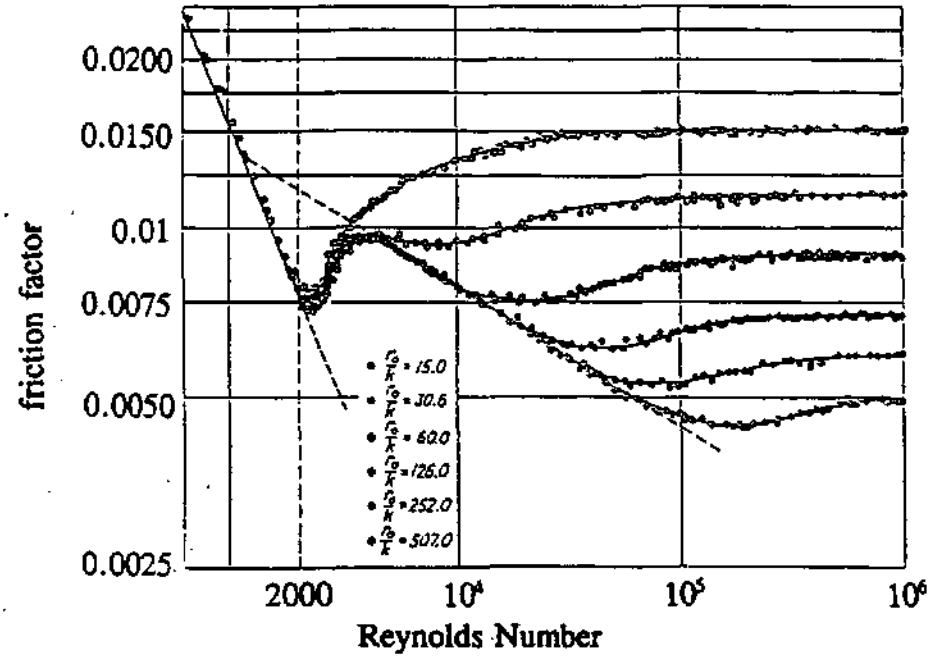

Figure C1 Resistance Coefficients for artificially roughened pipes (Rouse 1950)

As can be seen, f becomes independent of Re once flow is completely turbulent (that is, at high enough Re).

The smooth law relationship, first derived by Von Karman in 1930 and later put into a more convenient form by Prandtl, is given by

$$\frac{1}{\sqrt{f}} = 4\log_{10}(R_e\sqrt{f}) - 1.6$$

For rough flow at high Re, f is independent of Re and is given by

$$\frac{1}{\sqrt{f}} = 4\log_{10}(\frac{R}{k}) + 3.48$$

where R = pipe radius

Colebrook (1939), aided by C.M.White, mathematically described the transition region between smooth and fully rough laws by the equation

$$\frac{1}{\sqrt{f}} = -4\log_{10}(\frac{k}{3.71d} + \frac{1.26}{R_e\sqrt{f}}) \qquad \text{(C3)}$$

where d = pipe diameter

This equation, known as the *Colebrook-White Equation*, gives a smooth transition from smooth law to rough law while including both as special cases and was derived from experiments conducted on commercial pipes. In figure C2 below the deviation from Nikuradse's results is clearly shown. The dip-and-rise displayed by Nikuradse's results is typical of surfaces of regular roughness, while the behaviour of surfaces of random roughness closely follows that represented by equation C3. In general, commercial pipes fall into this random roughness category. Note, however, that for high enough u_* (hence Re) both curves converge, indicating that regular spacing is only a factor at low Reynolds numbers.

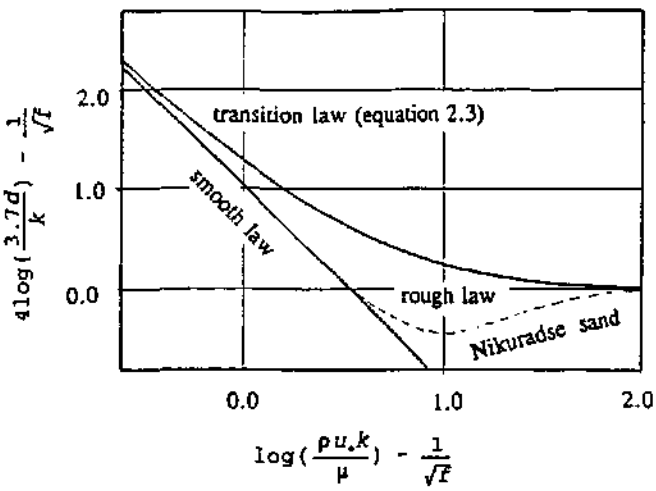

Figure C2 Transition Law (Colebrook 1939)

If Nikuradse's results are plotted in terms of the parameters $f^{-½}$ - 2log(r/k) and k/δ, the curve in figure (C3) is obtained. The fact that all of these data follow the same curve is evidence that the magnitude of δ relative to the bump heights actually does dictate whether flow is in the smooth or rough regime, as mentioned previously.

As can be seen, the Colebrook-White equation (equation C3) is not explicit in f, making solution for f an iterative process. Many formulae have been proposed for expressing f directly for the entire range of k/d and Re. Possibly the best yet[2] is that produced by Haaland (1983) :

$$\frac{1}{\sqrt{f}} = -3.6\log_{10}\left[\frac{6.9}{Re} + \left(\frac{k}{3.71d}\right)^{1.11}\right]$$

[2]Massey (1989) makes this recommendation.

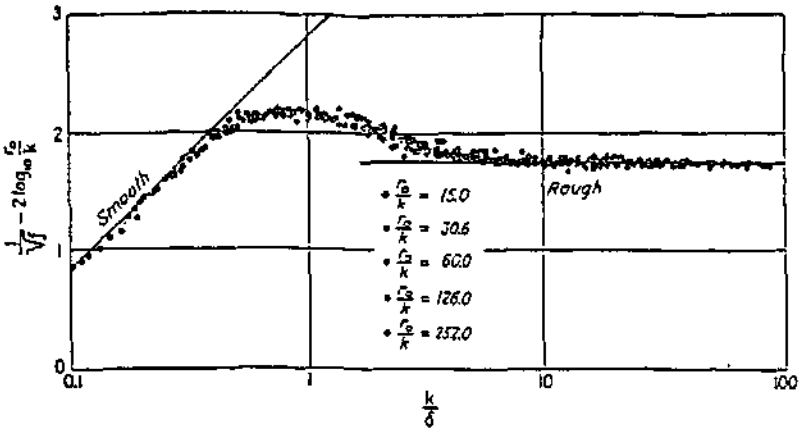

Figure C3 Variation in roughness effect with relative thickness of laminar sub-layer (Colebrook 1939)

Another way of simplifying the design procedure is to express equation C3 in chart form. Moody (1944) did this successfully and the chart he prepared, shown in figure C4 below, is still widely used in practice. Given both k/d and Re, the friction factor f may be read off directly. Figure C4 is known as the *Moody Diagram*.

Another roughness coefficient often encountered when dealing with head losses in conduits is "Manning's n", in spite of it originally having been developed for open channel flow. Use of Manning's n may be preferred to Darcy-Weisbach f in that n (like k) is independent of the diameter of the conduit. Specifying f alone for a pipe is not sufficient to describe the actual roughness. For the same boundary roughness in pipes of different diameter, different values of f result. The formula derived by Manning (1889) is given, in Metric units, by

$$u = \frac{1}{n} m^{\frac{2}{3}} S_0^{\frac{1}{2}}$$

where u = velocity
n = Manning's n
m = hydraulic radius
S_0 = bed slope

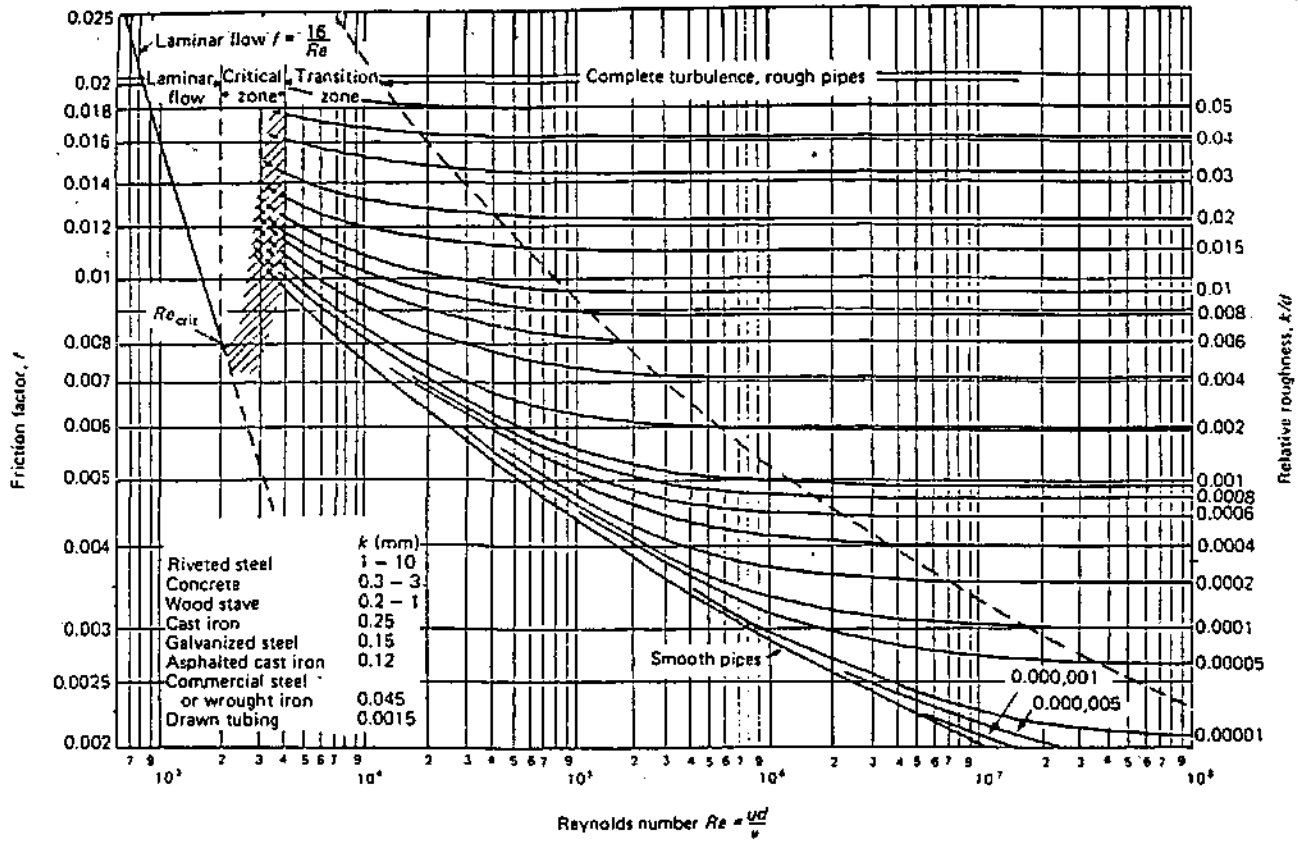

Figure C4 Moody Diagram (Massey 1989)

The Darcy-Weisbach friction factor, f, and Manning's n are related by

$$n = m^{\frac{1}{6}} \sqrt{\frac{f}{2g}} \qquad \text{(C4)}$$

or, for conduits flowing full

$$n = \left(\frac{d}{4}\right)^{\frac{1}{6}} \sqrt{\frac{f}{2g}}$$

Manning's n value is a purely empirical number (which is not dimensionless), as is the value used for k in finding f, and no greater accuracy is afforded by either one.

Equation (C3) has been shown to yield accurate results, provided that the correct value for k is used. It is in estimating the "roughness" k where discrepancies arise since k is the *equivalent grain diameter*, that is, the grain diameter which, if uniformly coating the inside of a smooth pipe, would, for the same Re, cause the same head loss as the pipe itself. This value of k is related *in some way* to the physical roughness of the pipe concerned. The use of k as a linear dimension representative of the roughness often leads to the assumption that k is equivalent to roughness height, h. This would appear incorrect as roughness height alone is not sufficient to completely describe the roughness.

Various authors have attempted to define roughness parameters k, f and n in terms of physical roughness dimensions. Others have made efforts to simplify the estimation of roughness parameters to be used for surfaces of particular characteristics.

C2 Fundamental Fluid Dynamics Relationships

The intention of this section is to be expository, not tutorial, so derivations of commonly used equations are omitted. If these are required, they may be found in fluid dynamics texts such as Batchelor (1967) or Hughes & Brighton (1967).

A start is made by stating the basic equations of continuity and momentum in differential form.

Continuity:

$$\frac{\partial \rho}{\partial t} + \frac{\partial}{\partial x}(\rho u) + \frac{\partial}{\partial y}(\rho v) + \frac{\partial}{\partial z}(\rho w) = 0 \qquad \text{(C5)}$$

where u, v, w are velocities in x, y, z directions

or, in tensor notation

$$\frac{\partial \rho}{\partial t} + \frac{\partial}{\partial x_i}(\rho u_i) = 0$$

For the case of incompressible fluid, density ρ is constant, and the continuity equation simplifies to

$$\frac{\partial u}{\partial x} + \frac{\partial v}{\partial y} + \frac{\partial w}{\partial z} = 0$$

Momentum:

The momentum integral equation (MIE) is :

$$F_s + \int_{cv} B.dv = \frac{\partial}{\partial t}\int_{cv} V\rho dv + \int_{cs} V\rho V.dA$$

where

F_s	=	total surface force vector
B	=	body force vector
V	=	velocity vector
CV	=	control volume
CS	=	control surface

By considering the forces on a block of fluid of dimensions $\Delta x, \Delta y, \Delta z$ in Cartesian co-ordinates, and by taking the limit as $\Delta x, \Delta y, \Delta z$ tend to zero and substituting into the MIE the following is obtained:

Considering the x-direction :

$$\rho\left(\frac{\partial u}{\partial t} + u\frac{\partial u}{\partial x} + v\frac{\partial u}{\partial y} + w\frac{\partial u}{\partial z}\right) = \frac{\partial \sigma_{11}}{\partial x} + \frac{\partial \sigma_{21}}{\partial y} + \frac{\partial \sigma_{31}}{\partial z} + B_x \qquad \text{(C6)}$$

where σ_{ij} is stress on face i in j direction

The above equations are theoretical, and cannot easily be used directly for real problems. In

the sub-section C3 following, these are extended to the practical situation of pipe flow, which is directly relevant to the purpose of this study.

C3 Turbulent Flow in Closed Conduits Flowing Full

In turbulent flow in pipes of constant cross-section, only the average motion is parallel to the axis of the conduit with individual fluid particles moving in erratic paths. Turbulent flow is characterised by the fact that, superimposed on the principal or average motion of the fluid, are random secondary movements. The velocity of a fluid particle in turbulent flow is made up of two components, a mean or time average component and a fluctuating component.

That is

$$u = \bar{u} + u'$$

where	u	=	velocity of fluid particle
	$\bar{u}$	=	mean (time average) velocity
	u'	=	fluctuating velocity component

At a particular point in the flow, velocity of the fluid varies randomly with time, as shown in figure C5 below.

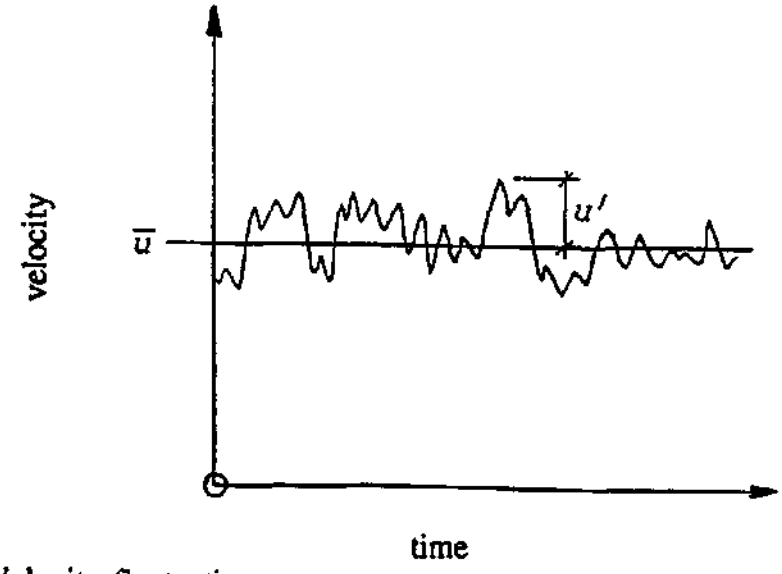

Figure C5 Velocity fluctuation

The time averaged velocity of the flow, $\bar{u}$ is defined as

$$\bar{u} = \frac{1}{T}\int_0^T u\, dt$$

where T is large.

Continuity Equation for turbulent flow

Taking the time average of equation C5,

$$\overline{\frac{\partial \rho}{\partial t} + \frac{\partial}{\partial x_i}(\rho u_i)} = 0$$

which implies

$$\frac{\partial \bar{\rho}}{\partial t} + \frac{\partial}{\partial x_i}(\bar{\rho}.\bar{u_i}) + \frac{\partial}{\partial x}(\overline{\rho u_i'}) = 0$$

which, for incompressible flow, reduces to

$$\frac{\partial \bar{u_i}}{\partial x_i} = 0$$

since ρ is constant.

Momentum Equation for Turbulent Flow

After substitution of

$$u_i = \bar{u}_i + u'$$
$$p = p + p'$$

and taking the time average of both sides, equation C6 becomes

$$\rho\left(\frac{\partial \bar{u_i}}{\partial t} + \bar{u_j}\frac{\partial \bar{u_i}}{\partial x_j}\right) = -\frac{\partial \bar{p}}{\partial x_j} + \frac{\partial}{\partial x_j}\left(\mu\frac{\partial \bar{u_i}}{\partial x_j} - \rho\overline{u_i' u_j'}\right) \qquad \text{(C7)}$$

Where $\rho u_i' u_j'$ are the Reynolds' stresses.

The equations represented by (C7) are known as the Navier Stokes Equations, and they give the complete solution to any flow, including turbulent flow. However, they are often computationally intractable and, for this reason, certain phenomenological theories have been developed to enable their use in practical situations.

Phenomenological Theories to describe turbulent flow

The last expression in brackets in equation (C7) is known as the shear stress tensor, τ_{ij}, and may be written in two dimensions as

$$\tau_{ij} = \mu\left(\frac{\partial \overline{u_i}}{\partial x_j} + \frac{\partial \overline{u_j}}{\partial x_i}\right) - \rho \overline{u_i' u_j'}$$

which shows that total shear stress is made up of laminar and turbulent components.

This is simplified by the concept of eddy viscosity, ϵ, defined implicitly in the relation

$$\tau_{ij} = (\mu + \rho\epsilon)\frac{\partial \overline{u_i}}{\partial x_j}$$

Eddy viscosity and Reynolds' stresses are thus related by the equation

$$\epsilon = -\overline{u_i' u_j'}\left[\frac{\partial \overline{u_i}}{\partial x_j}\right]^{-1}$$

Note that eddy viscosity is not constant, but varies according to flow conditions.

An important phenomenological theory is Prandtl's hypothesis of the mixing length. The mixing length l is defined as the average distance, perpendicular to the main flow direction, in which a small particle of fluid, moving toward slower moving layers, loses its extra momentum and takes on the velocity of its new surrounds. Mixing length is defined in the relation

$$\tau = \rho l^2 \left|\frac{\partial \bar{u}}{\partial y}\right| \frac{\partial \bar{u}}{\partial y} \qquad \text{(C8)}$$

If the assumption is made that mixing length l varies linearly with distance from the boundary, y, ie

$$l = \kappa y$$

where κ = constant

The constant κ is known as the universal turbulence constant.

Using this relation, equation (C8) may be written as

$$\tau = \rho \kappa^2 y^2 \left|\frac{\partial \bar{u}}{\partial y}\right|^2$$

LeGrange and Rooseboom (1993) showed by deterministic arguments using cylindrical eddies at the bed that $\kappa = (2\pi)^{-1/2} = 0.3989$. This matches the value of $\kappa = 0.40$ generally accepted and confirmed experimentally.

Substituting for κ

$$\tau = \frac{\rho}{2\pi} y^2 \left|\frac{\partial \bar{u}}{\partial y}\right|^2 \qquad \text{(C9)}$$

Using equation (C9) the shear stress at any level y from the boundary may be found, provided that the velocity gradient at this level is known.

The universal log law of the velocity distribution

From equation (C9), assuming that u varies in the y direction only, the partial becomes a full derivative, and

$$\frac{du}{dy} = \frac{\sqrt{2\pi\tau/\rho}}{y}$$

Using the boundary condition $\tau=\tau_0$ at $y=y_0$, this differential equation may be integrated to get

$$u = \sqrt{2\pi\tau_0/\rho}\ \ln(\frac{y}{y_0})$$

Introducing the shear velocity, $u_* = (\tau_0/\rho)^{1/2}$, the equation for the velocity distribution becomes

$$u = \sqrt{2\pi}\ u_*\ \ln(\frac{y}{y_0}) \qquad \text{(C10)}$$

which is known as the Universal Log Law. Through experimentation, the value for y_0 has been found to be given by

$$\ln y_0 = \ln(\frac{\nu}{u_*}) - 2.2$$

However, in spite of its name, equation (C10) does not apply over the entire body of the flow. This is because of the inclusion of u_* in the expression. Since u_* is proportional to the shear stress *at the bed*, τ_0, the expression only holds where $\tau \approx \tau_0$. That is, the universal log law is only applicable near the boundary. This is easily shown if equation (C10) is differentiated, and the resulting expression for du/dy is substituted into equation (C9). The result obtained is that $\tau=\tau_0$.

The correct velocity distribution

The correct velocity distribution may be derived by considering the variation of shear stress across the section of a pipe. Consider flow of a fluid in a circular pipe of radius R, as shown in figure C6 below.

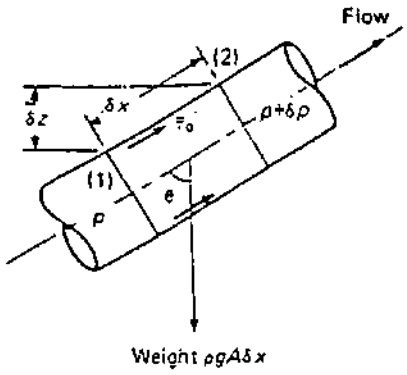

Figure C6 Fluid element in pipe flow (Massey 1989)

For fully-developed flow, a fluid element of length δx within the pipe experiences no net force. That is

$$pA - (p+\delta p)A - \rho gA.\delta x.\cos\theta + \bar{\tau}_0 P.\delta x = 0$$

where A = cross-sectional area
P = perimeter
τ_0 = mean boundary shear stress

which may be simplified to

$$\bar{\tau}_0 P.\delta x = A(\delta p + \rho g.\delta z)$$

For uniform boundary roughness in a circular section, τ_0 is constant around perimeter, P. In the limit as $\delta x \to 0$, the above equation simplifies to

$$\tau_0 = \frac{P}{A}\frac{dp^*}{dx}$$

where p^* = piezometric pressure = $p+\rho gz$

For a circular section flowing full, this may be written as

$$\tau_0 = \frac{R}{2}\frac{dp^*}{dx}$$

and this holds for cylindrical fluid elements of any radius $r < R$. Using the pipe boundary as

the origin for y, ie r=R-y,

$$\tau = \frac{R-y}{2}\frac{dp^*}{dx}$$

where τ = shear stress at R-y from boundary

Combining the relations for τ and τ_0 yields

$$\tau = \tau_0(\frac{R-y}{R})$$

This applies over the whole cross section, as opposed to only near the boundary and in addition applies in laminar or turbulent flow.

Combining equation (C9) with the linear shear stress variation above, yields

$$(\frac{du}{dy})^2 = \frac{2\pi}{y^2}\frac{1}{\rho}\frac{\tau_0(R-y)}{R} \qquad \text{(C11)}$$

Making the substitution

$$z = \sqrt{1-\frac{y}{R}}$$

then rearranging and integrating equation (C11) with respect to y, using the boundary condition at $y=R$, $u=u_R=u_{max}$,

$$u = u_*\sqrt{2\pi}(2z + \ln|\frac{z-1}{z+1}|) + u_R \qquad \text{(C12)}$$

Equation (C12) is the full velocity distribution for turbulent flow in a circular pipe and it holds throughout the flow, except for a very thin region near the wall (called the viscous sub-layer), which is defined and discussed later.

When z→1 (ie y→0), equation (C12) simplifies to equation (C10). This is shown in figure C7 below, where velocity u is plotted against y for equations (C10) and (C12), where u_R=1.48m/s, u.=0.0452m/s.

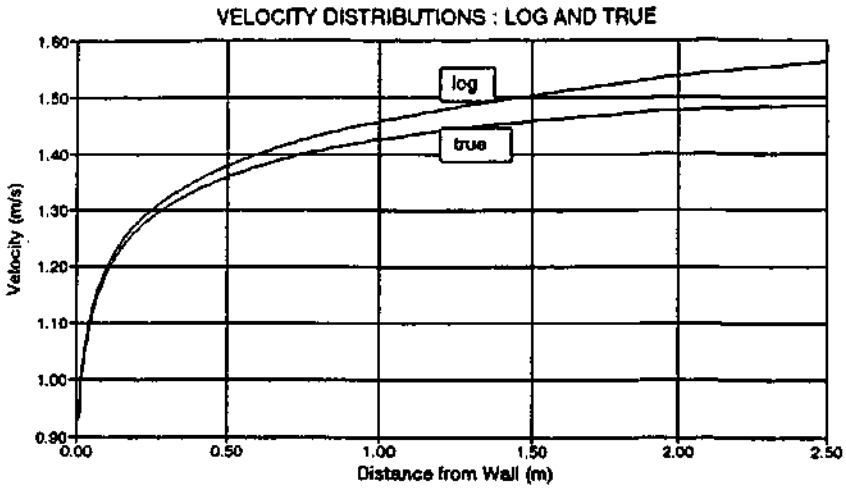

Figure C7 Time averaged velocity distributions across a pipe

Differentiating equation (C12) with respect to y yields

$$\frac{du}{dy} = u_*\sqrt{2\pi}\left[\frac{(1-y/R)^{\frac{1}{2}}}{y}\right]$$

and from this it may be seen that

for y=R du/dy = 0

for y=0 du/dy = $u_*(2\pi)^{1/2}/y$

If the log law equation (C10) is also differentiated with respect to y, the result is

$$\frac{du}{dy} = u_*\sqrt{2\pi}/y$$

By comparison with the derivative of equation (C12) it can be seen, once again, that the log law only holds near the boundary.

On these grounds it is concluded that equation (C12), the true velocity distribution in a pipe,

is more accurate than equation (C9), the universal log law. However, the term u_R (the velocity at the centre of the pipe) in equation (C12) needs further description.

Rearranging equation (C12), using $(2\pi)^{1/2} = 1/\kappa$, yields

$$\frac{\kappa u}{u_*} = 2\sqrt{1-\eta} + \ln\left|\frac{\sqrt{1-\eta}-1}{\sqrt{1-\eta}+1}\right| + C$$

where $\eta = y/R$

$C = \kappa u_R/u_*$

As $\eta \to 0$,

$$\frac{\kappa u}{u_*} \to 2\left(1-\frac{\eta}{2}\right) + \ln\left|\frac{-\eta/2}{2-\eta/2}\right| + C$$

where

$$\lim_{\eta \to 0} \sqrt{1-\eta} = 1-\frac{\eta}{2} + \ldots$$

That is

$$\frac{\kappa u}{u_*} \to \ln(\eta) + 2 - \ln(4) + C$$

From this

$$\frac{\kappa u}{u_*} = \ln\left(\frac{y}{R}\right) + 0.614 + C \qquad \text{(C13)}$$

In order to evaluate C, experimental data is used in the log law equation, which is valid near the wall. The required form of the log law must first be derived.

Recall the concept of eddy viscosity in the relation

$$\tau = \rho(\nu + \epsilon)\frac{du}{dy}$$

(ie by equation C9, $\epsilon = \kappa^2 y^2 \, du/dy$)

Close to the boundary, $\nu \gg \epsilon$ (ie the kinematic dominates over the eddy viscosity), which implies that

$$\tau = \rho\nu\frac{du}{dy} = \mu\frac{du}{dy}$$

Integration of this, using the boundary condition : at y=0, u=0 and $\tau=\tau_0$, yields

$$\frac{u}{u_*} = \frac{yu_*}{\nu} \qquad \text{(C14)}$$

O'Connor (1995) suggests that further from the wall (where $\epsilon > \nu$),

$$\frac{\epsilon}{\nu} \sim \kappa\frac{yu_*}{\nu} \qquad \text{(C15)}$$

Using this relation, by integration of equation (C9) O'Connor gives

$$\frac{u}{u_*} = \frac{1}{\kappa}\ln\left(\frac{yu_*}{\nu}\right) + B_0 \qquad \text{(C16)}$$

where B_0 = constant

This is another form of the log law, equation (C10). (Incidentally this derivation makes the error of including u_* into (C15), which again implies that $\tau=\tau_0$ which is not the case away from the wall).

O'Connor shows that the constant B_0 in equation (C16) has value $B_0 = 5.3 \pm 0.35$, which falls within the range for B_0 found experimentally by Hinze (1975) of $5.0 < B_0 < 5.5$.

From (C16), using $B_0=5.3$,

$$\frac{\kappa u}{u_*} = \ln(\frac{y}{R}) + \ln(\frac{u_* R}{\nu}) + 5.3\kappa \qquad \text{(C17)}$$

Since both the log law and the true velocity distribution (equations C10 and C12 respectively) hold near the boundary, equations (C17) and (C13) must be equivalent. This yields

$$C = \ln(\frac{u_* R}{\nu}) + 5.3\kappa - 0.614$$

Using κ=0.40,

$$u_R = 2.5u_*[\ \ln(\frac{u_* R}{\nu}) + 1.506]$$

which may be used in the true velocity distribution, equation (C12), to give

$$\frac{u}{u_*} = \frac{1}{\kappa}[2z + \ln|\frac{z-1}{z+1}| + \ln(\frac{u_* R}{\nu}) - 0.614] + 5.3 \qquad \text{(C18)}$$

This important equation will now be used to describe the friction factor in smooth pipes, and in a modified form to describe the velocity variation in the body of fully-developed rough turbulent flow.

Turbulent flow in smooth pipes

For smooth turbulent flow, there exists a thin region adjacent to the boundary called the laminar or viscous sub-layer. In this zone flow is always laminar, and du/dy is constant. A constant velocity gradient, du/dy, implies that shear stress, τ, is constant and equal therefore to τ_0. That is, although the shear stress does vary linearly over the entire section, it becomes nearly constant in the very thin region immediately adjacent to the boundary.

This approximation is reasonable when it is realised that δ, the thickness of the viscous sub-layer is less than 1 per cent of the radius of the conduit for low Re (30000) and less than 0.1 per cent for moderate Re (100000).

In figure C8 below, the deviation of the log law (equation C10) from the linear velocity distribution in the laminar sub-layer is shown. The thickness of the laminar sub-layer is denoted by δ.

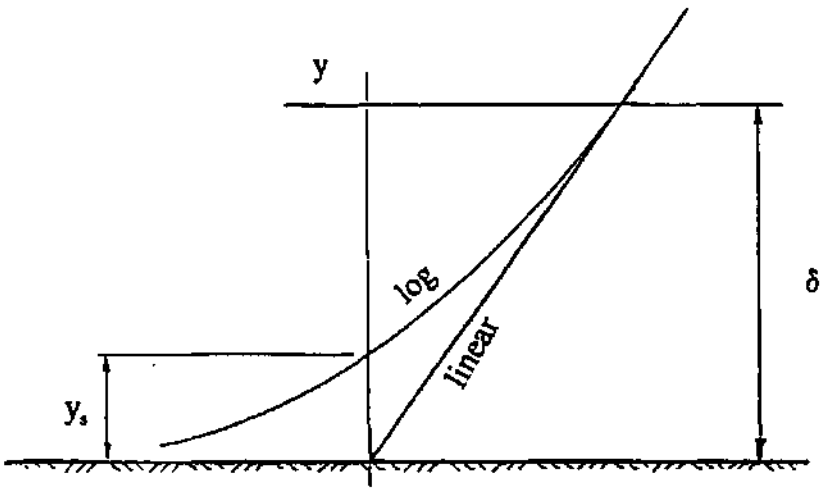

Figure C8 Velocity distribution in laminar sub-layer

Note that at $y=\delta$, $u=u_\delta$. The false origin of the log law is at $y=y_s$ where $y_s \simeq \delta/100$, so that $y_s < R/10^4$ in typical flow. This is the distance from the smooth boundary where, according to equation (C10), the velocity $u=0$, so can be thought to be the wall of the conduit from the turbulent velocity distribution's point of view.

LeGrange and Rooseboom (1993) indicated that power balance in an open channel may be written as :

Input stream power = Applied stream power

That is

$$\int_{y_s}^{D} \rho.g.S.u.dy = \int_{y_s}^{D} \tau \frac{du}{dy} dy$$

where D = depth of flow

Adapting this to pipe flow, the left hand side of the above equation becomes

$$power\ p = \int_{y_s}^{R} \rho.g.h_f.u.dy = \rho.g.h_f.Q$$

Power per unit length is therefore given by

$$\frac{p}{l} = \rho.g\frac{h_f}{l}Q = \int_{y_s}^{R} \tau\frac{du}{dy}2\pi(R-y)dy \qquad \text{(C19)}$$

Now, from equation (C11)

$$\frac{du}{dy} = u_*\sqrt{2\pi}[\frac{(1-y/R)^{\frac{1}{2}}}{y}] = u_*\sqrt{\frac{2\pi}{R}}[\frac{\sqrt{R-y}}{y}] \qquad \text{(C20)}$$

From C9

$$\tau\frac{du}{dy} = \frac{\rho}{2\pi}y^2(\frac{du}{dy})^3$$

and substituting for du/dy from C20,

$$\tau\frac{du}{dy} = \frac{\rho}{y}u_*^3\sqrt{2\pi}(\frac{R-y}{R})^{\frac{3}{2}} \qquad \text{(C21)}$$

so that (C19) becomes

$$\frac{p}{l} = \int_{y_s}^{R} \frac{\rho}{y}u_*^3\sqrt{2\pi}(\frac{R-y}{R})^{\frac{3}{2}}2\pi(R-y)\ dy$$

or

$$\frac{p}{l} = \rho u_*^3.\phi(R, y_s)$$

$$where \quad \phi(R, y_s) = \left(\frac{2\pi}{R}\right)^{\frac{3}{2}} \int_{y_s}^{R} \frac{(R-y)^{\frac{5}{2}}}{y}\, dy$$

By definition of friction factor, f

$$u_*^3 = \left(\frac{fu^2}{2}\right)^{\frac{3}{2}}$$

Combining the above two relations with equation (C19) yields

$$h_f = \frac{4flu^2}{2gd} \cdot \frac{f^{\frac{1}{2}}}{\pi d\sqrt{2}} \cdot \phi(R, y_s)$$

and this yields

$$\frac{f^{\frac{1}{2}}\sqrt{\pi}}{R^{\frac{5}{2}}} \int_{y_s}^{R} \frac{(R-y)^{\frac{5}{2}}}{y}\, dy = 1 \qquad \text{(C22)}$$

Integrating and simplifying gives

$$\frac{1}{\sqrt{f}} = -2\frac{\sqrt{\pi}}{R^{\frac{5}{2}}}\left[\frac{(R-y_s)^{\frac{5}{2}}}{5} + \frac{R(R-y_s)^{\frac{3}{2}}}{3} + R^2(R-y_s)^{\frac{1}{2}} + \frac{1}{2}R^{\frac{5}{2}}\ln\left(\frac{\left|(R-y_s)^{\frac{1}{2}} - R^{\frac{1}{2}}\right|}{(R-y_s)^{\frac{1}{2}} + R^{\frac{1}{2}}}\right)\right] \qquad \text{(C23)}$$

For $y_s \ll R$ (which is generally the case as seen above), the above equation (C23) may be approximated by the very much simpler form

$$\frac{1}{\sqrt{f}} = -2\sqrt{\pi}\left(\frac{1}{5} + \frac{1}{3} + 1 + \frac{1}{2}\ln\left(\frac{y_s}{2d}\right)\right)$$

which reduces to

$$\frac{1}{\sqrt{f}} = \sqrt{\pi}\left[\ln\left(\frac{2d}{y_s}\right) - \frac{46}{15}\right] \qquad \text{(C24)}$$

Within the viscous sub-layer, only laminar flow occurs and so the relation $\tau=\mu(du/dy)$ holds. This may be integrated using the boundary conditions $u=0$ and $\tau=\tau_0$ at $y=0$. Combining this with the log law and equation (C14) gives

$$\frac{u_\delta}{u_*} = \sqrt{\pi}\,\ln\left(\frac{\delta}{y_s}\right) = \frac{\delta u_*}{\nu}$$

Now, the thickness of the laminar sub-layer is given by (Rouse 1950)

$$\frac{\delta u_*}{\nu} = \frac{u_\delta}{u_*} = \sqrt{\pi}\,\ln\left(\frac{\delta}{y_s}\right) = 12 \pm 4$$

By experiment it has been found that (Rouse 1950)

$$\frac{\delta}{y_s} = 105$$

which implies that

$$\frac{\delta u_*}{\nu} = 11.63$$

which is within the expected range.

If it is assumed that this is an accurate relationship, then

$$y_s = \frac{\delta}{105} = \frac{11.63\nu}{105u_*}$$

and this when substituted into equation (C18) yields the following :

$$\frac{1}{\sqrt{f}} = \sqrt{\pi}\,\left[\ln\left(\frac{2d.105.u_*}{11.63\nu}\right) - \frac{46}{15}\right]$$

which simplifies to

$$\frac{1}{\sqrt{f}} = 4.08 \log_{10}(Re\sqrt{f}) - 0.921 \qquad \text{(C25)}$$

For comparison, Massey gives the following equation for turbulent flow in smooth pipes :

$$\frac{1}{\sqrt{f}} = 4\log_{10}(Re\sqrt{f}) - 0.4 \qquad \text{(C26)}$$

The difference between the constants in the above equation and equation (C25) is directly due to the sub-layer thickness estimate.

For $\delta u_*/\nu = 8$, constant = -2.84

$\delta u_*/\nu = 16$, constant = +1.61

$\delta u_*/\nu = 12.563$, constant = -0.4 (as in equation C26)

Since the values of $\delta u_*/\nu$ and δ/y_s are obtained experimentally, and not known to a high degree of accuracy, the constants in equations (C25) and (C26) are both acceptable.

Note that the only assumptions made here (other than Newtonian mechanics applied to fluid flow) are the experimentally-derived relationships :

- the value of the mixing length constant, κ, in the Prandtl mixing length law
- $\delta = 105y_s$ from experimental data.

These two assumptions are equivalent to fitting the constant in equations (C25) and (C26) to data derived from experiments on pipes flowing smoothly.

Thus, using basic fluid dynamic equations together with power balance in pipe flow over a smooth surface, the generally-accepted smooth law equation has been derived. Exactly the same principles will therefore be applied in deriving an equation for rough flow.

Turbulent flow in rough pipes

The geometry as used for smooth pipes needs to be modified for the derivation of rough flow equations. In a personal communication, Rooseboom (1995) suggested that energy lost in flow over rough surfaces is due to eddies formed at the boundary. He proposed a model (see LeGrange & Rooseboom 1993) of a cylindrical eddy formed behind a roughness element on the boundary, as shown in figure C9 below.

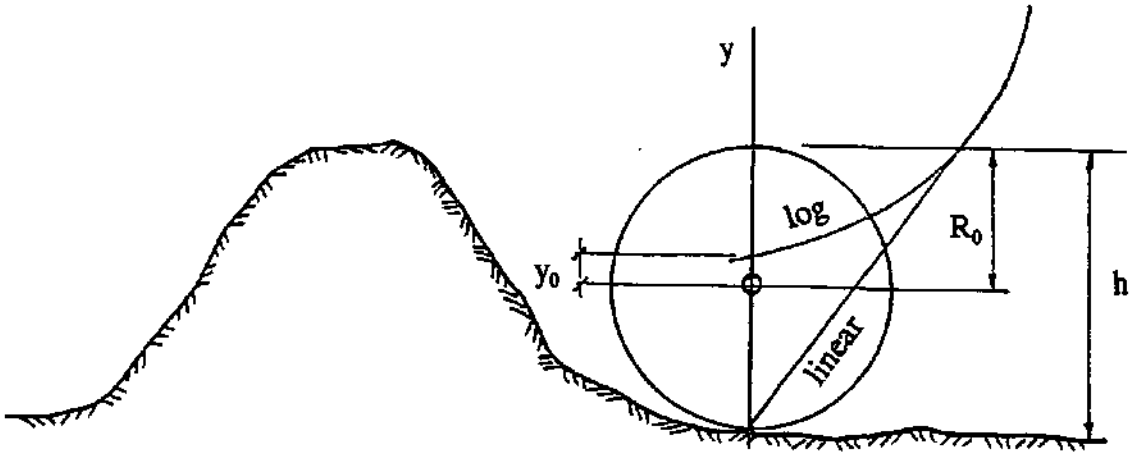

Figure C9 Eddy formed behind roughness element

In this model, the shear stress is assumed constant over the eddy as was done for the laminar sub-layer when dealing with a smooth boundary. This is predicted in the assumption that the eddy is not only rotating as a forced vortex (fixed cylinder) but rolling along the solid surface so that there is a linear variation of velocity vertically over its diameter. The diameter of the cylindrical eddy is equal to the height of the roughness element producing it, and the origin for y is at the centre of the eddy, O.

Input stream power may then be written

$$\int_{y_0}^{R} \rho.g.S_0.u \; dy$$

Using the same arguments and derivations as for the smooth boundary because the geometries

of the velocity distributions in figures C8 and C9 are the same, leads immediately to an equation like (C24),

$$\frac{1}{\sqrt{f}} = \sqrt{\pi}\,[\,\ln(\frac{2d}{y_0}) - \frac{46}{15}\,] \qquad \text{(C27)}$$

the only difference being that y_s is replaced by y_0.

Again, from the point of view of the velocity distribution, the wall of the pipe is at y_0, but the origin of the flow is at y=0, midway between troughs and crests of the bumps.

Now, using the linear velocity distribution over the eddy (implied by the constant shear stress assumption), at $y=R_0$, $u=2u_0$, where u_0 is the velocity at the centre of the eddy. The corresponding velocity at $y=R_0$ found using the log law (which has been shown to be valid near the boundary) is

$$u_0 = \frac{1}{2}\sqrt{2\pi}u_*\,\ln(\frac{R_0}{y_0}) \qquad \text{(C28)}$$

Not only must velocities from both the logarithmic and linear velocity distributions match at $y=R_0$, but so too must the velocity gradients. Using the linear velocity distribution,

$$\frac{du}{dy} = \frac{u}{y} = \frac{u_0}{R_0}$$

Using the logarithmic variation

$$\frac{u_0}{R_0} = \frac{\sqrt{2\pi}u_*}{y}$$

Substituting from equation C28 for u_0 yields

$$\frac{R_0}{y} = \frac{1}{2}\ln(\frac{R_0}{y_0})$$

and at the point where $y = R_0$,

$$\frac{R_0}{y_0} = \exp(2) = 7.39$$

To illustrate the application of this, consider an otherwise smooth surface uniformly covered with single-sized sand grains of diameter k. By definition, k is as quoted by Nikuradse (1933). The effective boundary of the flow occurs at k/2 from the smooth surface. The radius of the eddy resulting from one such sand grain is given by $R_0 = k/4$, as shown in figure C10 below.

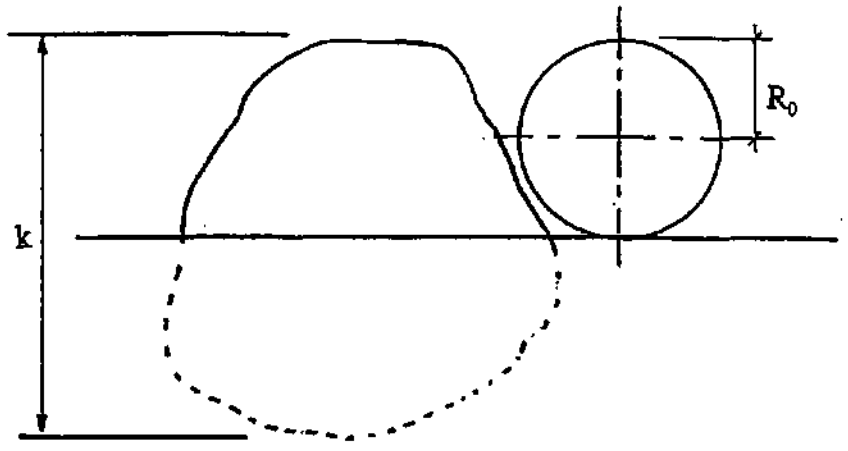

Figure C10 Grain diameter vs eddy size

Now, $R_0 = 7.39\ y_0$, and $k = 4R_0$.

Therefore

$$y_0 = \frac{k}{30} \qquad \text{(C29)}$$

which is a result quoted by many authors, corroborating the assumption made in the derivation of equation (C28).

This result may be used in equation (C27) to give

$$\frac{1}{\sqrt{f}} = 4.08 \log_{10}\left(\frac{d}{k}\right) + 1.82 \qquad \text{(C30)}$$

This compares favourably with the fully-developed turbulent flow equation for rough pipes found in Massey (equation 8.51) which is given by

$$\frac{1}{\sqrt{f}} = 4 \log_{10}\left(\frac{d}{k}\right) + 2.28 \qquad \text{(C31)}$$

Once again, the constants in the two equations differ. However, they do not differ by very much and the resulting f-values given are very similar as shown in Table C1 below.

Table C1 Comparison of equations (C30) and (C31)

k/d	f (C30)	f (C31)
0.0001	0.0030	0.0030
0.0004	0.0041	0.0040
0.001	0.0051	0.0049
0.004	0.0074	0.0071
0.01	0.0100	0.0095
0.04	0.0177	0.0161

The corroboration between these two equations demonstrates that the thinking behind the derivation of equation (C30) is a reasonable model of the reality which is phenomenologically described by equation (C31). This point is crucial, because the assumptions underlying the fluid interaction and the geometry of the boundary helps to give precision to the meaning of k and y_0. In particular, it is now clear that the "edge" of the pipe in rough turbulent flow is midway between troughs and crests of the roughness.

As further evidence of the correctness of the assumptions made here, using equation (C12), the velocity defect may be written

$$\frac{u_R - u}{u_*} = -\sqrt{2\pi}(2z + \ln|\frac{z-1}{z+1}|)$$

which is now compared to some experimental results.

Together with the log law, this is plotted against data obtained by Laufer (1954) in figure C11 below. As can be seen, the equation derived in this study (equation (C12)) fits these data very well.

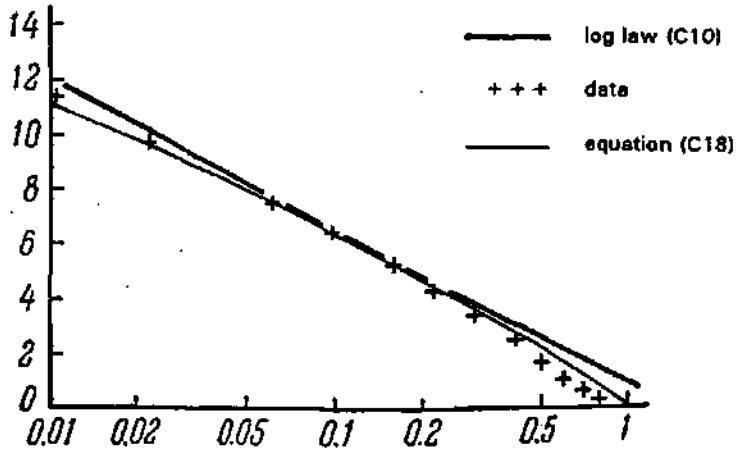

Figure C11 Verification of the velocity defect law for turbulent flow in a tube (Monin and Yaglom, 1971).

Turbulent Flow in a Wide Rectangular Channel

Although not of major significance in this study, the equation relating u and u_* for a wide rectangular channel may be derived using equation (C9).

The variation of shear stress with depth in such a channel is given by

$$\tau = \tau_0(\frac{D-y}{D})$$

where D = depth of flow

Substituting this into equation (C9) and performing the same operations as before yields

$$u = u_* \sqrt{2\pi} \left(2z + \ln\left|\frac{z-1}{z+1}\right|\right) + u_D$$

where u_D = velocity at y=D

When combined with power balance in an open channel, the resulting equation in terms of friction factor, f, is

$$\frac{1}{\sqrt{f}} = -2\frac{\sqrt{\pi}}{D^{\frac{3}{2}}}\left[\frac{(D-y_0)^{\frac{3}{2}}}{3} + D(D-y_0)^{\frac{1}{2}} + \frac{1}{2}D^{\frac{3}{2}}\ln\left(\frac{\left|(D-y_0)^{\frac{1}{2}} - D^{\frac{1}{2}}\right|}{(D-y_0)^{\frac{1}{2}} + D^{\frac{1}{2}}}\right)\right]$$

which is comparable to equation (C23) and, for $y_0 \ll D$, simplifies to

$$\frac{1}{\sqrt{f}} = \sqrt{\pi}\left[\ln\left(\frac{2D}{y_0}\right) - \frac{8}{3}\right]$$

APPENDIX D

SELECTION OF METHODS RELATING PHYSICAL ROUGHNESS TO HYDRAULIC RESISTANCE

In this appendix various methods of obtaining hydraulic resistance from physical roughness are examined. Firstly, it is shown how the methods proposed by Morris (1955 and 1959) were to be used, and then how these were found to be inappropriate. Thereafter the details of the data from concrete pipes and sinusoidal roughnesses, used for testing the remaining methods, are presented. Lastly, the actual test results of these methods when applied to the data under consideration are given, and from these the most accurate method(s) are selected.

D1 Methods suggested by Morris (1954 and 1959)

Morris (1954 & 1959) presented a rational method of calculating friction factor, f, using physical roughness dimensions for each of the five flow types he identified. The equations for each case will first be elaborated upon, and then it will be shown how these might be applied to the tunnels sampled in this study. His five sets are :

- For "smooth turbulent" flow, the friction factor may be obtained from the smooth law equation (from equation (C26))

$$\frac{1}{\sqrt{f}} = 4 \log_{10} Re\sqrt{f} - 0.4$$

- For "normal turbulent" flow

$$\frac{1}{\sqrt{f}} = 4 \log_{10}\left(\frac{r}{\lambda}\right) + 3.5$$

where r = radius of pipe

λ = longitudinal spacing of roughness elements.

- "Semi-smooth turbulent" flow (or isolated roughness flow) occurs when an otherwise

smooth surface is interspersed with isolated roughness elements. The overall friction factor is obtained by summing the f's due to the different textures. That is

$$f = f_s + \frac{C_D}{\lambda/h}\left(\frac{u_w}{\bar{u}}\right)^2\left(1-\frac{ns}{P}\right)$$

where

f_s	=	smooth conduit friction factor
n	=	number of individual elements in periphery
s	=	clear peripheral spacing between elements
P	=	wetted perimeter
C_D	=	coefficient of drag of elements
u_w	=	velocity at roughness crests

Nikuradse (1933) showed that

$$\left(\frac{u_w}{\bar{u}}\right)^2 = 16.8\, f_s$$

Morris suggested that if this is assumed to be valid here then, as an approximation, the above relation can be used to give

$$f = f_s\left[1+\frac{16.8\ C_D}{\lambda/h}\left(1-\frac{ns}{P}\right)\right] \qquad \text{(D1)}$$

Equation (D1) was tested by Morris using experimental test results and was shown to produce acceptable agreement with measured friction factors.

• When dealing with "hyper-turbulent" (or wake interference) flow, there is no part of the wall over which a laminar boundary layer exists. Because the wakes from successive elements interfere with each other, individual effects are not linearly additive. Morris gives the following equation for this type of flow :

$$\frac{1}{\sqrt{f}} = 4\log_{10}\left(\frac{r}{\lambda}\right) + 3.5 + \Phi\left(\frac{Re\sqrt{f}}{r/\lambda}\ ,\ shape\right) \qquad \text{(D2)}$$

The function Φ has been shown to decrease with increasing Re and may be regarded as a transition function, the magnitude of which decreases as the width of the zone of intense

turbulence near the wall decreases. The exact form of this transition function is dependent on the shapes of the roughness elements and must be determined experimentally. For high Re this equation approaches that for his "normal" turbulent flow, where f is primarily dependent on the roughness spacing and is described by the first two terms on the right-hand-side of equation (D2).

• For "quasi-smooth" or skimming flow, Morris proposed that the total energy consumed is a sum of that required to maintain the flow in a smooth pipe, and of that required to maintain the stable vortices situated between the closely-spaced roughness elements.

He suggests that an approximate friction factor equation for this is given by

$$f = f_s + \frac{(c_w u_w / \bar{u})^3}{\lambda/(\min [j, h])} \qquad \text{(D3)}$$

where c_w = constant such that $c_w u_w$ = velocity at vortex perimeter

If a surface has such variable roughness that flow of more than one type is produced, then Morris states that friction factors for each type may be added together to give the apparent friction factor for the surface as a whole.

For closely-spaced roughness elements, wake interference or hyper-turbulent flow is usually produced. Where there are, for example, two different sizes of roughness elements present, the overall effect is one of the combined effects of each of the two roughness sizes. If the roughness elements are predominantly of one size, with occasional larger elements, then the wake-interference phenomena will be controlled by the smaller elements, with the larger elements contributing to the overall roughness as isolated elements.

The experiments performed by Colebrook and White (1937) illustrated this. At low Re the thickness of the viscous sub-layer, δ, is large and the isolated roughness effect of the larger elements controlled the flow. As Re increases and δ decreases, so the smaller grains become more effective, producing wake-interference flow.

Morris states that wake-interference flow is not usually encountered in practice and that most commercial pipes would be more likely to exhibit skimming or isolated roughness flow.

In the early parts of this study, and drawing from Morris's arguments an initial attempt was made to link physical and hydraulic roughness at high Reynolds numbers. Isolated roughness flow was assumed, and data from the tunnels sampled in this study were considered, so that effects of roughness could be linearly added. Equation (D1) may be written as

$$f = f_s[1 + G.\frac{h}{\lambda}] \qquad \text{(D4)}$$

where

$$G = 16.8\ C_D(1 - \frac{ns}{P}) \qquad \text{(D5)}$$

is essentially constant for a given conduit.

By definition, the area under a power spectrum is equal to the variance of the input data. So, for frequency ϕ_i, the portion of the total variance associated with the corresponding wavelength, λ_i, is equal to $C_{xx}(\phi_i).d\phi$.

Now, from equation (2.1), $a=\sqrt{2}\sigma$, and the bump height h_i, which is twice the amplitude, associated with this elemental sinusoid is given by

$$h_i = 2\sqrt{2.C_{xx}(\phi_i).\Delta\phi}$$

Data from the scanner takes the form of distances measured from a base-line at 0.5mm intervals. Therefore, since frequency is the inverse of wavelength,

$$\frac{h}{\lambda} = 2.h.f$$

Substitution of this into equation (D4) gives :

$$f = f_s[1 + 4\sqrt{2}.G.\phi_i\sqrt{C_{XX}(\phi_i)}\ (\Delta\phi)^{\frac{1}{2}}]$$

This gives the contribution to the overall friction factor for the specific roughness of wavelength λ_i. In order to calculate this for the entire surface, the effects of all relevant wavelengths need to be summed. This leads to the formula

$$f = f_s[1 + \sum_{i=1}^{n} [\phi_i\sqrt{C_{XX}(\phi_i)}].4\sqrt{2}.G.(\Delta\phi)^{\frac{1}{2}}] \qquad \text{(D6)}$$

Once the power spectrum has been calculated, and the relevant information obtained from it, the only unknowns in this equation are G and $\Delta\phi$. The constant G is related to the coefficient of drag of the roughness elements (ie shape), as well as the proportion of area obstructing the flow. Morris (1959) gives values for C_D for various shapes of roughness elements. For completely random roughness, the value of (1-ns/P) must be equal to 0.5 (statistically). The problem arises in the selection of the value of $\Delta\phi$.

The concrete pipe data were used to calibrate this formula. Since f for these pipes is known, the value for the constant G may be found.

Equation (D6) requires calibration before it can be used directly in the calculation of friction factor as there is more than one unknown in the equation.

The smooth flow friction factor, f_s, may be found using equation (C26). The constant $G = 16.8\ C_D(1\text{-}ns/P)$.

Let

$$G' = 4\sqrt{2}\ (\Delta\phi)^{\frac{1}{2}}\ .G \qquad \text{(D7)}$$

Then equation (D6) may be re-stated as

$$f = f_s[1 + G'(\sum_{i=1}^{n} \phi_i \sqrt{C_{xx}(\phi_i)})] \qquad \text{(D8)}$$

The summation in this equation may be performed from the power spectrum calculated for each data set, and for known values of f and f_s, the equation may be solved for G'. This value of G' may then be used in the formula for data taken from a surface of unknown f. In this way the concrete pipe data (both f and f_s known) are used to evaluate the constant G', and, in so doing, calibrate equation (D6).

For each of the pipes sampled a value of G' was calculated, the mean of which was G'=0.174. As an initial test, the value of G'=0.17 was used in the formula applied to selected roughness data taken from sandstone, granite/gneiss and shotcrete surfaces.

From this initial test, it was found that resulting values for friction factor f were generally unacceptably high. Representative values from selected data sets for the different surface types are given below :

sandstone	f=0.0038	to	f=0.01005 (n=0.0144 to n=0.0235)
granite	f=0.00678	to	f=0.0086 (n=0.0182 to n=0.0205)
shotcrete	f=0.0101	to	f=0.0139 (n=0.0219 to n=0.0257)

Therefore, before proceeding further the method was checked and it was found that assumptions on which the various equations were based were not entirely applicable, because of the following argument.

The isolated roughness equation (equation D1) was made by Morris to depend on the relation, derived by Nikuradse, $(u_*/\bar{u})^2 = 16.8f_s$. This leads to equation (D4).

For any particular surface, Gh/λ is constant, being purely defined by roughness geometry. Therefore, by equation (D4), the ratio f/f_s must be constant. The Moody diagram indicates that for fully turbulent, rough flow, f becomes constant while f_s continues to decrease with increasing Re. Therefore f/f_s cannot remain constant over the whole range of Re applicable

in rough turbulent flow. This indicates that the method developed by Morris leading to equation (D8) above is not valid. Since flow in water tunnels is likely to occur for Reynolds number of the order of $5x10^6$, this method, which employs simple linear superposition of roughness effects, is discarded from further analysis.

D2 Concrete pipe and artificial sinusoidal roughnesses

Concrete Pipes

The scanner was used in the collection of roughness data from a number of spun concrete pipes ranging in diameter from 900mm to 1500mm. Assuming k=0,3mm (lower end of range suggested in Figure (C4) due to Massey, 1989) a value calculated using equation (C4) for Manning's n in such pipes yields n=0.0110. It is felt that this figure would apply only to those pipes manufactured under strict quality control, and that slightly higher values for n may be more representative of most pipes actually used in practice.

From the physical roughness data obtained by the scanner from the pipes sampled, values for Manning's n were estimated, using the various methods presented in Chapter 3. These results are presented in Table D1 below.

Table D1 Mean values for Manning's n in concrete pipes estimated by various methods

method	Manning's n
A : Heerman, equation (3.5)	0.0100
B : Colebrook-White, $k=h_\sigma=2.83\sigma$	0.0117
C : Colebrook-White, $k=2h_\sigma=5.66\sigma$	0.0126
D : Colebrook-White, $k=h_\lambda$	0.0113
E : Colebrook-White, $k=2h_\lambda$	0.0122
Expected value from eg. C4	0.0110

From Table D1 the following can be noted :

- Method A yields the most accurate results when compared to the expected value for n (exactly equal).

- Methods C and E (using k=2h) are the least accurate.

- Methods B and D are reasonably accurate and give very similar results on the expected "high" side of n=0.010.

Sinusoidal roughnesses

Not only did Heerman (1968) present a method for calculating f from physical roughness, but he also presented the experimental data on which this was based. A number of roughness types were tested, ranging from random soil roughness to artificial roughness comprising roughness elements of known size and shape stuck to a smooth boundary. In attempting to find a link, if any, between resistance to flow and longitudinal spacing of roughness, Heerman tested circular conduits with sinusoidal boundary roughness, using air as the fluid. The dimensions (namely amplitude and wavelength) of the sinusoids tested were given, and since these dimensions are sufficient to uniquely describe each sinusoid, roughness data of the same form could be analysed to test the methods presented in Chapter 4.

Heerman used nine different boundary sinusoids, consisting of three different wavelengths and three different amplitudes obtained by casting plaster in 150mm diameter pipe (the internal diameters varied with the roughness used). The standard deviations of the surfaces were measured by two methods. The first was from the average peak to valley amplitude ($\sigma 1$) and the second from equally-spaced measurements on the roughness profile ($\sigma 2$).

The dimensions of the nine different sinusoidal roughnesses are given in Table D2 below. The diameters of the pipes vary with the various roughness configurations. These diameters were measured by dividing the volume enclosed by a length of a pipe section by the length,

which is nearly equivalent to the suggestion made in Appendix C, which is that the effective wall should be at the mid range of the roughness elements.

Table D2 Sinusoidal Roughnesses (Heerman 1968)

pipe no.	dia (m)	wavelength (mm)	amplitude (mm)	$\sigma 1$ (mm)	$\sigma 2$ (mm)
1	0.1035	150	8.75	6.19	6.97
2	0.1025	76	8.50	6.01	7.07
3	0.1171	150	3.54	2.50	2.61
4	0.1161	76	3.26	2.31	2.47
5	0.1135	150	1.22	0.86	0.91
6	0.1148	76	1.55	1.10	1.15
7	0.1173	38	0.88	0.63	0.79
8	0.1159	38	2.65	1.88	1.93
9	0.1068	38	9.02	6.38	7.39

For each roughness, Heerman made head loss measurements at various values of Re. From each of these the shear velocity u_* was calculated, and this was used to calculate friction factor, f. Knowing the physical dimensions of boundary roughness and the corresponding f-value for each pipe, the methods of Chapter 4 could be tested for accuracy.

The results obtained by Heerman are presented graphically in Figure D1 below. Evident in this figure is that pipes of different roughness were not all tested over the same range of Re. There was some concern as to whether or not complete rough turbulence had been attained in each case, as the values for f for certain pipes appeared not to become constant with Re, and most formulae used for determination of f assume rough turbulence. Therefore, for the comparison of measured and calculated f-values, the friction factors for the highest Reynolds numbers in each pipe were used. Figure D2 shows these comparisons.

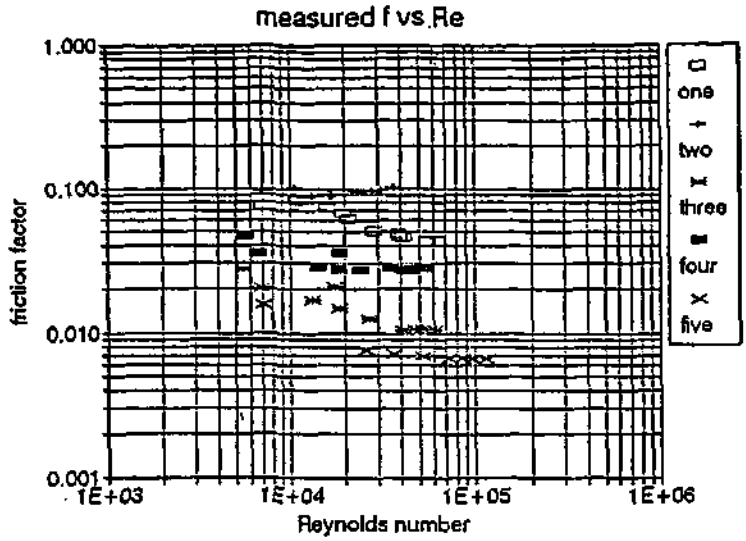

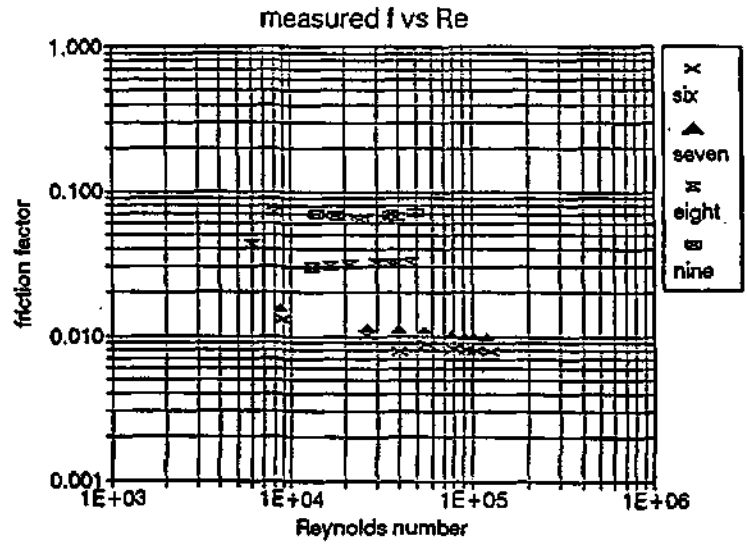

Figure D1 Friction factor vs Re for sinusoidal roughnesses

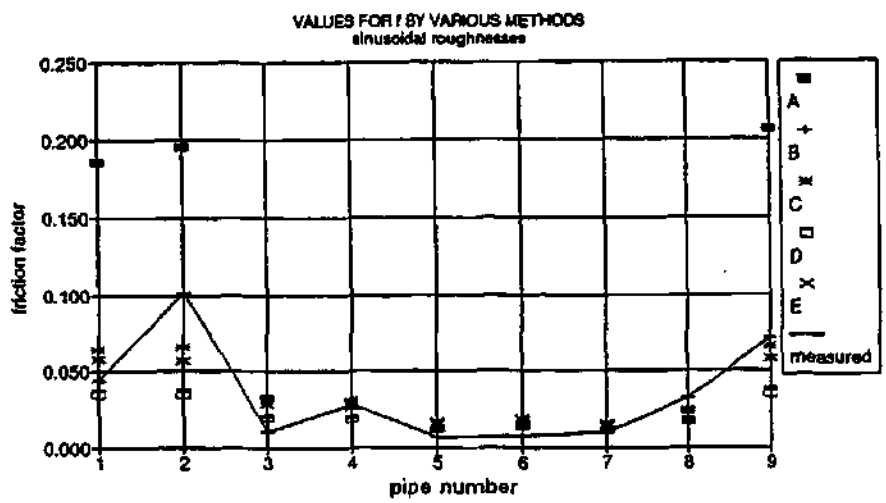

Figure D2 Comparison of f-values obtained by various methods

From figure D2, and by reference to the Moody diagram, it can be seen that pipes 1, 2 and 9 are unrealistically rough. This is also evident when considering the pipe geometry presented in Table D2. If the approximation is made that k=h (which has been shown to be reasonable), then k/d ratios for pipes 1, 2 and 9 are 0.17, 0.16 and 0.17 respectively, all of which are off the scale of the Moody diagram.

As shown in figure D2, all formulae proposed, including that by Heerman himself, give values of f very different to those measured in these three pipes. In the remaining pipes, the measured and calculated friction factors do seem to correspond fairly well.

It is true that the methods presented all assume fully-developed rough turbulent flow over surfaces of random roughness. Here, sinusoidal roughness is being considered which will (according to figure C2 and its associated argument) exhibit slightly different behaviour over the transition range of Re. The measured f-values used in this comparison are those taken at the highest values of Re. For pipes 3 to 8, these are as presented in Table D3, together with the corresponding approximate k/d values (calculated making the assumption that k=h).

Table D3 Reynolds number and k/d ratio

pipe number	Re	k/d
3	6.05×10^4	0.06
4	5.29×10^4	0.06
5	11.43×10^4	0.02
6	12.45×10^4	0.027
7	11.99×10^4	0.015
8	4.62×10^4	0.046

From the Moody diagram it can be seen that these combinations of Re and k/d all ensure that the respective f-values are for fully rough turbulent flow. Consequently, the characteristic "dip and rise" of the f-Re curve for pipes of regular (as opposed to random) roughness should not have any influence on the comparisons being made.

In order to select the formula (or method) yielding the most accurate values for f (compared to those measured), the sums of the squares of the deviations from the measured f-values for each method were calculated. The results for pipes 1, 2 and 9 were omitted. Table D4 below shows the values of the sums of squares for each method.

Table D4 Sums of Squares of differences between measured and predicted friction factors using Heerman's data

Method	sum of squares
A : Heerman	0.000637
B : $k=h_\sigma$	0.000461
C : $k=2h_\sigma$	0.000663
D : $k=h_\lambda$	0.000463
E : $k=2h_\lambda$	0.000612

From the above table, methods B and D are seen to be the most accurate. This indicates that the assumption that k=h is better than that of k=2h with the Colebrook-White equation. Also shown here is the lack of dependence on the method used for evaluating h (ie mean range and variance yield similar results for f). It is strange that method A (Heerman) does not yield results of a satisfactory degree of accuracy over surfaces created by him for his study, but is not surprising in the light of the careful fluid dynamic arguments presented in Appendix C.

Summary

From the testing of methods over the two different surface types given above, the most accurate method for the calculation of f from physical boundary roughness measurements is method B closely followed (within 0.5% of the sum of squares of difference) by method D. The method of choice is method D because it is more robust statistically than method B. This

method (D) involves the use of the roughness height, h_λ, calculated by the mean range technique. This value for h_λ is then used in the Colebrook-White equation with $k=h_\lambda$ to yield the estimate for friction factor.

It has also been shown that using the standard deviation instead of the mean range in the estimate of h yields results of a comparable degree of accuracy.

APPENDIX E

GUIDELINES FOR THE COLLECTION OF PHYSICAL ROUGHNESS DATA AND USE OF DATA ALREADY COLLECTED

The purpose of this chapter is provide all the necessary and useful information which would be required to either operate the scanner in collecting further physical roughness data, or to make full use of that data already collected and used in this study.

There are certain basic pieces of apparatus without which data collection is not possible. Other items which have been found useful are also mentioned here which, although not essential, have been found to improve efficiency.

E1 Basic Apparatus

* To start with, obviously the laser scanner itself is the single most important piece of apparatus. There is an on/off switch next to the fuse on the left hand side (as the scanner faces the wall) of the box mounted on top of the protective casing. On the right hand side is the power input. This power is delivered by the 12 Volt scanner batteries (of which there are four, two of which are connected in parallel for use at any one time - the other two are for backup). At the back of the box is the computer cable jack plug, as well as the wire to the laser unit itself, which sits within the casing.

* The scanner is supported by the T-bar leg, which has a height adjustor which is needed for triple-run scanning. All three of these are separate items.

* The computer and light used for photography are both powered by the 12 Volt accumulator. The computer has a rechargeable battery which supplies its power while the light is connected to the accumulator.

* The computer and scanner are connected via a cable which runs from the serial port of the computer to the jack plug at the back of the box on the scanner casing.

* The software that drives the apparatus is called "SCANNER.EXE" and is stored on the hard drive of the computer. It may also be found on the disk in the sleeve at the back of this document. A brief description of how this friendly program is used is given later. Because each data set is plotted on the screen, it was found convenient to run a batch file which would enter a spreadsheet for this plotting each time the program SCANNER was exited.

* Spraypaint and paper towel were used extensively in surface preparation. All wet areas were mopped dry, and over those zones where reflectivity was considered a potential problem, spraypaint was applied. A feel for those areas requiring painting is soon gained, and this speeds up the process.

* For the purpose of photographing the wall, it is considered essential that side-lighting be used. In this way the relief of the wall is highlighted. The light should be set up two to three metres upstream or downstream of the relevant wall section. Use of a low-light film, such as 400 ASA, is strongly recommended.

E2 Peripherals

* The painting guide is a strip of timber mounted on a cross-piece which may be inserted into the T-bar leg in the same way as the scanner. When this is done, the top of the horizontal timber lies slightly below the line along which the scanner will read when placed in the same position. Spraypaint is then applied along the top of this in a 50-70mm wide band. This ensures that the paint is applied in the correct place for the scanner to read over, and minimises wastage.

* The paint is also used to indicate chainage in the photographs where necessary (ie where there are no existing chainage plates).

* To minimise damage to delicate equipment, foam rubber was placed on the flatcar on top of which the apparatus was placed. This was particularly important for the trips into and out of the tunnel, which were done at higher speed than the short distances between set ups.

* A large plastic sheet was used to cover the equipment when not in use. This was done to prevent water dripping from the tunnel crown from damaging the apparatus.

* Since tunnels are notoriously wet and muddy, gumboots are considered essential footwear.

* A torch also proved useful, as did cap-lamps for hard hats, in the darkness of the tunnels.

* A battery charger was made for charging the scanner batteries. Use of this ensured that these batteries were always fully-charged, and could serve as a backup for the accumulator if needed. The charger was not needed inside tunnels.

E3 Operation

The finer details of the operation of the apparatus are given here, extending the overview given in Chapter 2.

Once all the equipment has been connected correctly, the scanner and computer are switched on. The program SCANNER is then run which immediately offers the user three options. Options 1 and 3 are self-explanatory, and option 2 should never need to be used, but was developed for the designer to check on the operation of the apparatus. The program then prompts the user for certain information pertaining to the section to be scanned. The date and time are inserted automatically from the system date and time of the computer. The data file path is specified for the place in which the roughness data is to be stored. The default of this is to store the data in the same place as that from which the program SCANNER was run. Under tunnel name, the operator may specify the prefix of the file save name. The default of this is to assign the prefix "DATA" to all files. The extension is the suffix for the file save name, and this is a number which is automatically incremented as data sets are obtained (ie from 001 for the first to, say, 010 for the tenth data set of that tunnel). For example, the sixth set of data will be named DATA.006. Chainage, rock type, rock condition and description are all to be entered by the user. Two step sizes are available, namely 0.5 and 0.25 mm. These are specified in hundredths of a millimetre, ie either 50 or 25 hundredths. The program will then prompt the user for verification of the input details of the scan about

to be performed. If the answer "y" for yes is given, the scanner is started. First the laser unit is moved to the end of the track, from which it will begin to scan. It then moves along, taking distance readings in the interval specified. The data read from the wall is passed immediately to the computer, and can be viewed on the screen as it passes into memory.

E4 Making use of Collected Data

All of the tunnel roughness data collected in this study have been stored in archive form on the stiffie diskettes in the sleeve at the back of this document. The file compressor, PKZIP, was used to compress the files, and is included on the diskettes, together with the program PKUNZIP, which uncompresses the files for use. Each complete set of compressed data files from a tunnel is stored under a relevant name. These names are as follows :

EMOL.ZIP	-	data from Emolweni Tunnel
CLER.ZIP	-	data from Clermont Tunnel
NGJS.ZIP	-	data from Ngoajane South Drive
NGJN.ZIP	-	data from Ngoajane North Drive

To uncompress any of these, run PKUNZIP. For example, to unzip the Emolweni Tunnel data, type "pkunzip emol". The program PKUNZIP together with the zipped file must be installed in the directory in which the unzipped data is required. Help in using PKZIP and PKUNZIP is obtained by typing "PKZIP", with no extension.

Data sets taken from individual setups are numbered sequentially, in the order in which they were taken, and are written in ASCII format, which may easily be imported into other packages for analysis.

Each file contains a descriptive header, as well as the physical roughness data. Figure E1 below shows the first few lines of the file called C:\QPRO\DATA.015. Below the header, the left-most number is the step number at which the corresponding distance reading was taken. The distance between steps is specified by the user as *stepsize* (in hundredths of a millimetre). Thus in figure E1 the interval is 0.5mm.

Operator Name : Pennington
Date : 06/03/1994
Time : 11:29
Data File Path : C:\QPRO\
Tunnel Name : DATA
Extension : 015
Chainage : 0000003900
Rock type : granite
Rock condition : dry, dusted
Description : fissured

Stepsize 1/100mm: 50
Distance = voltage/4.096*40.0
0000 Voltage= 0.000 Distance= 0.00
0001 Voltage= 3.955 Distance= 38.62
0002 Voltage= 3.943 Distance= 38.50
0003 Voltage= 3.945 Distance= 38.52
0004 Voltage= 3.951 Distance= 38.58
0005 Voltage= 4.008 Distance= 39.14

Figure E1 SCANNER data sample

APPENDIX F

PHOTOGRAPHS OF TUNNEL WALLS USING SIDE LIGHTING

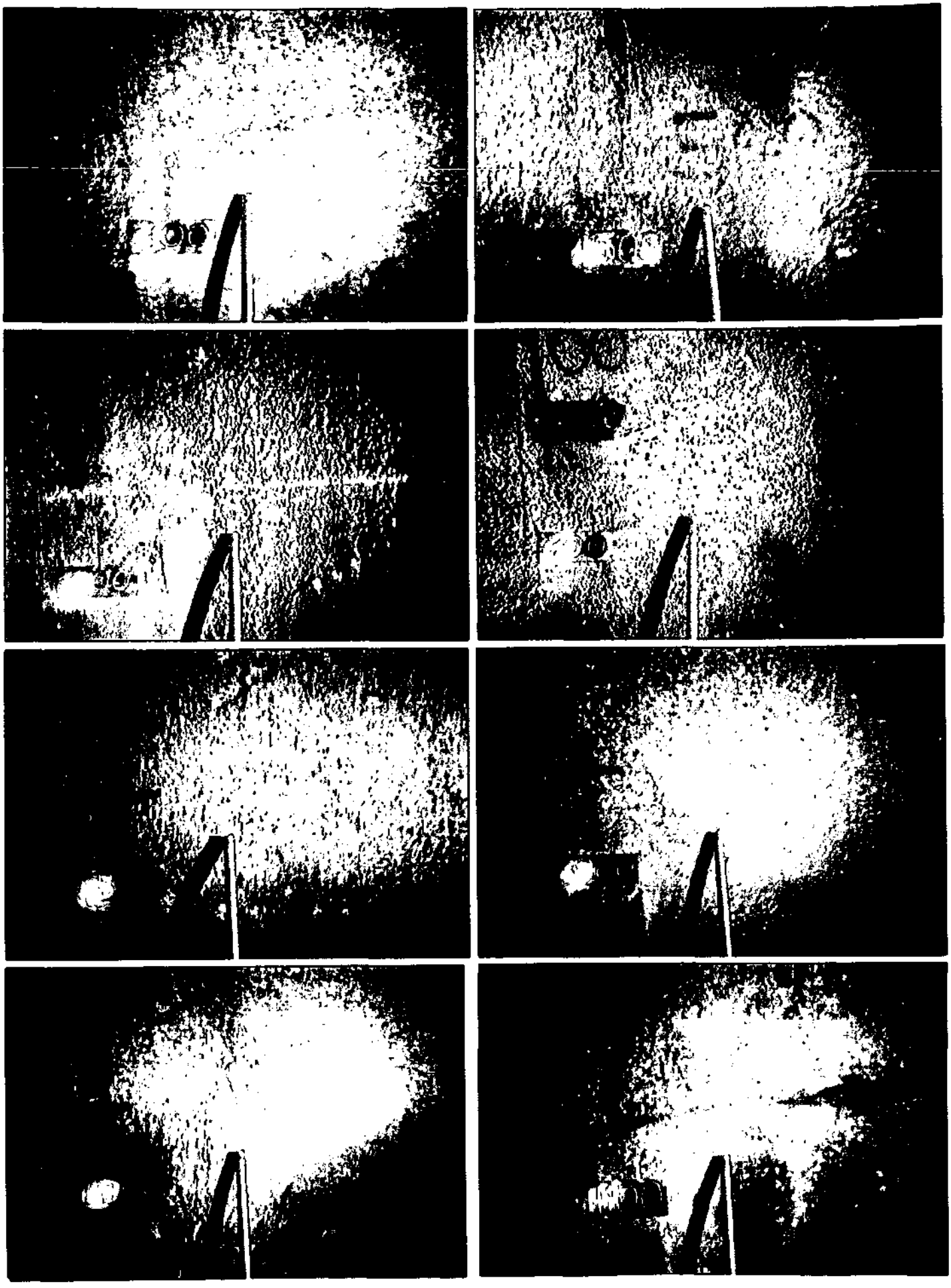

Plate F1 Emolweni Tunnel

Chainages 400 to 1100

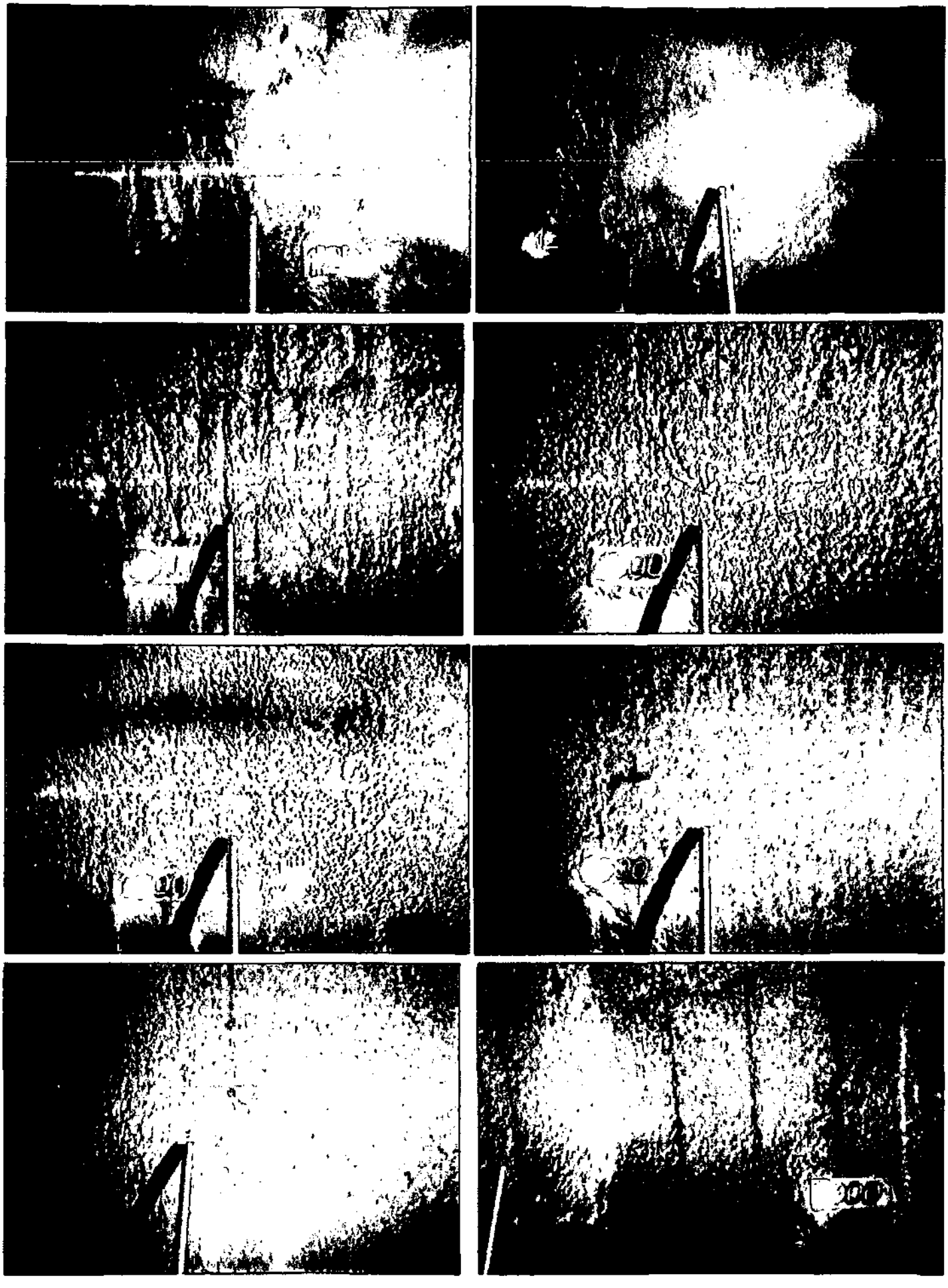

Plate F2 Emolweni Tunnel

Chainages 1200 to 1900

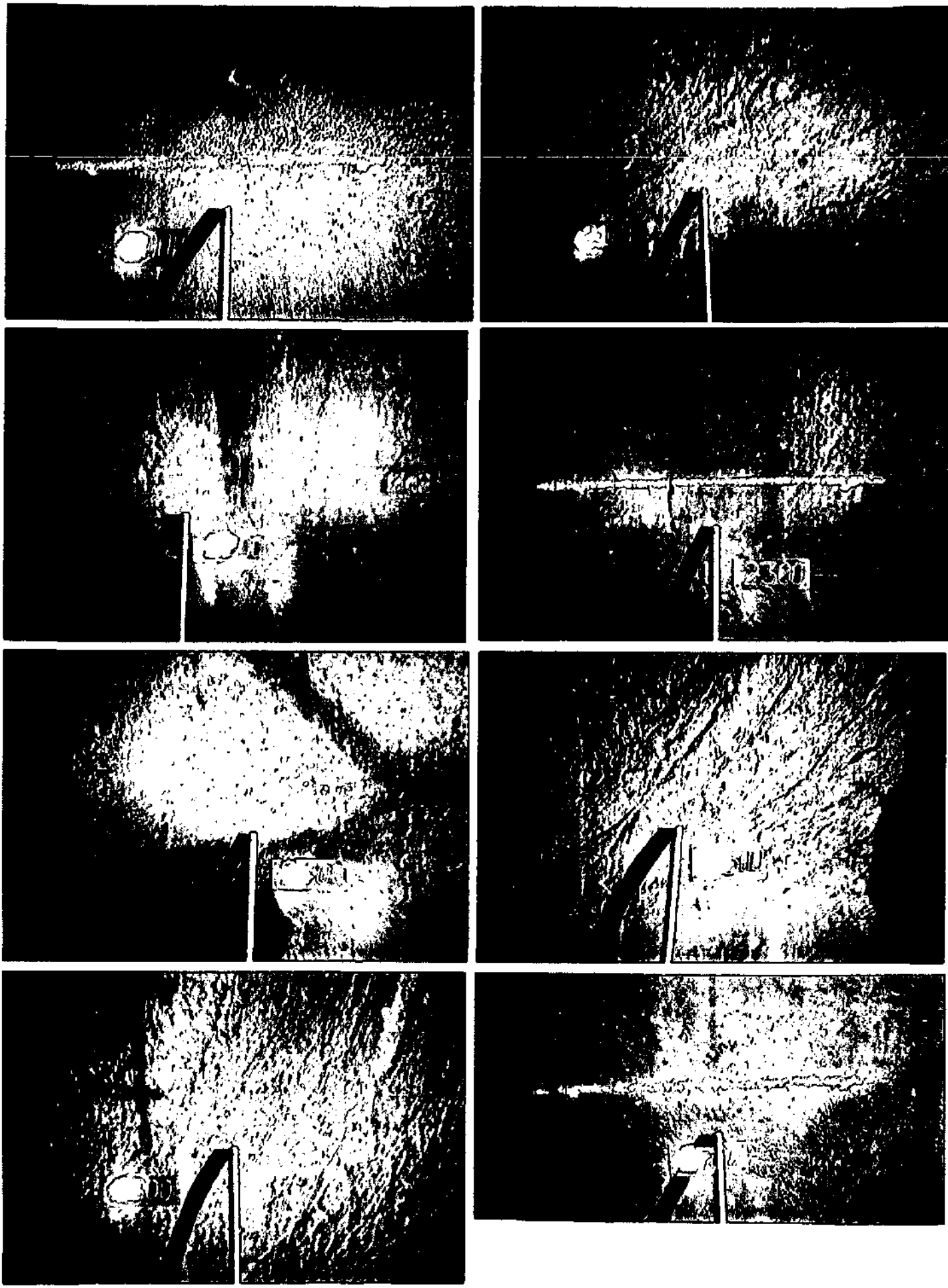

Plate F3 Emolweni Tunnel

Chainages 2000 to 2700

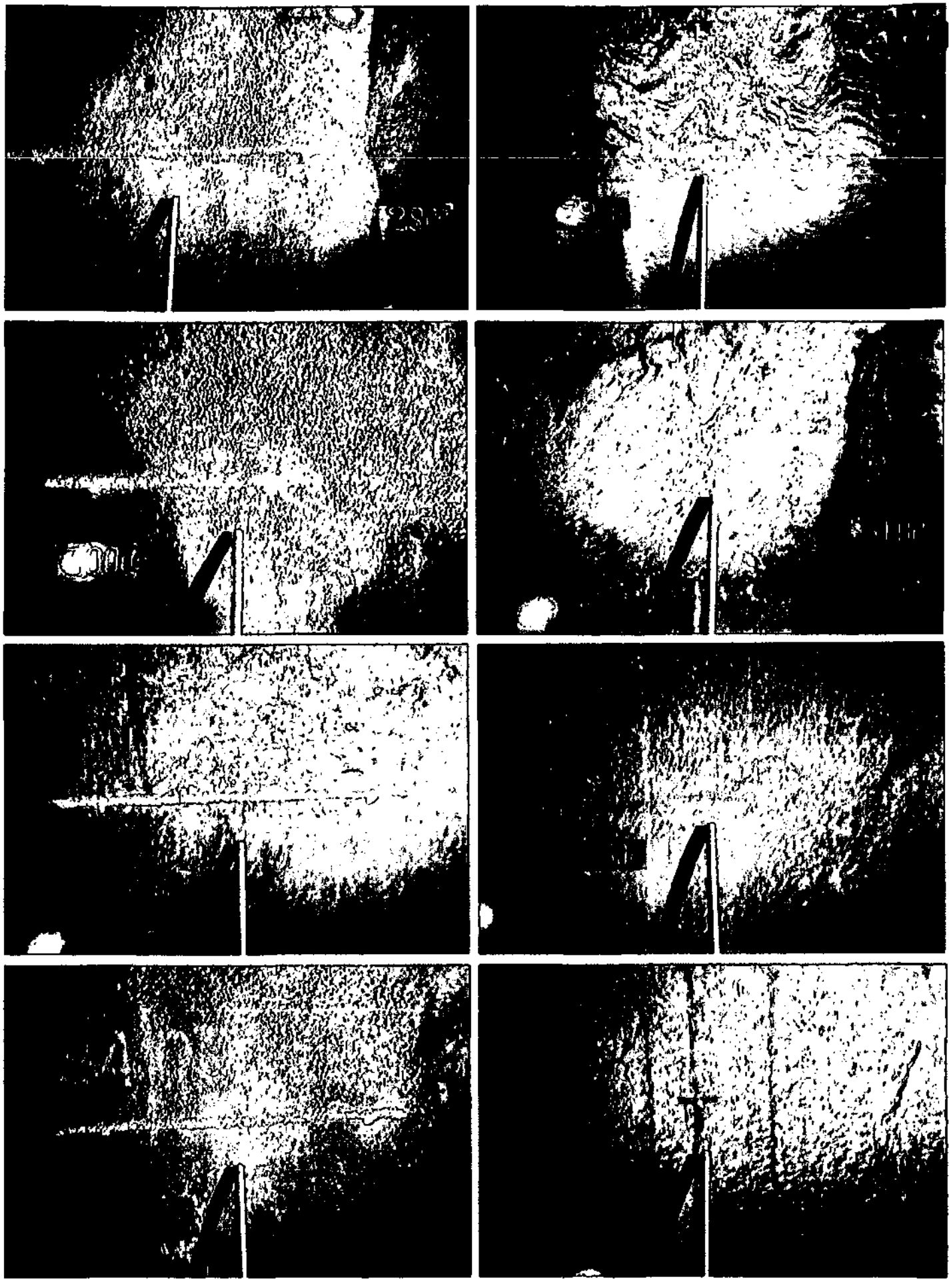

Plate F4 Emolweni Tunnel

Chainages 2800 to 3500

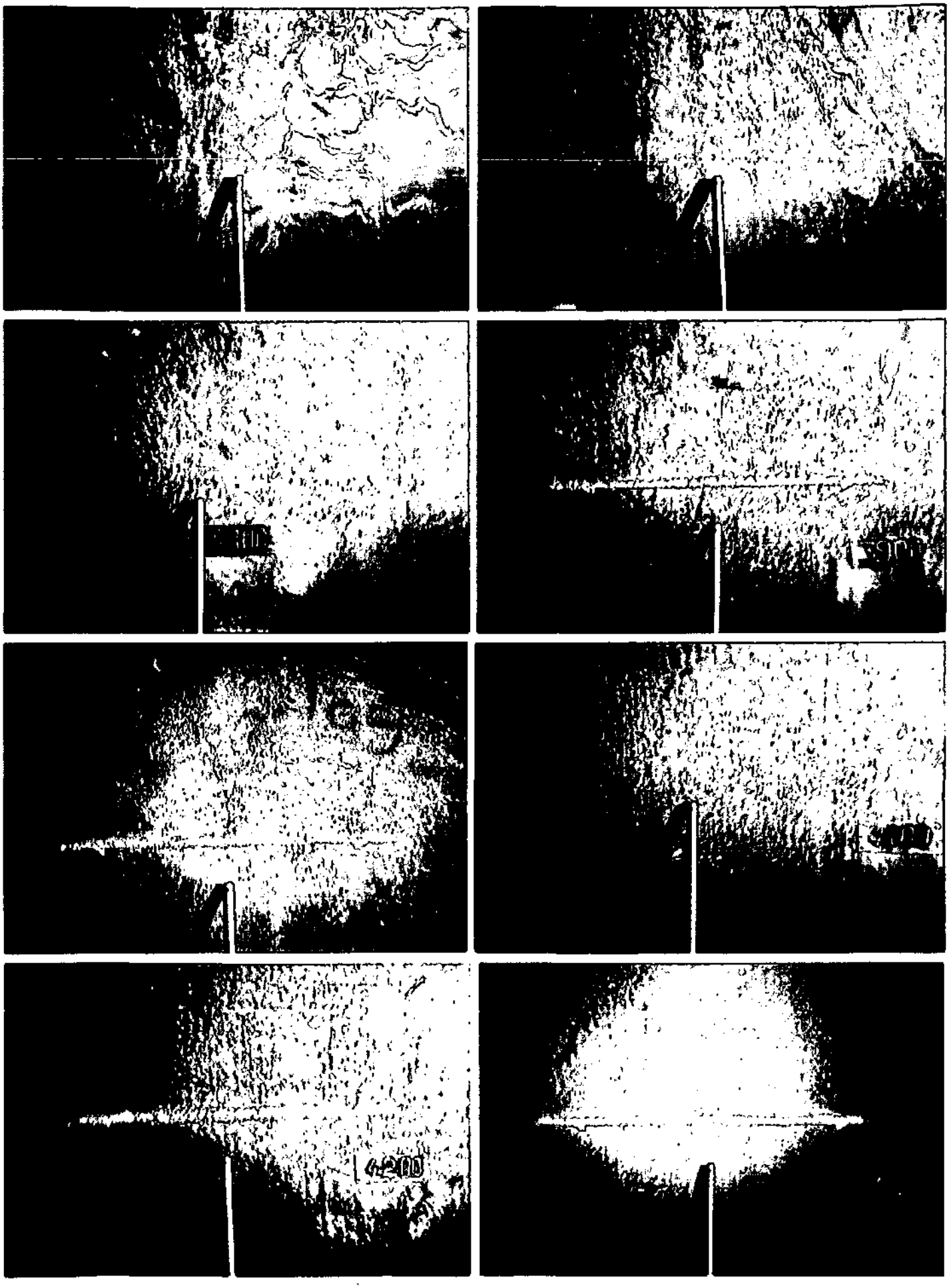

Plate F5 Emolweni Tunnel

Chainages 3600 to 4300

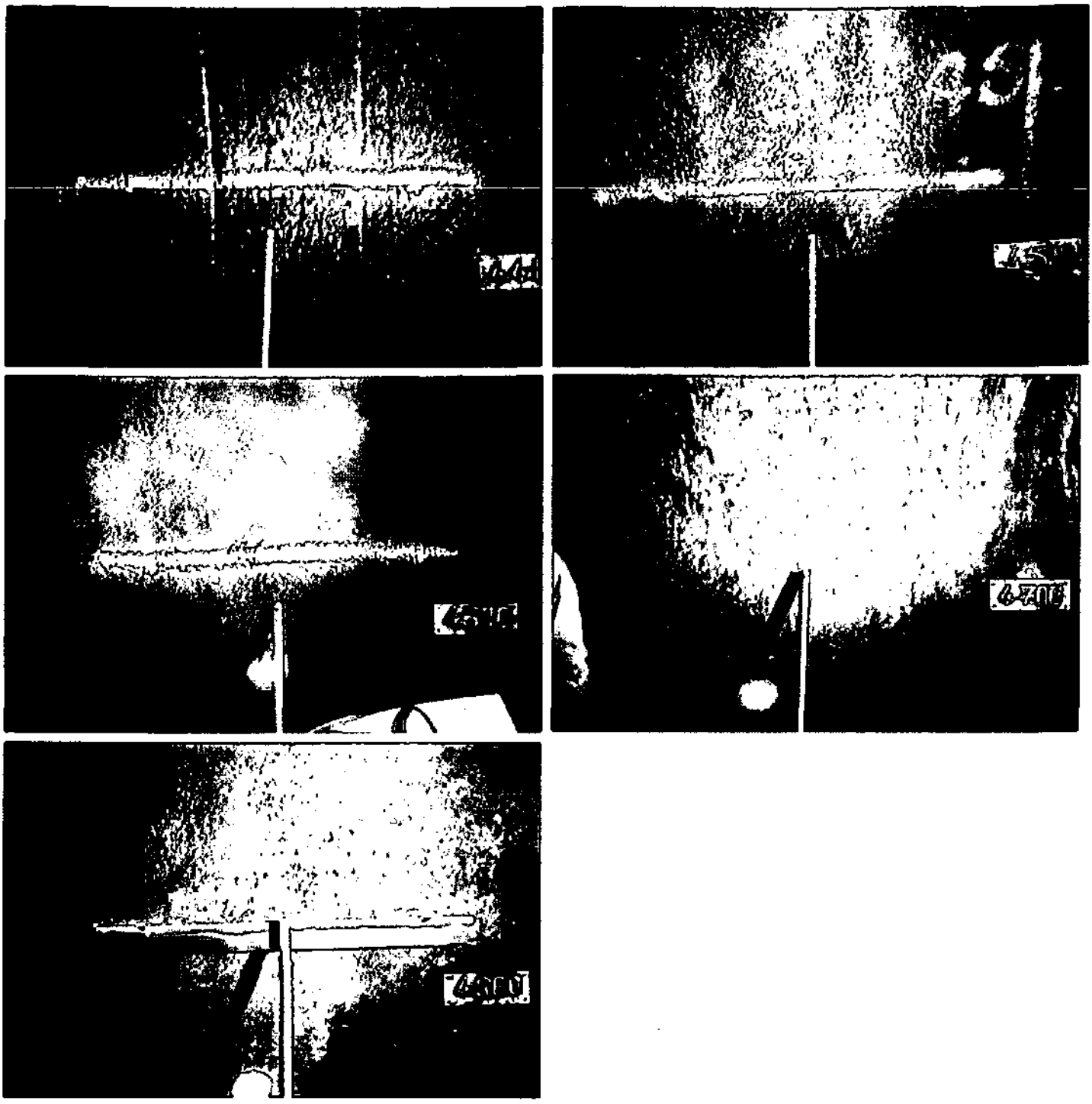

Plate F6 Emolweni Tunnel
Chainages 4400 to 4800

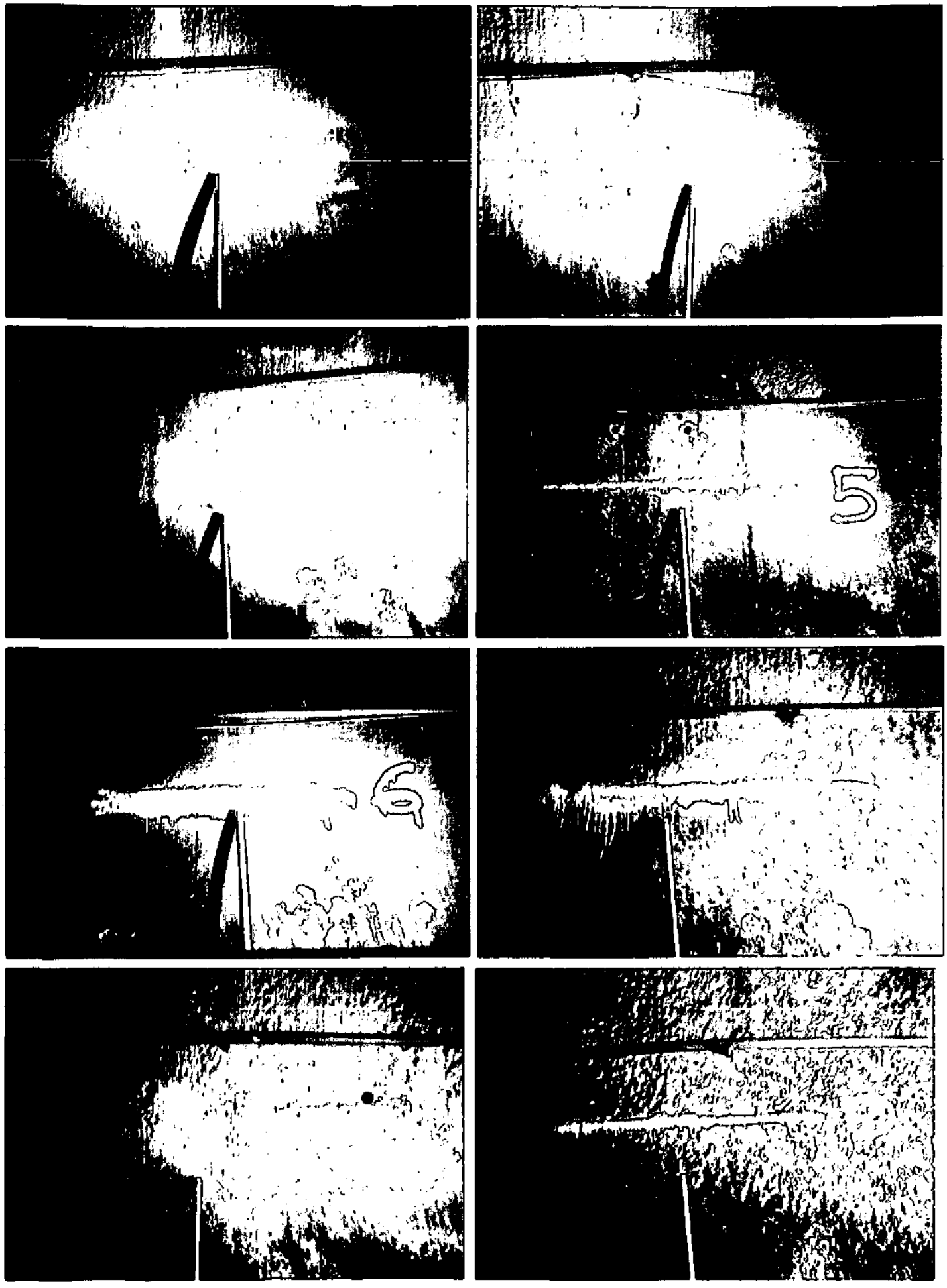

Plate F7 Ngoajane South Drive
Chainages 200 to 900

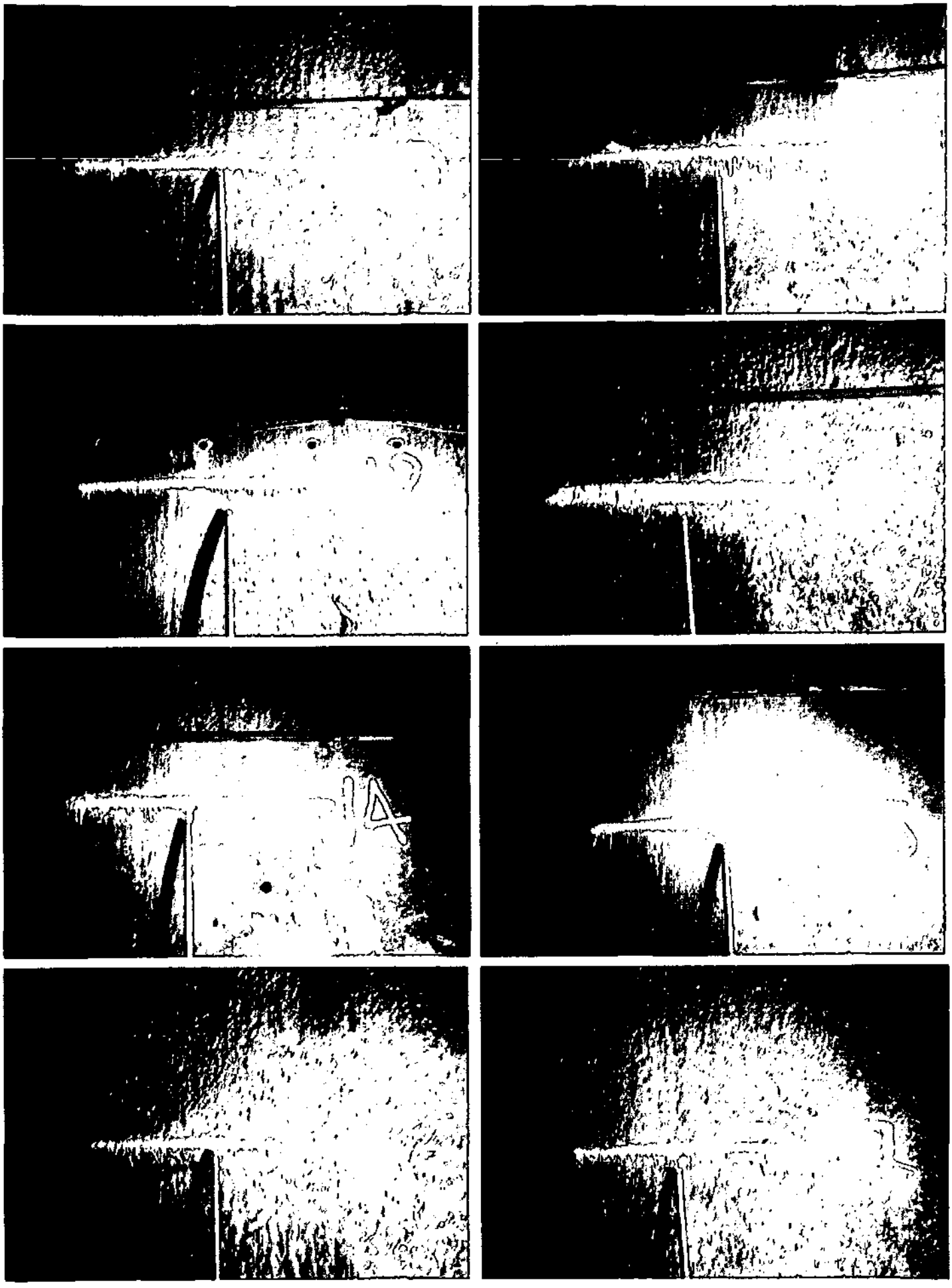

Plate F8 Ngoajane South Drive
Chainages 1000 to 1700

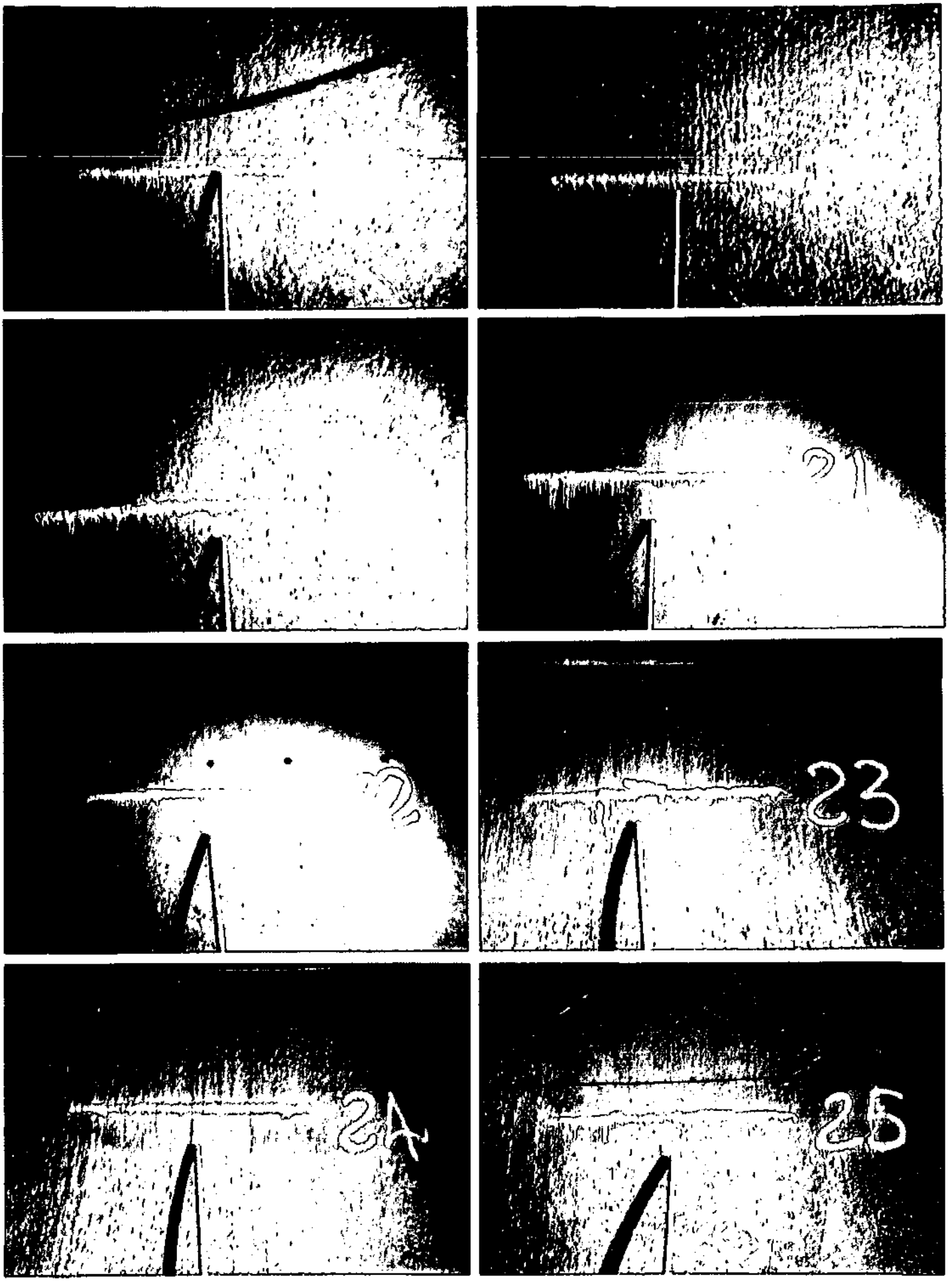

Plate F9 Ngoajane South Drive
Chainages 1800 to 2500

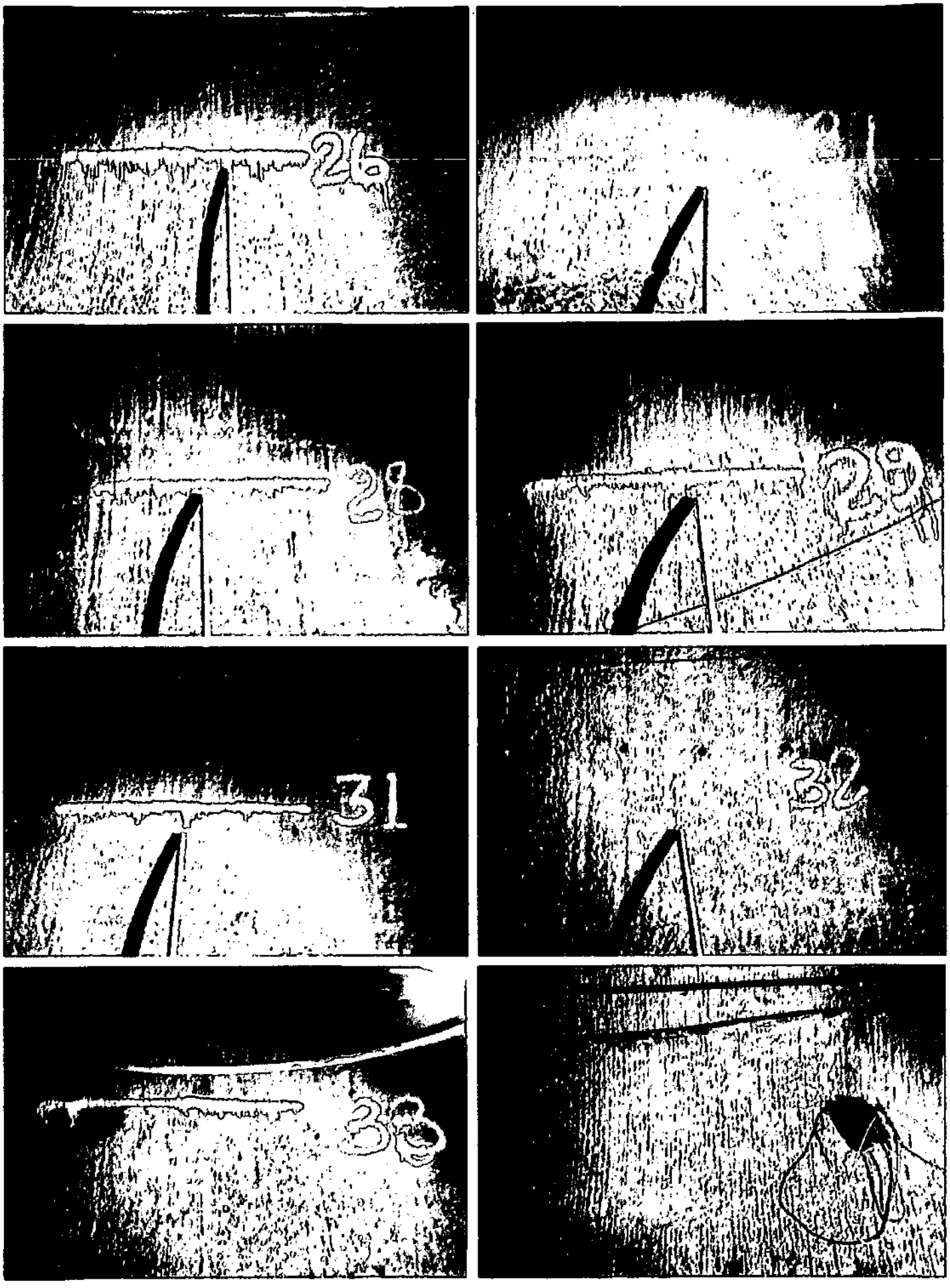

Plate F10 Ngoajane South Drive

Chainages 2600 to 3500

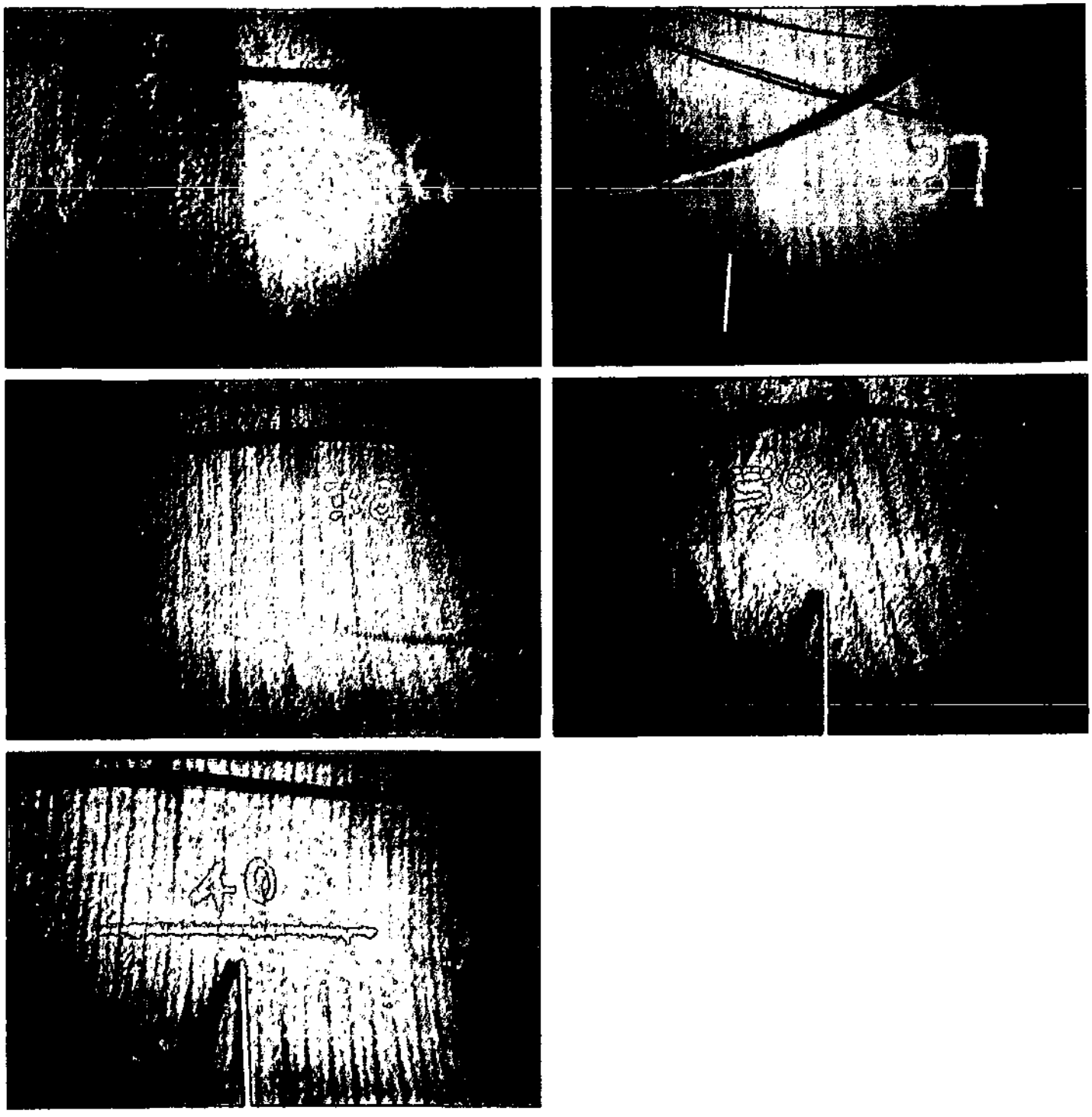

Plate F11 Ngoajane South Drive
Chainages 3600 to 4000

Plate F12 Clermont Tunnel
Chainages 2500 to 3867

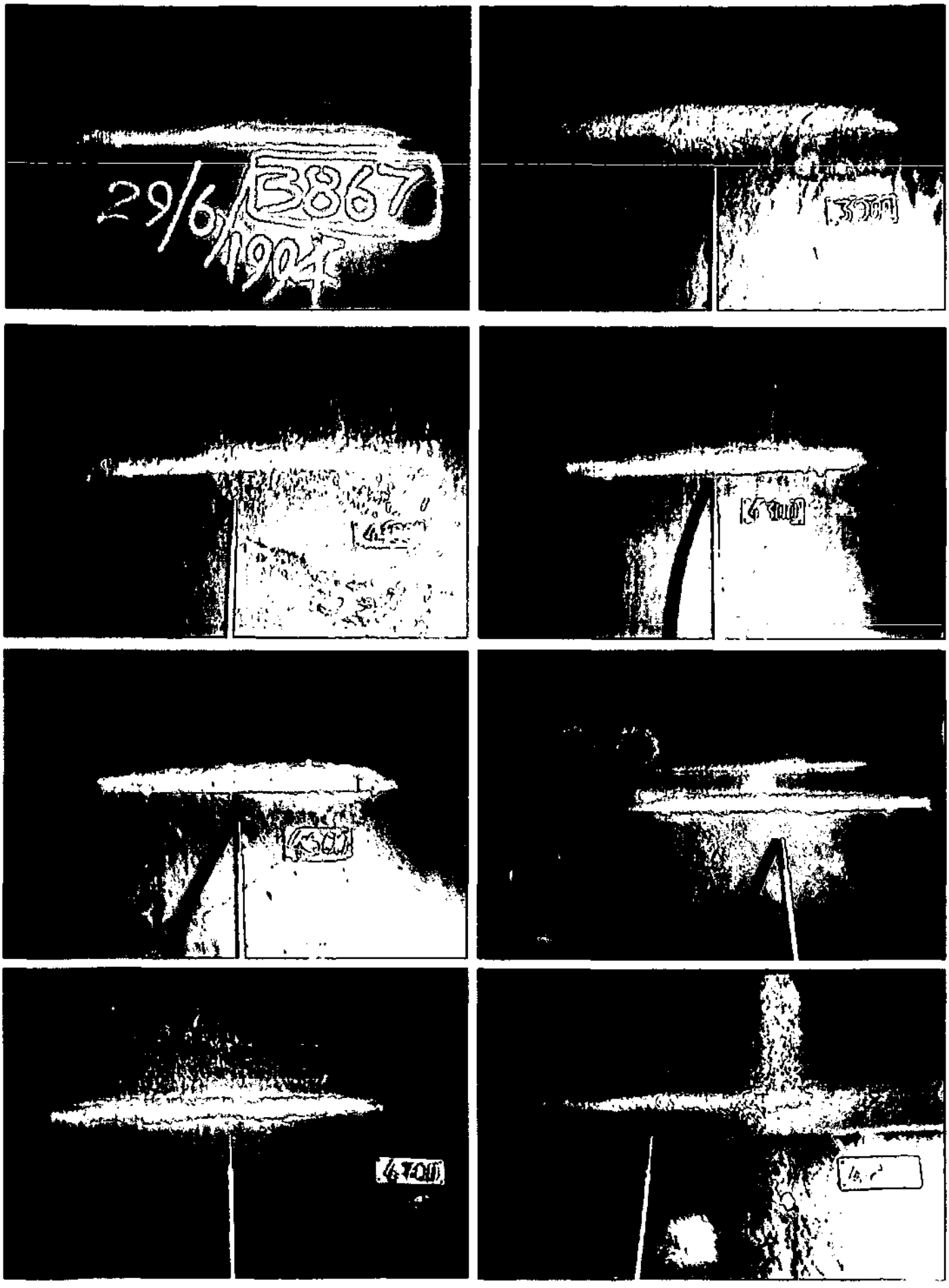

Plate F13 Clermont Tunnel

Chainages 3867 to 4800

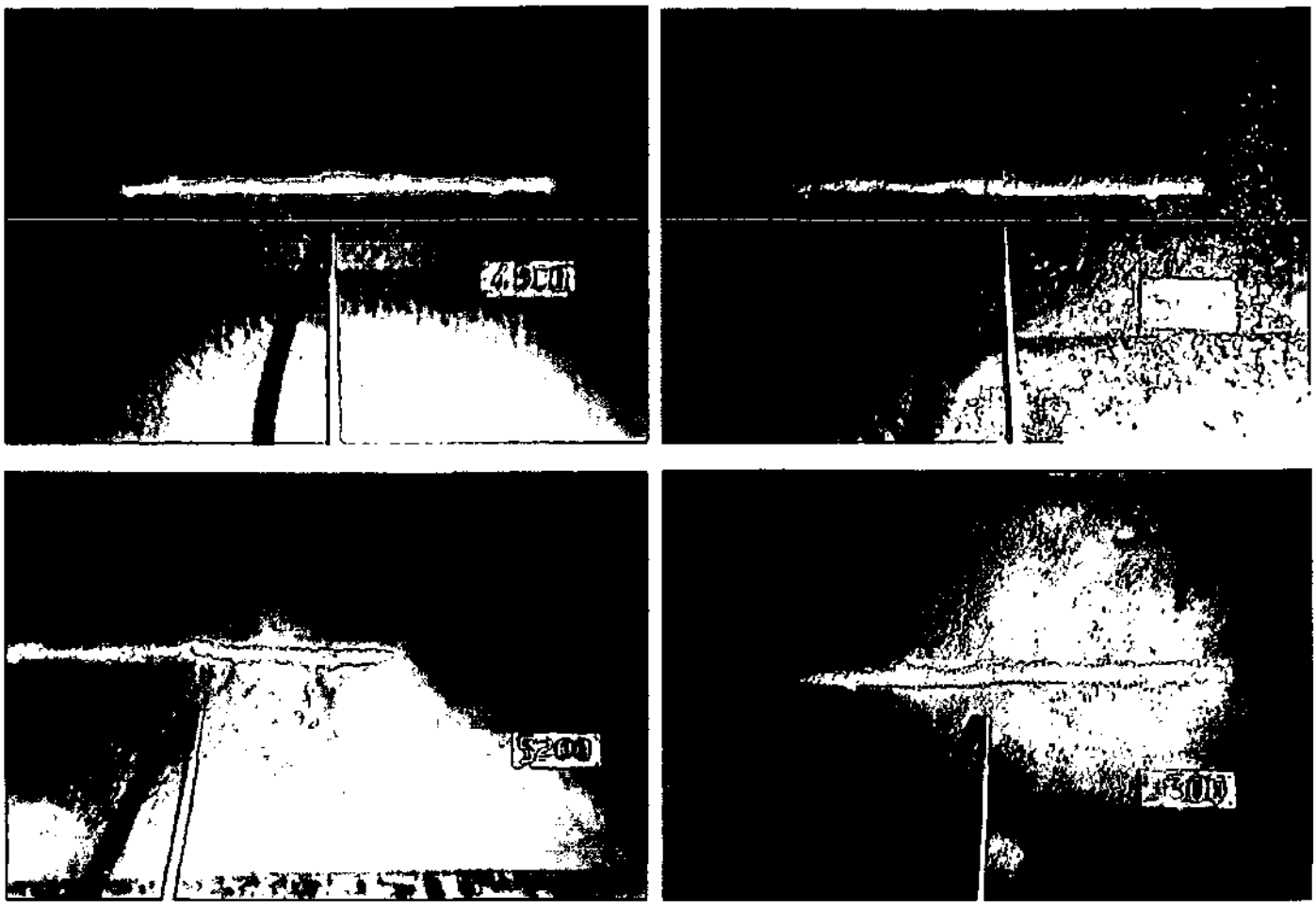

Plate F14 Clermont Tunnel

Chainages 4900 to 5300

REFERENCES

Ackers, P, (1963), Charts for the Hydraulic Design of Channels and Pipes, 2nd ed., London, HMSO.

Batchelor, GK, (1967), An Introduction to Fluid Dynamics, Cambridge University Press.

Box, GE & Jenkins, GM, (1970), Time Series Analysis Forecasting and Control, Holden Day, San Francisco.

Burchell, RS, (1983), Inanda-Wiggins Aqueduct : Absolute Roughness Measurements in a Machine-Bored Tunnel, Keeve Steyn Inc., Unpublished Report.

Chow, Ven Te, (1959), "Open Channel Hydraulics", Tokyo, McGraw-Hill Inc.

Colebrook, CF, (1939), Turbulent Flow in Pipes, with Particular Reference to the Transition Region between the Smooth and Rough Pipe Laws, *Journal of the Institution of Civil Engineers*, Vol.11, p.133-155.

Colebrook, CF & White, CM, (1937), Experiments with Fluid Friction in Roughened Pipes, *Proceedings, Royal Society of London*, Vol.161, p.367-381.

Haaland, SE (1983), Simple and Explicit Formulas for the Friction Factor in Turbulent Pipe Flow, *Journal of Fluids Engineering*, Vol.105, p.89-90.

Heerman, DF, (1968), Characterization of Hydraulic Roughness, Thesis submitted in partial fulfilment of requirements for PhD, Colorado State University, Colorado.

Highlands Delivery Tunnel Consultants, (1988), Delivery Tunnel Design Contract TCTA-01, Technical Memorandum H2, Tunnel Roughness Report, Unpublished.

Hinze, JO, (1959), Turbulence: an introduction to its Mechanism and Theory, McGraw Hill, New York.

Hughes, WF & Brighton, JA, (1967), Theory and Problems of Fluid Dynamics, Schaum Publishing Company, New York.

Jenkins, GM & Watts, DG, (1968), Spectral Analysis and its Applications, Holden-Day, San Francisco.

Kumar, S & Robertson, JA, (1980), General Algorithm for Rough Conduit Resistance, *Journal of the Hydraulics Division, ASCE*, Vol.106, p.1745-1764.

Laufer, J, (1954), The Structure of Turbulence in Fully-Developed Pipe Flow, *National Advisory Commission for Aeronautics*, Report No. 1174.

LeCoq, R & Marin, G, (c1976)[1], Evaluation des Pertes de Charges des Galleries D'Amenee D'Eau Forees au Tunnelier et Non-Revetues, Translation by J Capell, (1994), Keeve Steyn Inc, Unpublished.

LeGrange du PA, & Rooseboom A, (1993), The Development of a Model to Simulate Channel Deformation in Alluvial Rivers, WRC Report No. 236/1/93, BKS Inc.

Manning, R, (1889), On the Flow of Water in Open Channels and Pipes, *Transactions, Institution of Civil Engineers of Ireland*, Vol.20, p.161-207.

Massey, BS, (1989), "Mechanics of Fluids", 6th ed., London, Chapman and Hall.

May, DK, Peterson, AW & Rajaratnam, N, (1986), A study of Manning's Roughness Coefficient for Commercial Concrete and Plastic Pipes, Technical Report, T.Blench Hydraulics Laboratory, University of Alberta, Edmonton, Canada.

Monin, AS & Yaglom, AM, (1971), Statistical Fluid Mechanics, MIT Press, Massachusetts.

Moody, LF, (1944), Friction Factors for Pipe Flow, *Transactions, American Society of Mechanical Engineers*, Vol.66, p.671-684.

Morris, HM, (1955), Flow in Rough Conduits (with discussion), *Transactions, American Society of Civil Engineers*, Vol.120, p.373-410.

Morris, HM, (1959), Design Methods for Flow in Rough Conduits, *Transactions, American Society of Civil Engineers*, p.454-490.

Nikuradse, J, (1933), Stromungsgesetze in Rauhen Rohren, *Verein Deutscher Ingenieure, Forschungsheft*, Vol.361. English translation: *Petroleum Engineer*, (1940), March p.164-166; May p.75, 78, 80, 82; June p.124, 127, 128, 130; July p.38, 40, 42; August p.83, 84, 87.

O'Connor, DJ, (1995), "Inner Region of Smooth Pipes and Open Channels", *ASCE Journal, Hydraulics Division*, Vol.121, No.7, July, p.555-560.

Pegram, GGS, (1993), Hydraulic Roughness of Tunnels Bored by Machine through Various Rock Types: Proposal to Water Research Commission.

Rouse, H, (1950), Engineering Hydraulics, Proceedings of the Fourth Hydraulics Conference, Iowa Institute of Hydraulic Research, 1949, Wiley, New York.

---

[1]This document was supplied to the Author without quoting its original source. The suppliers of it do not, themselves, know the source and a thorough search for it was made (in vain). It may be possible that this document was never published, as no other authors encountered have quoted LeCocq and Marin as a reference. From reading the document it is apparent that it was written either late in 1976 or some time thereafter. The original was written in French.

Schumway, RH, (1988), Applied Statistical Time Series Analysis, Prentice Hall, New Jersey.

Shipton, RJ & Graze, HR, (1976), Flow in Corrugated Pipes, *Journal of the Hydraulics Division, ASCE,* Vol.102, p.1343-1351.

Streeter, VL, (1936), Frictional Resistance in Artificially Roughened Pipes, *Transactions, American Society of Civil Engineers*, Vol.101, p.681-704.

Stutsman, RD, (1988), TBM Tunnel Friction Factors for the Kerckhoff 2 Project, *Water Power '87*, Brian W Clowes ed., p.1710-1725.

Tullis, JP & Utah State University Foundation, (1986), "Friction Factor Tests on Concrete Pipe", Utah State University Foundation.

Wallis, S, (1992), Lesotho Highlands Water Project, Surrey, Laserline.

Wallis, S, (1993), Lesotho Highlands Water Project Volume 2, Surrey, Laserline.